Novel Protein-Based Solutions for Organophosphorus Nerve Agent Detection and Elimination

Andrew C. Hemmert

A dissertation submitted to the faculty of the University of North Carolina at Chapel Hill
in partial fulfillment of the requirements for the degree of Doctor of Philosophy
in the Department of Biochemistry and Biophysics

Chapel Hill
2010

Approved by:
Matthew Redinbo, Ph.D.
Richard Wolfenden, Ph.D.
Edward Collins, Ph.D.
Henrick Dohlman, Ph.D.
Brian Kuhlman, Ph.D.

ABSTRACT

Andrew C. Hemmert
Novel Protein-Based Solutions for Organophosphorus Nerve Agent Detection and Elimination
(Under the direction of Professor Matthew R. Redinbo)

Organophosphorus (OP) nerve agents are some of the deadliest chemicals ever synthesized by man. These toxins, which include sarin, soman, cyclosarin, tabun, and VX, inhibit the neurotransmitter-regulating enzyme, acetylcholinesterase (AChE). This leads to continual acetylcholine muscarinic and nicotinic receptor stimulus and may eventually result in death due to prolonged muscles contraction and diaphragm incapacitation. Current treatments for OP poisoning include injections of atropine, to dampen acetylcholine stimulation, a strong-nucleophile oxime, such a 2-pralidoxime, to reactivate inhibited AChE, and diazepam for seizures. These treatments are limited, however, because they do not protect against poisoning, cannot be administered prior to exposure, and don't address the long-term side effects associated with nerve agent poisoning. Additionally, there is no broad-spectrum oxime effective against all nerve agents. A better therapeutic would be a prophylactic molecule capable of catalytically degrading the OP prior to AChE inhibition.

Protein-based therapeutics are an emerging remedy for OP toxicity. It has been shown that pre-administration of excess AChE in mice can protein against 8-10 normally lethal doses of soman. Current enzyme therapeutics can be categorized as either

stoichiometric or catalytic. Stoichiometric OP binders, such as AChE or the homologous butyrylcholinesterase (BChE), benefit from nanomolar (nM) dissociation constants, but suffer in their ability to recover after OP exposure, thereby requiring large enzyme doses for effective treatment. Catalytic protein therapeutics, including serum paraoxonase (PON1) or the bacterial organophosphate hydrolase (OPH) exhibit rapid rates of *in vitro* nerve agent hydrolysis, but are limited by high dissociation constants, making them ineffective *in vivo*.

Human carboxylesterase 1 (hCE1) is a liver serine hydrolase in the same α/β super family as AChE and BChE, which may have more favorable attributes as an OP bioscavenger. Indeed rodents express a serum carboxylesterase that affords them high levels of protection against OPs. Using structural and biochemical studies, we determined the stereopreference, rates of spontaneous reactivation, and availability of rapid oxime-assisted reactivation of hCE1 with nerve agents. Next, using structurally guided protein design, we engineered a form of the hCE1 that combines the benefits of both bioscavenger classes, exhibiting nM dissociation constants and enhanced rates of hydrolysis, up to 48,700-fold, against the nerve agents sarin, soman, and cyclosarin. Finally, novel mutants of hCE1 were developed that exhibit-increased rates of reactivation against specific agents, and can be utilized to detect and identify chemical agents.

DEDICATION

To my wife Rachael and my son Isaac. Your sacrifices, encouragement, and laughter have helped me pursue my passion.

ACKNOWLEDGEMENTS

I would first like to thank Dr. Matthew Redinbo for his mentorship and financial support during my graduate career. He has enabled me to grow as a person, scientist, and leader through giving of his time, teaching-moments, and encouragement. I would also like to thank my committee members for their time and enthusiasm. Dick, Ed, Brian, and Henrick are inspiring role models and I aim to model my scientific career after theirs. Thanks to my collaborators Doug Cerasoli and Tammy Otto at the USAMRICD, as well as Phil Potter and Monika Wierdl at St. Jude's Childrens Research Hospital. Without their efforts I would not have been able to complete such an exciting project in the same amount of time. They all greatly contributed to my success.

I appreciate the support and help of my current and past co-workers in the Redinbo lab. Eric Ortlund, Mike Miley, Scott Lujan, and Chris Fleming mentored me at the beginning of my career, helping me get my project off the ground and were always willing to listen to my ideas and questions. Special thanks to Sarah Kennedy and Rebekah Nash for their friendship, willingness to listen, and technical assistance; they helped me stay centered. Thanks to Steven Lewis, Jacob Grohman, Lauren Hall, and Jillian Tyrrell for their assistance on my project during their respective rotations. Lastly I want to thank Jon Edwards, Ben Hill, and Holden Higgenbotham for their hard work in getting Identizyme Defense Technologies, Inc. off the ground. I wish them all success in their future endeavors.

I greatly appreciate the guidance and friendship of my undergraduate research mentor, Dr. Bellamkonda Kishore at the University of Utah. He gave me an opportunity to discover my life's passion, and always told horribly lame jokes. I never felt like an inexperienced undergraduate in his lab, and he is a great friend. I would like to thank my high school chemistry teacher, Doug Tate. Before I took his class, I remember wanting to never study chemistry. He was a fantastic teacher and his threats to kick my butt all over the school when I didn't reach the potential that he saw, were very motivating. I will always be grateful to him.

Finally I want to thank my wife, Rachael, my in-laws Gary and Teresa Beckstrand, and my parents Russ and Tammy Hemmert. They have provided a constant stream of support and motivation throughout the past five years. I look forward to sharing my successes with them, because I know they will always be proud of me. The addition of my son Isaac has been an added joy to graduate school, not only in making life a little more challenging, but by also providing constant love, fun, and laughter. I hope he finds happiness in his life, and is able to find a career he loves, as much as I love mine.

PREFACE

It was during my junior year of an undergraduate degree in chemistry at the University of Utah that I discovered I wanted to be a scientist. Up until that point I had always enjoyed chemistry and seemed to excel in all my science classes. At the time I was taking MCAT prep classes and finalizing the requirements for Medical School. The thought of working tirelessly in a large concrete chemistry building wasn't appealing. That fall semester, during a biochemistry lecture taught by Dr. Dale Poulter, I was captivated by his description of how multiple proteins function to create life. We were learning about pyrimidine biosynthesis and he described how the growing substrate is transferred from one protein machine to another, finally creating the essential building block for life. I was mesmerized with the ideas of protein nano-machines. The thoughts and impressions from those lectures spilled over into the research lab where I was studying the expression and regulation of water channels in kidneys. I became fascinated in how these tiny pores tightly regulated water during various hydration states. Then it happened, I saw my first crystal structure, Aquaporin 2. After studying the atomic resolution details, I came up with an idea to change this protein into a nano-machine for chemical transport. Could I mutate residues within this channel to make it now selective for small molecules or solvents? The ideas of creating novel proteins has been my obsession ever since.

I was able to pursue my passion of developing novel proteins under the guidance of Matthew Redinbo. Dr. Redinbo, a highly regarded scientist in X-ray crystallography and xenobiotic metabolism, allowed me to work on a project that utilized protein structure to rationally develop novel enzyme activity, or to answer the question, "Can I mutate these residues to make it now do this?" The project of developing human carboxylesterase 1 into a nerve agent-metabolizing enzyme has been one of the most fulfilling pursuits of my life so far. Not only has it enabled me to learn numerous scientific techniques, taught me to dissect scientific literature, and lead research groups from academia, industry, and government, it has allowed me to be creative and push the boundaries on what I thought I could do. As a result of this project I am going to continue product driven research and aim to work on projects that allow me to answer the questions, "Can I make this protein do something new?"

Here I present the work completed during my graduate career under the direction of Dr. Redinbo. In chapter one, I describe the history, chemical structures, and current treatment for organophosphorus nerve agent poisoning. Due to the deficiencies in these antidotes, I will also summarize the current research on developing protein-based therapies, or bioscavengers, to protect against chemical agent poisoning. In chapter two, I introduce the enzyme human carboxylesterase 1 (hCE1), describe how this protein interacts with nerve agents, and lay out the differences of this enzyme over current bioscavengers. In chapter three, I will present the novel mutations we introduced into hCE1 to generate rate enhancements in nerve agent hydrolysis by as much as 48,700-fold over the wild type enzyme. I will also compare the catalytic properties of the hCE1 dyad mutant against other bioscavengers. Lastly, I will discuss where this designed enzyme

fits within the field of rational protein design. In chapter four, I present a novel patent-protected application that incorporates some of the mutant proteins I have generated during my graduate career for nerve agent detection and identification. Finally in chapter five, I report other data I have generated for hCE1 mutants regarding chemotherapy prodrug activation and unique structural loops of this carboxylesterase compared to other similar enzymes.

TABLE OF CONTENTS

LIST OF TABLES

LIST OF FIGURES

Chapter 1.

Chapter 2.

LIST OF ABBREVIATIONS AND SYMBOLS

2-PAM	2-pralidoxime
Å	angstrom
AChE	Acetylcholinesterase
A_{max}	maximal percent reactivation
Atropine	(8-methyl-8-azabicyclo[3.2.1]oct-3-yl) 3-hydroxy-2-phenylpropanoate
BChE	Butyrylcholinesterase
CE	Carboxylesterase
CPT-11	Irinotecan
CWC	Chemical Weapons Convention
Cyclosarin	cyclohexyl methylphosphonofluoridate
DAM	diacetylmonoxime
DFPase	Fluorophosphatase
Diazepam	7-chloro-1,3-dihydro-1-methyl-5-phenyl-1,4-benzodiazepin-2(2H)-one
DMS	Differential Ion Mobility Spectroscopy
ER	Endoplasmic Reticulum
GA	Tabun
GB	Sarin
HAZMAT	Hazardous materials

hCE1	Human Carboxylesterase 1
hiCE	Human Intestinal Carboxylesterase
HSA	Human Serum Albumin
k_2	rate of phosphonylation
kcal	kilocalorie
K_d	dissocation constant
kDa	kilodalton
k_i	bimolecular rate of inhibition
k_{obs}	observed rate of reactivation
LB	Lysogeny Broth
LCt_{50}	mean lethal concentration
LD	loop deletion
LD_{50}	percutaneous lethal dose
mg	milligram
mM	millimolar
N.D.	no data
nm	nanometer
nM	nanomolar
oNPA	*ortho*-nitrophenyl acetate
OP	organophosphorus
OPH	Organophosphorus Hydrolase
PCR	Polymerase Chain Reaction
PDB	Protein Data Bank

PEG	polyethylene glycol
pKa	acid dissociation constant
pNPB	*para*-nitrophenyl butyrate
PON1	Serum Paraoxonase
r.m.s.d.	root mean square deviation
rCE	Rabbit Liver Carboxylesterase
rsCE	Rat Serum Carboxylesterase
S.E.	standard error
Sarin	isopropyl methylphosphonofluoridate
SN-38	7-ethyl-10-hydroxycamptothecin
Soman	pinacolyl methyl phosphonofluoridate
Tabun	ethyl N,N-dimethylphosphoramidocyanidate
USAMRICD	United States Army Medical Research Institute of Chemical Defense
VX	O-ethyl S-[2-(diisopropylamino)ethyl] methylphosphonothiolate
μL	microliter
μM	micromolar

Chapter 1. Organophosphorus Nerve Agents

1.1 History of Organophosphate Nerve Agents

Organophosphate (OP) nerve agents are some of the deadliest chemicals ever synthesized by man. This class of chemical agent was accidentally discovered in 1936 by Dr. Gerhard Schrader of I.G. Farben in Germany while attempting to develop new insecticides (*1*). Controlled animal studies with ethyl *N,N*-dimethylphosphoramidocyanidate, now known as Tabun, reported lethality within 20 minutes of exposure. After accidentally spilling a small drop on the laboratory bench, both Dr. Schrader and his assistant were the first human test subjects of OP poisoning, experiencing miosis and difficulty breathing that kept them away from the lab for 3 weeks (*1*). Their discovery was reported to the Nazi Ministry of War and large-scale production began on this new, more deadly, chemical warfare agent. In 1938 Dr. Schrader and his group discovered a second nerve agent, one that was 10 times more effective in animal tests as Tabun, isopropyl methylphosphonofluoridate, named in acronymic form after the discovering scientists as sarin (**S**chrader, **A**mbrose, **R**udriger, and van der L**in**de) (*2*). The additional G-agents (G for German) soman (pinacolyl methyl phosphonofluoridate) and cyclosarin (cyclohexyl methylphosphonofluoridate), were further developed in Germany during World War II (*3*). Even though Nazi Germany filled bombs, shells, and rockets with Tabun, for differing reasons, none of these weapons were

ever used on the battlefield. The Allied forces only discovered these toxic agents after Germany was overrun (*2*).

After World War II ended, the U.S., Soviet Union, and England incorporated the German nerve agent technology into their arsenal and began constructing weapons filed with sarin. In 1952 a British scientist, Dr. Ranajit Ghosh, discovered *O*-ethyl *S*-[2-(diisopropylamino)ethyl] methylphosphonothiolate, now known as VX, during his research to develop an insecticide replacement for DTT. A derivative of this compound was briefly commercialized as a pesticide called Amiton, but quickly recognized as being too toxic for general use (*1*). The secret of VX (V for venomous) nerve agent was passed to the U.S., where it was incorporated into ammunition and land mines, and eventually leaked to the Soviet Union, where additional V-agents have been developed (*4*). Like Nazi Germany, the U.S. never released nerve agents on the battlefield, but in 1968 an accidental VX release in Skull Valley, Utah sickened or killed over 6000 sheep (*5*). Because of this and a similar accident in Okinawa, Japan a year later, U.S. production of chemical agents was halted in 1969 (*1*).

Since their inception the most significant use of OP nerve agents was the Iraqi deployment of nerve and chemical agents against Iran during the Iran-Iraq war (*6*). This was infamously followed in 1988 by massive Iraqi chemical agent attacks on their own people in Halabja resulting in over 5000 total casualties. It is thought that tabun and sarin were deployed (*1, 7*). Following this horrific event, many industrialized countries, including the U.S. and Russia, began again to produce nerve agents, focusing however on the creation of binary agents, or two less-than-lethal precursors, that form deadly agents when combined (*1, 4*). This escalation continued until 1993 when many countries signed the Chemical Weapons

Convention (CWC), which banned all chemical weapon development, production, acquisition, stockpiling, transfer, or use and also required the destruction of existing stockpiles (*8*).

Despite the adoption of the CWC, nerve agents are a continued threat. There are reportedly more than 200,000 tons of nerve agents in existence worldwide (*9*). In 1995 the religious doomsday cult Aum Shinrikyo attempted twice to publicly release sarin. First they targeted the apartment complex of three judges who ruled against them in a land deal trial. During the attack, the wind changed direction and the judges were not killed, but became ill. Overall seven people died and 144 civilians were injured in that attempt. More publicized however was their second attempt in which they released dilute sarin gas into the Tokyo subway system on 5 trains simultaneously. Twelve passengers died and 5500 sought medical treatment (*10-12*). Although these are limited examples of military and terrorist use, they may not accurately reflect the potential of future threats (*1*).

1.2 Chemistry of Organophosphate Toxicology

OP nerve agents are alkylphosphonic esters that contain different alkyl, alkoxy, and potent-leaving groups **(Figure 1.1)**. The volatility and toxicity of each agent depends on arrangement of these groups around the chiral phosphate **(Table 1.1)**. Sarin is the most volatile nerve agent (22,000 mg/m^3) compared to the volatility of VX (10.5 mg/m^3) and is the most likely agent to exist as an actual "nerve gas" (*13*). Tabun contains a cyanide leaving group, dimethylamine alky group, and an ester linked ethyl group. This is the least stable and toxic nerve agent with a half-time of hydrolysis in water at pH 7 of 8.5 hours. Sarin, soman, and cyclosarin all share common methyl alkyl and fluoride leaving groups, but differ,

in alkoxy group; isopropyl, pinacolyl, and cyclohexyl respectively. Soman has a half-time of hydrolysis of 80 hours at 20^{o}C, pH 7 (*14*). Lastly VX is composed of ethoxy, methyl, and a large diisopropylamino thioester leaving group. This thioester is charged at physiological pH, which as discussed later, enhances the impact of this nerve agent. VX is also the least volatile and most persistent of all the nerve agents, behaving similar to gasoline, and having a half-time of hydrolysis at 25^{o}C and pH 7 of 30 days (*14*).

Nerve agents exist in racemic mixtures, but their toxicity is greatly affected by stereochemistry. The central phosphate is chiral exhibiting P_R and P_S isomers. The P_S isomers of sarin, soman, and Cyclosarin are up to 5,000-fold more toxic than the respective P_R isomers (*15*). Soman contains and additional chiral center in the pinacolyl alkoxy moiety, the C_R enantiomer is slightly more potent than C_S. P_S VX is approximately 100-times more toxic than the P_R isomer.

1.3 Mechanism of Nerve Agent Toxicity

Nerve agents exert their toxic affects by inhibiting serine hydrolase enzymes. The critical target is the neurotransmitter-regulating enzyme acetylcholinesterase (AChE) (*16*). Additional targets include butyrylcholinestease (BChE), carboxylesterases (CEs), human serum albumin (HSA), and serum paraoxonase (PON1) (*17-19*). AChE is responsible for hydrolyzing acetylcholine, which transmits stimulation through muscarinic and nicotinic receptors in neuromuscular junctions (*20*). OP nerve agents bind and covalently modify the catalytic serine in the enzyme's active site. If greater than 40% of this enzyme becomes irreversibly inhibited, the resulting buildup of acetylcholine will continually stimulate the central and peripheral nervous systems, leading to a cholinergic crisis (*21*). Symptoms

include; miosis, increased bronchial secretions and constriction, sweating, incontinence, tremors, convulsions, seizures, and eventually diaphragm incapacitation. Death from OP nerve agents is generally attributed to respiratory failure (*21, 22*).

The most common routes of OP poisoning are inhalation or dermal contact. As shown in **Table 1.2**, the LCt_{50}, or mean lethal concentration, ranges from 50 mg-min/m^3 for VX up 400 mg-min/m^3 with tabun. VX is the most toxic followed by cyclosarin, soman, sarin, and tabun. If percutaneous exposure occurs, again VX has the lowest LD_{50} (analogous to LCt_{50}) at 10 mg. This is proportional to the amount of liquid needed to fill in two columns of the Lincoln Memorial on a U.S. penny (*7*). Cyclosarin is the next toxic with an LD_{50} of 30 mg, followed by soman (50 mg), tabun (1000 mg) and sarin (1700 mg) (*13*).

1.4 Treatments for Nerve Agent Exposure

Current treatments for nerve agent poisoning include injections of three different drugs (*23*). The first, atropine is a competitive antagonist of the muscarinic acetylcholine receptors and reduces parasympathetic activity of all muscles and glands (*24*). This tropane alkaloid is derived from the deadly nightshade plant (*Atropa belladonna*) and is a core medicine in the World Health Organizations "Essential Drugs List" (*25*). The second drug is a strong nucleophile oxime, such as 2-pralidoxime (2-PAM) or obidoxime (*24*). These molecules react with the phosphonylated catalytic serine in AChE and attempt to remove the covalent adduct. This is limited in that there is no broad-spectrum oxime and reactivity differs for each agent (*26*). For example, 2-PAM is effective against sarin or VX poisoning, but is non-reactive with tabun, soman, or cyclosarin (*26*). Additionally, if the phosphonylated serine has undergone a process known as "aging", the oxime antidote is

completely ineffective (*27*). Aging is a time-dependent dealkylation of the nerve agent adduct. Soman inhibited AChE has been shown to age in as quickly as 2 minutes. The mechanism behind aging will be discussed in greater detail in chapter two. Lastly, diazepam is given to the victim to help reduce the impending seizures associated with nerve agent poisoning (*24*).

This treatment regimen has been utilized since the 1950's and has several limitations (*28*). Atropine and oximes are toxic and cannot be administered prior to exposure. Excess atropine produces an effect opposite that of OP nerve agents reducing peripheral nervous system activity. Patients with atropine toxicity experience dry mouth, blurred vision, tachycardia, increased temperature, and increased minute ventilation (*29*). Besides reactivating inhibited AChE, oximes also affect release of acetylcholine from cholinergic synapses, allosterically modulate muscarinic receptors in peripheral and central synapses, and influence nicotinic receptor associated ion-channels (*30*).

In addition to these side effects atropine, oxime, and diazepam don't protect against any of the long-term side effects of OP poisoning (*31, 32*). These include; anxiety, psychomotor depression, intellectual impairment, and sleep disturbances (*21*). A review of manufacturer workers accidentally exposed to high doses of sarin reported high incidence of self-described memory disturbances, difficulty maintaining alertness, and appropriate focusing of attention (*33*).

1.5 Bioscavengers

To protect against the short- and long-term affects of nerve agent poisoning researchers are currently developing bioscavengers (*34*). These are molecules that can be

administered prior to exposure and could sequester the nerve agent before AChE inhibition. Current bioscavenger targets include monoclonal antibodies, serum AChE, plasma BChE, serum PON1, organophosphorus hydrolase (OPH) and CEs (*16-18, 35-38*). As early as 1957 it was observed that excess pretreatment of rats with fluorophosphatase (DFPase), an enzyme homologous with PON1, greater than 80% of the animals survived, whereas all the control unprotected rats died (*39*). It has also been shown that prophylactic treatment with excess AChE not only protected mice against 8-10 LD_{50} of soman but also prevented long-term side effects compared to traditional oxime therapies (*40*).

Current bioscavengers are either stoichiometric or catalytic **(Table 1.3)** (*34*). Stoichiometic binders such as AChE, BChE, and CEs act as molecular sponges binding one nerve agent per active site (*22*). Recombinant BChE is aggressively being developed for this purpose, including the generation of transgenic goats that secrete BChE in their milk (*41, 42*). The benefits of BChE are that it binds nerve agents with nanomolar (nM) affinity, exhibits stereopreferences for the more toxic P_S nerve agent isomers, and has high circulation mean retention times (*43*). AChE and BChE are non-catalytic, exhibiting spontaneous rates of nerve agent hydrolysis less than 1×10^{-5} min^{-1}, therefore these stoichiometric scavengers would require large protein concentrations to afford effective protection. It has been calculated that a dose of 250 mg BChE/70 kg person would be sufficient to protect red blood cell AChE above 30% after one soman LD_{50} (*44*).

Multiple catalytic bioscavengers, such as PON1, DFPase, and OPH are being investigated as an alternative to stoichiometric scavengers. If an enzyme were capable of efficiently hydrolyzing nerve agents, much less protein would be required. These enzymes rapidly hydrolyze OP nerve agents *in vitro* with rates of hydrolysis as high as 840 min^{-1} (*37*).

Despite the enzymatic rates of hydrolysis, PON1, DPFase, and OPH suffer from high dissociation constants (mM range) and are ineffective *in vivo* (*36, 37*). Additionally, these enzymes selectively bind and hydrolyze the less toxic P_R nerve agent isomers (*45*). The catalytic mechanisms of PON1 and DFPase are poorly understood and numerous investigations are underway to elucidate the residues necessary for substrate binding and hydrolysis (*36, 46*). Recently, through rational structural design, investigators were able to shift the stereopreference of DFPase for cyclosarin (*45*).

Whether in military combat or targeted terrorist attacks, the threat for nerve agent poisoning has not diminished. These toxins potently target AChE in neuromuscular junctions and may result in death through suffocation. Current treatments for nerve agent poisoning are limited in that they might prevent death but provide no protection and don't reduce the debilitating long-term side effects. Novel bioscavenger therapies are currently being developed to sequester and detoxifying nerve agents prior to AChE inhibition. Despite the respective advantages of either the stoichiometric or catalytic enzymes, they both suffer from limitations that prevents their incorporation as a therapeutic. Additional work needs to be done on generating an efficient catalytic bioscavenger.

1.6 Figures and Tables

Figures and tables are listed in the same order they appear in the text of chapter 1.

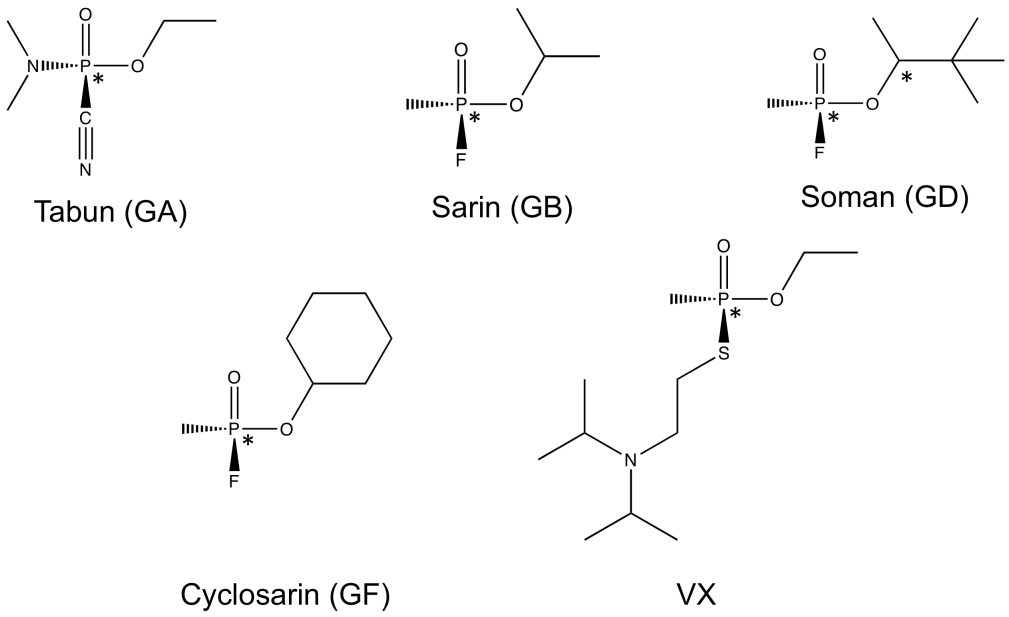

Figure 1.1 Chemical structures of OP nerve agents. Each nerve agent is given a common (e.g. tabun, sarin, etc.) and NATO name (e.g. GA, GB). Nerve agents exist as racemic mixtures around a chiral phosphate (*). Soman has an additional chiral center in the pinacolyl alkoxy group.

	Molecular Weight (g)	Melting Point (^oC)	Boiling Point (^oC)	Vapor Pressure (mmHg, 25^oC)	Volatility (mg/m^3, 25^oC)
Tabun	162.12	-50	240	0.07	610
Sarin	140.10	-57	147	2.90	22,000
Soman	182.20	-42	198	0.40	3,900
Cyclosarin	180.16	-30	239	0.07	581
VX	267.40	-51	298	0.007	10.50

Table 1.1 Physical properties of OP nerve agents. They all exhibit similar properties except for sarin and VX. Sarin has the lowest boiling point and is the most volatile. This agent is the most likely to be present as a "nerve gas". VX is the most persistent OP with low vapor pressure and volatility. CBWinfo.com

	LCt_{50} (mg•min/m^3)	LD_{50} (mg)
Tabun	135	4,000
Sarin	70	1,700
Soman	70	350
Cyclosarin	50	30
VX	30	10

Table 1.2 OP toxicological data. LCt_{50} is the lethal concentration at which a gas kills 50% of the exposed population. LD_{50} is the percutaneous dose that will kill half the exposed population. CBWinfo.com

	MW (kDa)	k_{react} (min^{-1})	K_m (M)	k_{react}/K_m ($min^{-1}M^{-1}$)
AChE[a]	56	$< 5 \times 10^{-5}$	6×10^{-7}	83
BChE[b]	65	$< 5 \times 10^{-5}$	4×10^{-7}	125
PON1[c]	43	669	6.2×10^{-4}	1×10^{6}
OPH[d]	35	300	5×10^{-4}	6×10^{5}

Table 1.3 Kinetic constants of current bioscavengers for soman. Acetylcholinesterase (AChE) and butyrylcholinesterase (BChE) are stoichiometric scavengers with nM binding constants (K_m) but slow rates of spontaneous hydrolysis (k_{react}). PON1 and OPH rapidly hydrolyze soman by poorly bind the substrate [a](*47*), [b](*48*), [c](*49*), [d](*50*).

REFERENCES

1. Salem, H., Ternay, A., and Smart, J. (2008) Brief History and Use of Chemical Warfare Agents in Warfare and Terrorism, in *Chemical Warfare Agents-Chemistry, Pharamcology, Toxicology, and Therapeutics* (Romano Jr., J. A., Lukey, B. J., and Salem, H., Eds.) 2nd Edition ed., CRC Press, Boca Raton.

2. Harris, R., and Paxman, J. (1982) *A Higher Form of Killing: The Secret Story of Chemical and Biological Warfare.*, Hill and Wang, New York.

3. SIPRI (1971) *The Rise of CB Weapons*, Humanities Press, New York.

4. Mirzayanov, V. (2009) *State Secrets: An insider's chronicle of the russian chemical weapons progam*, Outskirts Press, Denver.

5. Davidson, L., and J, B. (2001) Toxic Utah: A land littered with poison, in *Deseret News*, Salt Lake City.

6. Pringle, L. (1993) *Chemical and Biological Warfare*, Enslow Publishers, Inc., Hillside.

7. Newmark, J. (2007) Nerve agents, *Neurologist 13*, 20-32.

8. Trapp, R. (2006) Worldwide governmental efforts to locate and destroy chemical weapons and weapons materials: minimizing risk in transport and destruction, *Ann N Y Acad Sci 1076*, 527-539.

9. LeJeune, K. E., Dravis, B. C., Yang, F., Hetro, A. D., Doctor, B. P., and Russell, A. J. (1998) Fighting nerve agent chemical weapons with enzyme technology, *Ann N Y Acad Sci 864*, 153-170.

10. Biema, D. (1995) Prophet of poison, in *Time*, pp 27-33.

11. Ohbu, S., and Yamashina, A. (1997) Sarin poisoning on Tokyo subway, *Southern Medical Journal 90*, 587-693.

12. Okumura, T., Hisaoka, T., Yamada, A., Naito, T., Isonuma, H., Okumura, S., Miura, K., Sakurada, M., Maekawa, H., Ishimatsu, S., Takasu, N., and Suzuki, K. (2005) The Tokyo subway sarin attack--lessons learned, *Toxicol Appl Pharmacol 207*, 471-476.

13. FAS. (2010) Nerve Agents, in *Chemical Weapons Information*, Federation of American Scientists.

14. Kikilo, P., Fedoreno, V., and Ternay, A. (2008) Chemistry of Chemical Warfare Agents, in *Chemical Warfare Agents: Chemistry, Pharmacology, Toxicology, and Therapeutics* (Romano Jr., J. A., Lukey, B. J., and Salem, H., Eds.), pp 36-40, CRC Press, Boca Raton, FL.

15. Kovarik, Z., Radic, Z., Berman, H. A., and Taylor, P. (2006) Mutation of acetylcholinesterase to enhance oxime-assisted catalytic turnover of methylphosphonates, *Toxicology*.

16. Shafferman, A., Ordentlich, A., Barak, D., Stein, D., Ariel, N., and Velan, B. (1996) Aging of phosphylated human acetylcholinesterase: catalytic processes mediated by aromatic and polar residues of the active centre, *Biochem J 318 (Pt 3)*, 833-840.

17. Li, B., Nachon, F., Froment, M. T., Verdier, L., Debouzy, J. C., Brasme, B., Gillon, E., Schopfer, L. M., Lockridge, O., and Masson, P. (2008) Binding and hydrolysis of soman by human serum albumin, *Chem Res Toxicol 21*, 421-431.

18. Maxwell, D. M., and Brecht, K. M. (2001) Carboxylesterase: specificity and spontaneous reactivation of an endogenous scavenger for organophosphorus compounds, *J Appl Toxicol 21 Suppl 1*, S103-107.

19. Raveh, L., Grunwald, J., Marcus, D., Papier, Y., Cohen, E., and Ashani, Y. (1993) Human butyrylcholinesterase as a general prophylactic antidote for nerve agent toxicity. In vitro and in vivo quantitative characterization, *Biochem Pharmacol 45*, 2465-2474.

20. Germann, W., and Stanfield, C. (2005) *Principles of Human Physiology*, 2nd Edition ed., Pearson Education, San Franciso, CA.

21. McDonough, J. H., and Romano Jr., J. A. (2008) Health Effects of Low-Level Exposure to Nerve Agents, in *Chemical Warfare Agents: Chemistry, Pharmacology, Toxicology, and Therapeutics* (Romano Jr., J. A., Lukey, B. J., and Salem, H., Eds.), pp 71-76, CRC Press, Boca Raton, FL.

22. Saxena, A., Luo, C., Nageswararao, C., Maxwell, D. M., and Doctor, B. P. (2010) Novel Approaches to Medical Protection against Chemical Warfare Nerve Agents, in *Chemical Warfare Agents: Chemistry, Pharmacology, Toxicology, and Therapeutics* (Romano Jr., J. A., Lukey, B. J., and Salem, H., Eds.), pp 145-159, CRC Press, Boca Raton, FL.

23. Gray, A. P. (1984) Design and structure-activity relationships of antidotes to organophosphorus anticholinesterase agents, *Drug Metab Rev 15*, 557-589.

24. Musilek, K., Dolezal, M., Gunn-Moore, F., and Kuca, K. (2009) Design, evaluation and structure-Activity relationship studies of the AChE reactivators against organophosphorus pesticides, *Med Res Rev 21*, 21.

25. Wikipedia. (2010) Atropine.

26. Kuca, K., Jun, D., and Bajgar, J. (2007) Currently used cholinesterase reactivators against nerve agent intoxication: comparison of their effectivity in vitro, *Drug Chem Toxicol 30*, 31-40.

27. Jokanovic, M. (2009) Current understanding of the mechanisms involved in metabolic detoxification of warfare nerve agents, *Toxicol Lett 188*, 1-10.

28. Dunn, M. A., and Sidell, F. R. (1989) Progress in medical defense against nerve agents, *Jama 262*, 649-652.

29. Arendse, R., and Irusen, E. (2009) An atropine and glycopyrrolate combination reduces mortality in organophosphate poisoning, *Hum Exp Toxicol 28*, 715-720.

30. Bartosova, L., Kuca, K., Kunesova, G., and Jun, D. (2006) The acute toxicity of acetylcholinesterase reactivators in mice in relation to their structure, *Neurotox Res 9*, 291-296.

31. Maxwell, D. M., and Koplovitz, I. (1990) Effect of endogenous carboxylesterase on HI-6 protection against soman toxicity, *J Pharmacol Exp Ther 254*, 440-444.

32. Leadbeater, L., Inns, R. H., and Rylands, J. M. (1985) Treatment of poisoning by soman, *Fundam Appl Toxicol 5*, S225-231.

33. Metcalf, D. R., and Holmes, J. H. (1969) VII. Toxicology and physiology. EEG, psychological, and neurological alterations in humans with organophosphorus exposure, *Ann N Y Acad Sci 160*, 357-365.

34. Lenz, D. E., Yeung, D., Smith, J. R., Sweeney, R. E., Lumley, L. A., and Cerasoli, D. M. (2007) Stoichiometric and catalytic scavengers as protection against nerve agent toxicity: a mini review, *Toxicology 233*, 31-39.

35. Hemmert, A., Otto, M. F., Wierdl, M., Edwards, C. C., Fleming, C. D., MacDonald, M., Cashman, J. R., Potter, P. M., Cerasoli, D. M., and Redinbo, M. R. (2010) Human Carboxylesterase 1 Stereoselectively Binds the Nerve Agent Cyclosarin and Spontaneously Hydrolyzes the Nerve Agent Sarin, *Molecular Pharmacology IN PRESS*.

36. Otto, T. C., Harsch, C. K., Yeung, D. T., Magliery, T. J., Cerasoli, D. M., and Lenz, D. E. (2009) Dramatic differences in organophosphorus hydrolase activity between

human and chimeric recombinant mammalian paraoxonase-1 enzymes, *Biochemistry 48*, 10416-10422.

37. Reeves, T. E., Wales, M. E., Grimsley, J. K., Li, P., Cerasoli, D. M., and Wild, J. R. (2008) Balancing the stability and the catalytic specificities of OP hydrolases with enhanced V-agent activities, *Protein Eng Des Sel 21*, 405-412.

38. Saxena, A., Sun, W., Luo, C., Myers, T. M., Koplovitz, I., Lenz, D. E., and Doctor, B. P. (2006) Bioscavenger for protection from toxicity of organophosphorus compounds, *J Mol Neurosci 30*, 145-148.

39. Cohen, J. A., and Warringa, M. G. (1957) Purification and properties of dialkylfluorophosphatase, *Biochim Biophys Acta 26*, 29-39.

40. Maxwell, D. M. (1992) The specificity of carboxylesterase protection against the toxicity of organophosphorus compounds, *Toxicol Appl Pharmacol 114*, 306-312.

41. Huang, Y. J., Lundy, P. M., Lazaris, A., Huang, Y., Baldassarre, H., Wang, B., Turcotte, C., Cote, M., Bellemare, A., Bilodeau, A. S., Brouillard, S., Touati, M., Herskovits, P., Begin, I., Neveu, N., Brochu, E., Pierson, J., Hockley, D. K., Cerasoli, D. M., Lenz, D. E., Wilgus, H., Karatzas, C. N., and Langermann, S. (2008) Substantially improved pharmacokinetics of recombinant human butyrylcholinesterase by fusion to human serum albumin, *BMC Biotechnol 8*, 50.

42. Huang, Y. J., Huang, Y., Baldassarre, H., Wang, B., Lazaris, A., Leduc, M., Bilodeau, A. S., Bellemare, A., Cote, M., Herskovits, P., Touati, M., Turcotte, C., Valeanu, L., Lemee, N., Wilgus, H., Begin, I., Bhatia, B., Rao, K., Neveu, N., Brochu, E., Pierson, J., Hockley, D. K., Cerasoli, D. M., Lenz, D. E., Karatzas, C. N., and Langermann, S. (2007) Recombinant human butyrylcholinesterase from milk of transgenic animals to protect against organophosphate poisoning, *Proc Natl Acad Sci U S A 104*, 13603-13608.

43. Raveh, L., Grauer, E., Grunwald, J., Cohen, E., and Ashani, Y. (1997) The stoichiometry of protection against soman and VX toxicity in monkeys pretreated with human butyrylcholinesterase, *Toxicol Appl Pharmacol 145*, 43-53.

44. Ashani, Y., and Pistinner, S. (2004) Estimation of the upper limit of human butyrylcholinesterase dose required for protection against organophosphates toxicity: a mathematically based toxicokinetic model, *Toxicol Sci 77*, 358-367.

45. Melzer, M., Chen, J. C., Heidenreich, A., Gab, J., Koller, M., Kehe, K., and Blum, M. M. (2009) Reversed enantioselectivity of diisopropyl fluorophosphatase against organophosphorus nerve agents by rational design, *J Am Chem Soc 131*, 17226-17232.

46. Hu, X., Jiang, X., Lenz, D. E., Cerasoli, D. M., and Wallqvist, A. (2009) In silico analyses of substrate interactions with human serum paraoxonase 1, *Proteins 75*, 486-498.

47. Forsberg, A., and Puu, G. (1984) Kinetics for the inhibition of acetylcholinesterase from the electric eel by some organophosphates and carbamates, *Eur J Biochem 140*, 153-156.

48. Millard, C. B., Lockridge, O., and Broomfield, C. A. (1998) Organophosphorus acid anhydride hydrolase activity in human butyrylcholinesterase: synergy results in a somanase, *Biochemistry 37*, 237-247.

49. Yeung, D. T., Smith, J. R., Sweeney, R. E., Lenz, D. E., and Cerasoli, D. M. (2007) Direct detection of stereospecific soman hydrolysis by wild-type human serum paraoxonase, *Febs J 274*, 1183-1191.

50. Di Sioudi, B. D., Miller, C. E., Lai, K., Grimsley, J. K., and Wild, J. R. (1999) Rational design of organophosphorus hydrolase for altered substrate specificities, *Chem Biol Interact 119-120*, 211-223.

Chapter 2. Human Carboxylesterase 1 and Organophosphorus Nerve Agents

2.1 Carboxylesterases and OP nerve agents

As previously mentioned OP nerve agents target hydrolase enzymes, covalently modifying the catalytic machinery within the enzyme's active site. AChE is the lethal target of OP inhibition, but other enzymes affected by nerve agent poisoning include BChE, HSA, PON1, and CEs (*1-4*). Because of the deficiencies with current antidotal therapies, researchers are investigating the use of prophylactic enzymes to circulate in the blood stream and scavenge nerve agents before AChE is inhibited (*5*). Examples of these bioscavengers can be observed in nature. Rats and mice contain high levels of circulating serum CEs, that affords them exception protection against OP nerve agents (*2*). Indeed, based on their serum CE levels, mice are naturally protected against up to 16 LD_{50}s of soman compared to mammals that don't express a serum CE, such as rabbits or guinea pigs (*6*). In addition, these murine CEs exhibit 100-faster rates of spontaneous reactivation (k_{react}~1 x 10^{-3} min^{-1}) for nerve agents than AChE and BChE and don't undergo the dead-end aging process that plagues these cholinesterases (*2, 7*). Humans don't express a serum carboxylesterase (*8*), but based on the benefits of the rat and mouse serum CEs, the enzyme human carboxylesterase 1 (hCE1) might be an effective bioscavenger.

2.2 Human Carboxylesterase 1 (hCE1)

hCE1 is the most highly expressed carboxylesterase in the human body (*9*). This 62-kDa enzyme is a member of the α/β serine hydrolase superfamily, and shares 33% and 34% homology to AChE and BChE, respectively (*10*). It is primarily found in the liver, but is also expressed in the lung, intestine, kidneys, testes, heart, monocytes, and macrophages (*11*). Within hepatocytes, hCE1 is localized and retained in the endoplasmic reticulum a KDEL like retention motif (HVEL) (*12*). Physiologically, hCE1 helps to regulate cholesterol by hydrolyzing cholesterol esters into free cholesterol prior to incorporation into extracellular high density lipoprotein (HDL) (*9*). This enzyme, also know as egasyn, and has been implicated in regulating C-reactive protein and β-glucoronidase release from the liver (*13*). Lastly, hCE1 is critical member of the Phase I drug metabolism pathway to hydrolyze compounds containing ester, thioester, and amide containing xenobiotics (*9*).

The first atomic crystal structure of hCE1 was solved in 2003 in complex with analogs of heroine and cocaine, two substrates processed by this enzyme (*14*). hCE1 shows an α/β hydrolase fold composed of three domains; catalytic, αβ, and regulatory **(Figure 2.1)**. A large active site cavity is formed at the interface of these domains and contains the catalytic residues serine 221 (S221), histidine 468 (H468), and glutamine 354 (E354). This pocket is divided into two regions around S221: a large, flexible hydrophobic pocket, and a smaller, rigid, charged pocket. With the assistance of an oxyanion hole, formed by three glycine residues (G141, G142, and G143), hCE1 utilizes the catalytic triad in a ping-pong mechanism to hydrolyze a variety of substrates (*11*). Additional crystal structures of hCE1 solved in complex with the Alzheimer's drug tacrine, the cholesterol lowering drug

mevastatin, and the breast cancer drug tamoxifen, illustrate the promiscuous nature of this enzyme (*15, 16*).

2.3 hCE1 and OP Nerve Agents

By definition hCE1 is a B-esterase because it is inhibited by OP nerve agents (*17*). Other B-esterases include AChE and BChE, while PON1 is an A-esterase (*17*). Like AChE and BChE, OP nerve agents are hemisubstrates of hCE1, forming a covalent acyl-enzyme intermediate **(Scheme 2.1)**. In 2007 two atomic resolution crystal structures were solved of hCE1 in complex with the OP nerve agents soman and tabun (*18*). In the hCE1-soman complex a non-aged, P_R, acyl-enzyme intermediate adduct was observed, the first time this soman-adduct form had been seen. In AChE and BChE soman ages rapidly and up to this point all other esterase-soman crystal structure were in the aged state (*19, 20*). The soman alkoxy group was positioned in the larger, flexible binding pocket and the P_R stereochemistry adduct suggests that hCE1 had preferentially reacted with the less toxic P_R soman isomer. Even though a stereo-inversion occurs upon collapse of the first transition state, a change in priority ranking around the phosphate after leaving group dissocation, causes the same stereochemistry to be retained within the OP adduct (*21*). In the hCE1-tabun structure a non-aged P_S isomer was observed, again implying stereopreference for the P_S substrate.

These crystal structures provided initial information about the interactions of hCE1 and nerve agents, but they also raised a number of questions. In both crystal structures hCE1 had reacted with the less-toxic OP enantiomer. Was this also the case with sarin, cyclosarin, and VX? Does hCE1 exhibit an absolute steropreference for P_R or P_S enantiomers? Why wasn't an aged soman adduct observed in hCE1? Is hCE1 resistant to aging? Lastly, can this

human CE, like the murine CEs, spontaneous reactivate any OP nerve agents? To effectively gauge the ability of hCE1 to act as a bioscavenger and answer these questions, additional structural and biochemical experiments were necessary.

2.4 Expression and Purification of hCE1

Before structural and biochemical studies could be pursued recombinantely expressed protein is required. Purified hCE1 was produced through baculovirus mediated insect cell expression (*14, 16, 18, 22*). This enzyme requires specific post-translational glycosylations that are either not made, or overly produced by more traditional expression systems such as *Escherichia Coli* (*E.Coli*) or *Saccharomyces Cerevisiae* (*23*). hCE1 (GenBank accession NC_000016) was inserted into a pFastbac1 (Invitrogen) plasmid through ligation of a PCR amplification gene with sense and anti-sense primers containing *EcoR1* and *Pst1* restriction site, respectively. The C-terminal ER retention sequence was removed during the PCR cloning process to enable protein secretion (*23*). Following ligation, plasmids were transformed into DH10Bac *E.Coli*, where with help of the pMON7124 helper plasmid, the gene-encoding region is transposed via a mini-Tn7 element into the mini-*att*Tn7 attachment site on the bacmid. Utilizing the aid of antibiotic resistance and colorimetric *LacZ*$^{-}$ selection, recombinant bacmid DNA was isolated prior to insect cell infection. SF21 insect cells were transfected with hCE1-containing bacmid via lipofectamin DNA delivery. Three generations of viral titers were prepared from transfected cells in serum free media. Each generation was selected for maximal protein expression through limited dilutions and hCE1 activity assays. Finally, secreted protein was collected 72 hours after from SF21 cells were infected with 3rd generation titer. Protein expression is controlled by the multiple nuclear polyhedrosis virus

polyhedrin promoter and is maximally produced 30-72 hours post infection. hCE1 was then purified through dialysis, isoelectric focusing, and size exclusion chromatography.

For smaller scale biochemical experiments hCE1 was produced by transfecting COS-7 cells with a pCI-neo mammalian vector containing hCE1 (*24, 25*). Wild type and mutant forms of hCE1 were ligated into pCI-neo using T4 DNA Ligase and custom sense and anti-sense PCR primers containing *EcoR1* and *Sma1* restriction sites, respectively. Prior to COS-7 transfection, plasmids were isolated through an endo-toxin free maxiprep kit (Qiagen) and sequence verified (UNC genome sequencing facility). Using a Bio-Rad electroporator and a capacitance extender, COS-7 cells were electroporated with 20 μg of hCE1 pCI-neo plasmid in 200 μL PBS buffer (*26*). After transfection, cells were plated on 75-cm2 flasks in fresh media, harvested by trypsinization after 48 hours, and frozen in liquid nitrogen.

2.5 Additional hCE1-OP Crystal Structures

To determine crystal structures of hCE1 in complex with the sarin, cyclosarin, and VX, purified protein was sent to the United States Army Medical Research Institute of Chemical Defense (USAMRICD) where it was exposed to ~1000-fold molar excess of racemic respective OP agents. After 1 hour of OP exposure, excess unbound agent was removed by passing the protein sample over P-10 Sephadex G-25 spin columns (GE Healthcare). These DNA desalting columns have been shown to efficiently remove OP nerve agents (*18, 22*). By measuring production of nitrophenol at 410 nm, the column eluate was tested to confirm that hCE1 activity had been inhibited. Uninhibited hCE1 efficiently hydrolyzes *para*-nitrophenyl butyrate (pNPB, Sigma) to form nitrophenol. To ensure that all excess agent had been removed, the ability of column flow-through to further inhibit BChE

was also measured. Based on these two experiments we determined that hCE1 was not inhibited by VX. Excess VX had been removed from the sample, and yet full enzyme activity remained. Sarin and cyclosarin exposed samples were completely inhibited. The thioester leaving group in VX is charged at physiological pH, poorly inhibiting hCE1. This inability to interact with charged substrates is also observed in the murine serum CEs (*7*), making VX a potent cholinesterase inhibitor. No further structural studies of VX were pursued.

Sarin and cyclosarin inhibited samples were concentrated to 3 mg/ml, and set up for protein crystallization using the sitting drop vapor diffusion method. Plate like crystals (600 μM x 100 μM x 50 μM) of hCE1-cyclosarin were grown after 8 weeks in 10% PEG 3350, 0.3 M Li_2SO_4, 0.1 M Citrate pH 5.5, 0.1 M NaCl, 0.1 M LiCl, and 5% glycerol. Despite multiple attempts and varying conditions, hCE1-sarin samples never crystallized. The basis for these crystals not forming will be discussed later.

Prior to cooling to 100K for X-ray beam exposure and data collection, hCE1-cyclosarin crystals were serially cryoprotected into a 30% sucrose plus mother liquor solution. X-ray diffraction data were collected at the Argonne National Laboratory (Argonne, IL) on beamline 22-ID (SER-CAT). Data were indexed and scaled using the XDS package (*27*). Molecular replacement was conducted using MolRep in the CCP4i Suite (*28*) (v. 6.1.0) with one trimer of the hCE1-tacrine structure (RSCB PDB accession code 1MX1 (*15*)) as the search model. The hCE1-cyclosarin model was refined using rigid body, simulated annealing, and group *B*-factor refinements in CNS (*29*) that included an overall anisotropic *B*-factor, bulk solvent correction, and non-crystallographic symmetry (NCS) restraints for regions outside the active site. Prior to any structural refinements, a subset

(7%) of the data were set aside for cross-validation by R_{free} calculation. Manual building was conducted in Coot (*30*) with σ_a-weighted composite omit, difference density, and simulated annealing omit maps. Data collection and refinement statistics were summarized and are presented in **Table 2.1**. The final structure was validated using PROCHECK (*31*), and all figures were generated in PyMol (DeLano Scientific, Palo Alto, CA). Coordinates and structure factors have been deposited at the PDB with accession code 3K9B.

2.6 Crystal Structure of the hCE1-Cyclosarin Complex.

The crystal structure of hCE1 in a covalent acyl-enzyme intermediate complex with the OP nerve agent cyclosarin was determined by molecular replacement and refined to 3.1 Å resolution (**Table 2.1**). The hCE1-cyclosarin structure was similar to ligand complexes of this enzyme described previously, with a root-mean-square deviation (r.m.s.d.) of 0.48 Å over 1,354 equivalent Cα positions when compared to the hCE1-tacrine structure (*15*). The initial maps were of good quality for the majority of the polypeptide, with the exception of the acyl-loop (residues 304-318) that caps the active site and five short loops (340-342, 369-374, 406-410, 450-454, 483-488) between secondary structural elements. When positioned provisionally, these disordered regions displayed *B*-factors of >90 $Å^2$; in contrast, the average *B*-factor of the ordered regions of the final model was 54 $Å^2$. Two of these regions (369-374, 450-454) were also disordered in the structure of a rabbit liver CE, which shares 81 % sequence identity and 0.42 Å r.m.s.d. over 401 equivalent Cα positions relative to hCE1 (*32*). The model of hCE1 complexed with cyclosarin was refined to final *R* factors of 26.6% (R_{cryst}) and 29.9% (R_{free}) **(Table 2.1)**.

Each hCE1 monomer, supported by two disulfide links (Cys87-Cys116, Cys274-Cys285), contained two ligand binding sites within three domains **(**see **Figure 2.1)**(*32*). The hCE1-trimer was formed through C3 symmetry around respective α/β domains and buries 475 $Å^2$ of solvent-accessible surface area per protein monomer. The primary ligand binding site, the active site, was located at the interface of the three domains in each monomer as previously discussed. The second ligand-binding site (or Z-site) was on the enzyme's surface at the interface between the regulatory and catalytic domains. Previous crystal structures of hCE1 in complex with OP nerve agents soman and tabun contained sucrose, the cryoprotectant, in the Z-site (*18*). Ser 369, which forms a hydrogen bond with the O1 of sucrose in these other structures, was disordered in the hCE1-cyclosarin structure and no ligand molecule was observed in this site. The catalytic domain also contained a high-mannose glycosylation site at Asn79. Density was observed near Asn79 but neither *N*-acetylglucosamine nor terminal sialic acid could be reliably built and refined into this region.

As outlined in **Scheme 2.1** cyclosarin inhibits hCE1 by forming a covalent adduct with the catalytic serine. In the structure of the hCE1-cyclosarin complex, a covalent cyclosarin adduct was easily identified in initial difference density ($F_0 - F_c$) maps as a 6 σ electron density peak approximately 1.6 Å away from the S221 Oγ, which corresponded to the nerve agent phosphate. At lower σ levels (2.5-4 σ), additional density for the complete molecule was apparent. The cyclosarin model was built into the observed density, refined, and P_R stereochemistry was assigned around the chiral phosphate **(Figure 2.2)**. The acyl-enzyme adduct was stabilized by two hydrogen bonds. These occur between the cyclosarin phosphoryl oxygen atom and hydrogen atoms present on the amide nitrogens of the oxyanion hole (2.6 Å and 2.4 Å, respectively). The *O*-cyclohexyl alkoxy group is located within in the

larger, flexible pocket of the active site and is stabilized by interactions with Leu363 of the regulatory domain. The stereochemistry and alkoxy placement was confirmed with a 3.1 Å resolution simulated annealing omit map, contoured to 5 σ **(Figure 2.3)**. The opposite P_S isomer was also built into the starting model and one round of refinement was performed. Clear positive and negative density from a difference density map ($|F_0 - F_c|, \phi_{calc}$) verified the P_R assignment as consistent with the biochemical results **(Figure 2.4)**.

This is the first crystal structure of any protein covalently bound to cyclosarin and as with the previous hCE1 OP crystal structures, the hCE1-cyclosarin structure is in a non-aged state and bound to the less-toxic P_R isomer. This bulky cyclohexyl group is positioned towards the large, flexible pocket in the active site. The smaller, rigid pocket cannot accommodate this large alkoxy group, a requirement for P_S binding. To confirm the observed OP stereoprefence and understand the binding affinity of hCE1 for P_R and P_S nerve agent isomers, the bimolecular rates of inhibition for nerve agents with hCE1 were determined.

2.7 Bimolecular Rates of Inhibition for OPs in hCE1

Sarin, soman, and cyclosarin contain a chiral phosphorus atom and exist as racemic mixtures of P_R and P_S stereoisomers. Soman also has an asymmetric carbon (Cα) in the pinacolyl group. The P_S isomers of sarin, soman and cyclosarin inhibit AChE more potently than the P_R forms; for example, the preference of P_S vs. P_R soman is 5,000-fold for AChE (*33*). Using OP nerve agent analogs containing a thiomethyl-leaving group prepared as purified stereoisomers (**Figure 2.5**), we determined the stereoselectivity of hCE1 inhibition by analogs of sarin, soman, and cyclosarin **(Figure 2.6)**. These analogs have been shown by

MALDI-TOF mass spectrometry to yield, among other products, acyl-enzyme adducts identical to those from authentic agents when used to inhibit BChE (*34*). The thiomethyl-leaving group that replaces the fluoride atom decreases the toxicity of the analogs by slowing the rate of phosphonylation (k_2) compared to *bona fide* agents; however, the dissociation constants (K_d) remain similar (*35*). The decrease in k_2 results in a reduction in the bimolecular rate of inhibition (k_i) by 2-3 orders of magnitude when compared to the corresponding nerve agent (*6*).

Samples of purified hCE1 at 100 nM were inhibited at room temperature with increasing concentrations of stereogenic OP nerve agent analogs. Aliquots of enzyme incubated with stereoisomer analogs of sarin (P_R, P_S), P_S soman, and P_S cyclosarin were removed at various time points (up to 1 hr) and the level of active enzyme that remained was determined by comparing pNPB hydrolysis relative to an uninhibited sample. Because the P_R soman and P_R cyclosarin analogs react more quickly with hCE1, the impacts these analogs had on hCE1 were measured continuously (for up to 15 min) by adding increasing concentrations of analog to enzyme samples containing pNPB and measuring loss of functional activity over time. These data, collected at 410 nm and 25 ^{o}C on a Pherastar microplate reader (BMG Labtech), were corrected for spontaneous pNPB hydrolysis and fit to equation 1 (*36*):

$$\frac{\Delta t}{\Delta \ln v} = \frac{K_d}{k_2} * \frac{1}{[IX](1-\alpha)} + \frac{1}{k_2} \qquad \textbf{(1)}$$

where K_d was the dissociation constant, k_2 the unimolecular phosphorylation rate constant, v the remaining percent enzyme activity, [IX] was the OP analog concentration, α was $[S]/(K_M + [S])$, in which $[S]$ was the substrate concentration and K_M was the Michaelis-

Menton constant. All experiments were performed in triplicate. Data were analyzed in KaleidaGraph 4 (Synergy Software, Reading, PA) to determine k_i ($k_i = k_2 / K_d$) values.

P_R analogs of soman and cyclosarin inhibited hCE1 1,700- and 2,900-fold more efficiently than the P_S isomers, respectively. In contrast, hCE1 exhibited a 5-fold preference for the P_S vs. P_R form of the sarin analogs. This strong hCE1 preference for the P_R isomers of cyclosarin and soman analogs is opposite to the stereopreference observed for AChE with *bona fide* nerve agents. A structural comparison of the hCE1-soman and hCE1-cyclosarin crystal structures with AChE-soman (RSCB PDB code 2WGO (*33*)) reveals that the bulky P_R *O*-alkoxy group is positioned into the larger hydrophobic binding pocket of hCE1. In contrast, this region is occupied in AChE by a long acyl loop that dips into the active site pocket and precludes binding of P_R nerve agents (*18, 33*). Therefore, the geometry of the hCE1 active site size dictates the enantiomeric binding of the bulkier nerve agents soman and cyclosarin.

With the smaller nerve agent sarin, hCE1 demonstrated only a 5-fold preference for the P_S isomer of the sarin nerve agent analog. Our structures indicate that while both isomers of sarin will fit in the active site of the enzyme, only P_S sarin is capable of forming stabilizing hydrophobic contacts with Phe101 and Leu97; P_R sarin would not form analogous interactions **(Figure 2.7)**. These structural considerations, in part, explain the observed strong preference for P_R soman and cyclosarin, and the relatively weak preference for P_S sarin exhibited by hCE1. Taken together, these results demonstrate that hCE1 exhibits a strong preference for the P_R soman and cyclosarin analogs, and a smaller preference for the P_S isomer of the smaller, sarin analog.

2.8 Spontaneous Nerve Agent Reactivation in hCE1

After the formation of the acyl-enzyme intermediate, proteins exposed to OP nerve agents may remain stably adducted, permanently inhibited (aged), or undergo spontaneous hydrolysis (hereafter referred to as reactivation) reversing the phosphonylation and returning the enzyme to normal function (*37, 38*) **(Scheme 2.2)**. To test the ability of hCE1 to reactivate after inhibition by nerve agents, the enzyme was challenged with racemic mixtures of the OP nerve agents soman, sarin, and cyclosarin. Fifty μL of COS cell lysate expressing a non-secreted form of hCE1, prepared as previously described (*24*), was inhibited with a ~1000- fold molar excess of racemic OP agents sarin, soman, or cyclosarin for 10 min. Excess agent was removed by passing inhibited samples over a PD-10 Sephadex G-25 size exclusion column (GE Healthcare). The column eluate was diluted 10-fold in 0.1 M potassium phosphate buffer, pH 7.4 and tested for the presence or absence of CE activity and complete removal of excess agent, as previously described. Aliquots were removed over time (up to 80 hrs) and the percent enzyme activity was measured by pNPB hydrolysis relative to an uninhibited sample. The rate of reactivation (k_{obs}) and maximal percent recovery (A_{max}) were determined by fitting the data to equation 2:

$$A = A_0 + A_{max}(1 - e^{-k_{obs}t}) \qquad \textbf{(2)}$$

where A was percent activity at time, t, and A_0 was initial activity at t=0. The experiments were conducted in triplicate and data were analyzed with Sigma Plot v.8.02 (Systat, Chicago, IL).

We found that only samples inhibited with sarin exhibited spontaneous reactivation **(Figure 2.8)**, with a half time of 45 hours (k_{obs}=2.58 ± 0.06 x 10^{-4} min^{-1}). When carried out to 300 hours, a maximum activity of 84 ± 6% was recovered **(Figure 2.9)**. The rate of

reactivation was approximately 10-fold slower than that measured for rat serum CE (*2*), but 10-fold faster than BChE (*39*). In contrast, AChE exhibits no reactivation following sarin inhibition (*39*). hCE1 inhibited with soman and cyclosarin, however, exhibited poor reactivation and achieved a maximum recovery of activity of only ~10% even after 300 hours. These data establish that reactivation of hCE1 only occurs following exposure to sarin, and explain why no hCE1-sarin crystals formed. hCE1 requires a substrate in the active site for crystal formation and by the time samples were returned to UNC-CH for crystallization most of the sarin had already been hydrolyzed.

2.9 Oxime Assisted Reactivation in hCE1

An alternative mechanism for nerve agent reactivation is through oxime assistance. Strong oxime nucleophiles like 2-PAM and obidoxime are known to reactivate OP-inhibited esterases, particularly AChE, by promoting the dephosphonylation of the active site serine. These cationic oximes are currently used as part of post-exposure therapy and are appropriate for the anionic choline binding gorge in cholinesterases (*40*). Carboxylesterases such as hCE1 react poorly with charged substrates (*7*); however, the ability of a neutral oxime like diacetyl monoxime (DAM) to reactivate inhibited hCE1 had not been reported in the literature. Thus, we tested whether DAM would reactivate hCE1 that had been exposed to racemic nerve agents or stereogenic nerve agent analogs. The combination of oximes and stoichiometric bioscavengers had been utilized to make a pseudo-catalytic bioscavenger (*3*).

Fifty μL of COS cell lysate containing hCE1 were inhibited and excess agent was removed as previously described. The OP analogs were utilized in a similar fashion to racemic nerve agents, but required a longer incubation time (up to 1 hr). Upon column

elution, samples were diluted 10-fold into 1 mM DAM (Sigma), which had been previously prepared in 0.1 M potassium phosphate pH 7.4 and kept on ice. DAM had no inhibitory effect on hCE1 at this concentration. Aliquots were removed over time and enzyme activity was measured as described above. The rates of reactivation (k_{obs}) and maximal percent reactivation (A_{max}) were determined for each agent/analog by subtracting background oxime-induced pNPB hydrolysis and fitting the data to equation 2.

We found that DAM enhanced the reactivation of sarin-inhibited hCE1, but not enzyme inhibited by soman or cyclosarin **(Figure 2.10 A)**. In the presence of DAM, sarin-inhibited hCE1 exhibited a half time of reactivation of 41 minutes (k_{obs}=0.0168 ± 0.0003 min^{-1} mM^{-1}), approximately 66-fold faster than that observed without the oxime (see **Figure 2.8**). In addition, similar to spontaneous reactivation, the maximal recovery of hCE1 that was observed in the presence of DAM was 89 ± 4%. Thus, the neutral oxime DAM increased the rate of reactivation of sarin-inhibited hCE1 by more than 65-fold.

We next examined the ability of DAM to enhance the reactivation of hCE1 inhibited with pure enantiomeric P_R or P_S isoforms of the nerve agent analogs (see **Figure 2.5**). We found that hCE1 inhibited with the P_S sarin analog exhibited reactivation with a half-time of 30 minutes (k_{obs}=0.023 ± 0.004 min^{-1} mM^{-1}), while hCE1 inhibited by the P_R sarin analog exhibited no detectable reactivation (**Figure 2.10 B**). In contrast, hCE1 samples inhibited with P_S soman and cyclosarin analogs were capable of marginal reactivation, while respective P_R analogs displayed no recovery **(Figures 2.10 C and 2.10 D)**. Taken together, these data suggest that the reactivation of hCE1 in the presence of the sarin analog was due to the hydrolysis of the P_S isomer, while the P_R isomer cannot be removed from the active site even in the presence of DAM.

2.10 Aging in OP-inhibited hCE1

The alternative end result to reactivation after acyl-enzyme intermediate formation is aging (see **Scheme 2.2**). Aging in serine hydrolases involves the time-dependent dealkylation of the bound adduct, resulting in a permanently phosphorylated catalytic serine residue (*37*). This process is rapid for soman in the active site of AChE ($t_{1/2}$ of ~2 minutes), and is the primary cause of the toxicity of this agent (*33*). Once aging has occurred, nerve agent adducts are inert even to strong oximes. We explored the propensity of hCE1 to age in the presence of nerve agent analog P_S stereoisomers by measuring the loss in the maximal level of DAM-mediated reactivation *(*A_{max}) over time.

Samples of 1 μM purified hCE1 were inhibited with a 1,000-fold molar excess of the P_S sarin, soman, and cyclosarin analogs for 60 minutes at room temperature. Complete inhibition was verified by the absence of pNPB hydrolysis. Excess unbound agent was removed by size exclusion chromatography as previously described, and aliquots were diluted 1:10 into 1 mM DAM every 12 hours for 48 hours. After dilution into DAM, each sample was incubated for 24 hours to achieve maximal DAM-assisted reactivation, and then enzyme activity was measured and percent reactivation was determined relative to an uninhibited sample. Maximum percent reactivation (A_{max}) was plotted against the incubation time in the absence of DAM and fit to **equation 3** (*41*):

$$A_{max} = A_{max0} \exp^{-k_a t} \qquad \textbf{(3)}$$

where A_{max0} was the maximum recovery at time=0, and k_a was the rate of aging.

If the nerve agent analog adduct undergoes time-dependent dealkylation, one would expect an exponential decay for A_{max} (*41*). Over 48 hours, no change in A_{max} was observed

for any of the agent analogs **(Figure 2.11)**. For example, after two hours exposure of hCE1 to the P_S sarin analog, DAM was capable of reactivating ~60% of the enzyme activity (see **Figure 2.10 B**); however, even after 46 additional hours of incubation with this sarin analog, the same fraction of enzyme activity, recovered by DAM, was observed **(Figure 2.11)**. Thus, sarin-inhibited hCE1 does not appear to undergo the same first-order aging process that has been observed with AChE and BChE. hCE1 and rat serum CE do not contain three specific residues essential for aging in the cholinesterases, thereby limiting the potential for this dead-end process (*2*).

2.11 Mechanism for Sarin Reactivation in hCE1

These data clearly show that hCE1 is able to reactivate, either spontaneously or oxime-assisted, following sarin inhibition. Additionally, it is clear that only the P_S isomer is being hydrolyzed to reactivate the enzyme. Finally, this isomer does not undergo that dead-end aging process observed in AChE and BChE. Using these data and prior literature we generated a model to explain how hCE1 might preferentially reactivate P_S sarin (**Figure 2.12**). Early work investigating the influence of pH on spontaneous reactivation in AChE identified the importance of two ionizable residues with pKa values of 6.9 and 9.8, suggesting possible His and Tyr residues, respectively (*42*). In the hCE1 active site, the catalytic His468 neighbors P_S sarin and Tyr152 is located approximately 8 Å away. These two residues are connected via a hydrogen-bonding network through Glu200 (**Figure 2.12**). It has been observed in the structure of the AChE covalent complex with non-aged P_S VX that the protonated Nε2 of His440 (H468 in hCE1) rotates away from Ser200 (Ser221 in hCE1) to form a hydrogen-bond with Glu199 (Glu220 in hCE1) (*20*). The Nε2 movement

would be expected to be blocked in hCE1 by larger alkoxy groups, such as the *O*-pinacolyl group in soman, and is not observed in a non-aged AChE soman structure (*33*). If this shift occurs in hCE1 with P_S sarin, however, the His468 Nε2 rotation to Glu220 would reorient the remaining His468 nitrogen, Nδ1, formerly hydrogen-bonded to Glu354. It would then be positioned to interact with the P_S sarin O2 atom and may act as a general base for hydrolytic dephosphonylation (**Figure 2.12**). An analogous orientation of the O2 atom of P_R sarin would not be possible while still maintaining interactions with the oxyanion hole (see **Figure 2.7**). By this model, hCE1 will only reactivate after inhibition with P_S sarin, consistent with the experimental results presented above. However, the rate of reactivation is observed to be poor, likely due to the weak nucleophilicity of Tyr152 at pH 7.4.

Finally we considered what the fate of the P_R-hCE1 adducts are if they do not age, and the state of the remaining percent of P_S-hCE1 adducts that do not undergo reactivation. For complexes of P_R organophosphates and hCE1, we propose that they remain at the acyl-enzyme intermediate stage of the enzyme's reaction mechanism. This state has been observed in the hCE1-P_R soman and hCE1-P_R cyclosarin crystal structures, and via MALDI-TOF analysis of BChE inhibited by P_R analogs of sarin, soman, and cyclosarin (*34*). For the 40% of P_S-sarin analog complexes with hCE1 that do not undergo reactivation, we propose that an alternate S221 state is created. In addition to forming adducts identical to authentic agents, the thiomethyl-nerve agent analogs utilized in this study have been shown to undergo a unique reaction, where the *O*-alkoxy rather than the thiomethyl group is displaced upon collapse of the original pentahedral intermediate (*34*). Therefore, dehydroalanine formation at the catalytic serine might also occur with these nerve agent analogs. Mass spectrometry studies were attempted to confirm or deny the presence of this adduct in hCE1;

unfortunately, the peptide fragment containing S221 could not be isolated and no useful data were obtained (personal communication with Dr. Oksana Lockridge).

2.12 Summary of hCE1 and Nerve Agents

These studies establish the stereopreference of wild type hCE1 for nerve agent analogs of cyclosarin, soman and sarin, and confirm this preference for cyclosarin with crystallographic data. Unfortunately, wild type hCE1 exhibits opposite stereoprefence to AChE for soman and cyclosarin. These data reveal that the native form of hCE1 is capable of reactivation after incubation with the nerve agent sarin, and that the rate of reactivation is enhanced with the neutral oxime DAM. Lastly, hCE1 does not undergo the dead-end aging process observed with the cholinesterases. The ability to spontaneously reactivate the more toxic form of sarin and not age in the process qualifies hCE1 as a stronger bioscavenger candidate against this agent than the other stoichiometric scavengers. These data are published in molecular pharmacology (*22*). In Chapter 3, I will present how we used these data to design mutant forms of hCE1 with enhanced rates of nerve agent hydrolysis for not only sarin, but also soman and cyclosarin.

2.13 Figures and Tables

Figures and tables are listed in the same order they appear in the text of chapter 2.

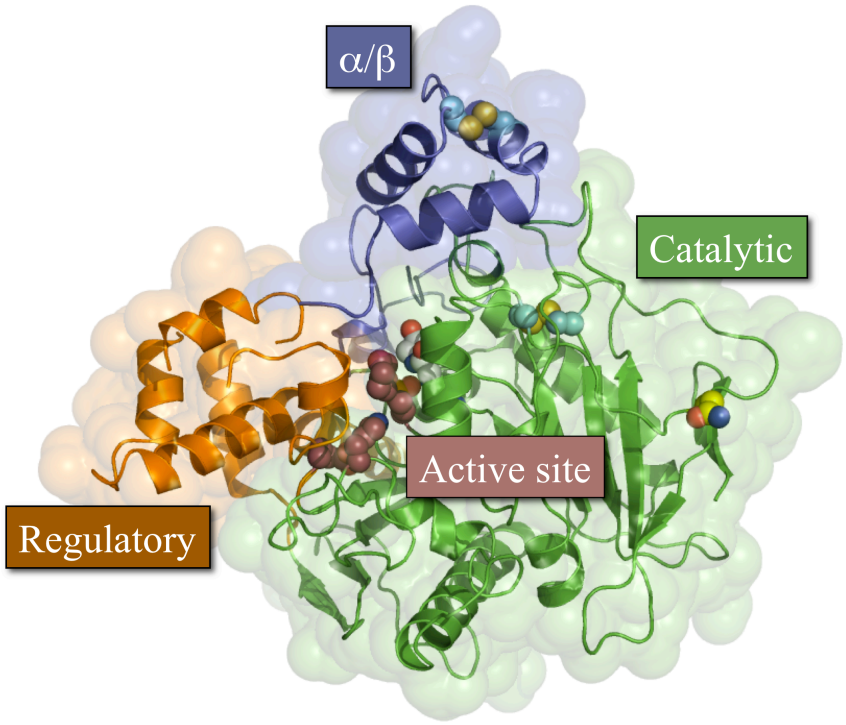

Figure 2.1 hCE1 monomer. Each protein monomer has three domains; the α/β domain (blue) forms the trimer interface and caps the active site, the regulatory region (orange) contains the secondary surface binding site (Z-site) and Glu354 of the catalytic triad, and the catalytic domain (green) contains the central β-sheet conserved in serine hydrolases, as well as the two catalytic residues His468 and Ser221. There are two disulfide bonds (cyan), one in the α/β domain and the other in the catalytic domain, and one glycosylation site, at Asn79 (yellow).

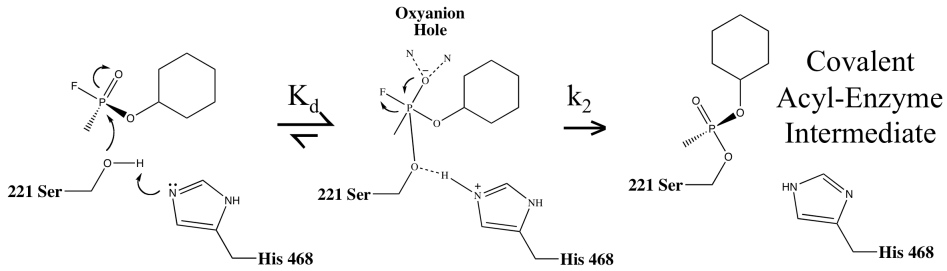

Scheme 2.1 Chemical scheme of hCE1 reacting with cyclosarin. Glu354 (not shown) deprotonates Nδ1 of His468, causing Nε2 to deprotonate Ser221, enabling nucleophilic attack on the phosphonyl center. After collapse of the pentahedral transition state, a stable covalent acyl-enzyme intermediate is formed.

hCE1-Cyclosarin	
Resolution (Å)	48-3.1 (3.3-3.1)
Space group	$P2_12_12_1$
Asymmetric unit	one trimer
Cell constants (Å, deg)	a = 55.6
	b = 179.9
	c = 200.6
	$\alpha = \beta = \gamma = 90$
Total reflections	256,334
Unique reflections	36,488
Mean redundancy[a]	7.0 (6.2)
R_{sym} (%)[a,b]	13.1 (48.1)
Wilson B factor (Å^2)	53.9
Completeness[a]	98.0 (94.0)
Mean I/σ[a]	13.6 (4.5)
R_{cryst} (%)[c]	26.6
R_{free} (%)[d]	29.9
RCSB access code	3K9B

TABLE 2.1 Crystallographic data collection and refinement statistics.

[a]Number in parenthesis is for the highest shell.

[b] $R_{sym} = \Sigma|I - \langle I \rangle|\Sigma I$, where I is the observed intensity and $\langle I \rangle$ is the average intensity of multiple symmetry-related observations of that reflection.

[c] $R_{cryst} = \Sigma ||F_o| - |F_c|| / \Sigma|F_o|$, where F_o and F_c are the observed and calculated structure factors, respectively.

[d] $R_{free} = \Sigma ||F_o| - |F_c|| / \Sigma|F_o|$ for 7% of the data not used at any stage of structural refinement.

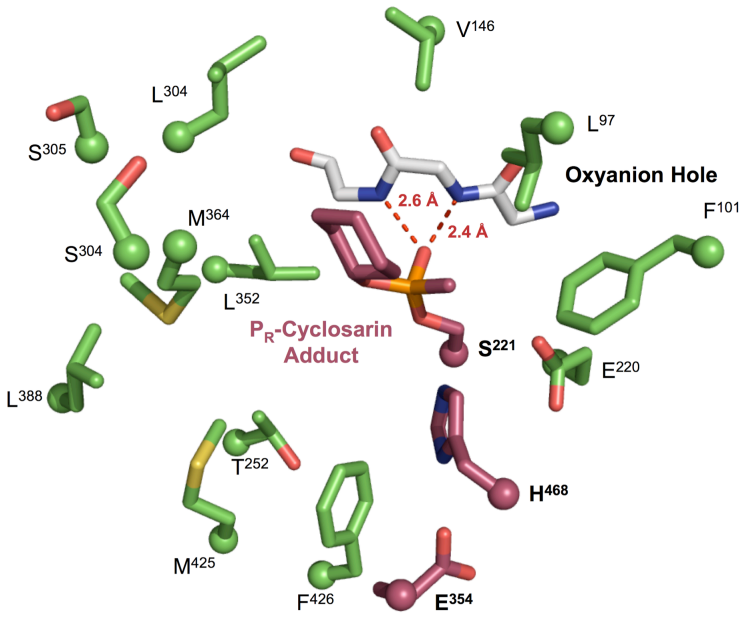

Figure 2.2 hCE1-cyclosarin complex. Cut away view of the hCE1-cyclosarin active site. The catalytic triad and cyclosarin molecule are shown in purple, oxyanion hole in white, and the surrounding residues in green. Hydrogen bonds between the phosphoryl oxygen and the backbone nitrogen atoms in the oxyanion hole are shown in red.

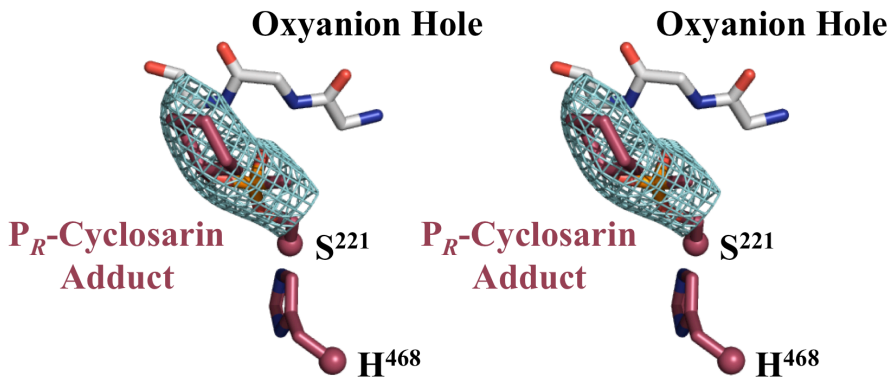

Figure 2.3 hCE1-cyclosarin adduct stereochemistry. S221 and H468 of the catalytic triad and the cyclosarin adduct are shown in purple. The oxyanion hole is colored white. Stereoview of a 3.1 Å resolution $F_o - F_c$ simulated annealing omit map (blue, contoured to 5 σ) calculated for the P_R-cyclosarin adduct.

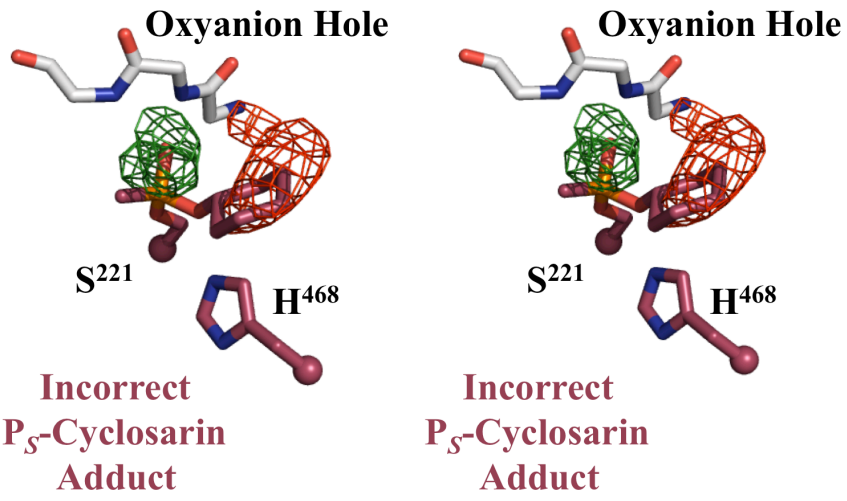

Figure 2.4 Incorrect hCE1-cyclosarin adduct stereochemistry. Stereoview of initial difference density maps for the incorrect P_S-cyclosarin adduct (green for positive, shown at 3 σ; red for negative, shown at -3 σ).

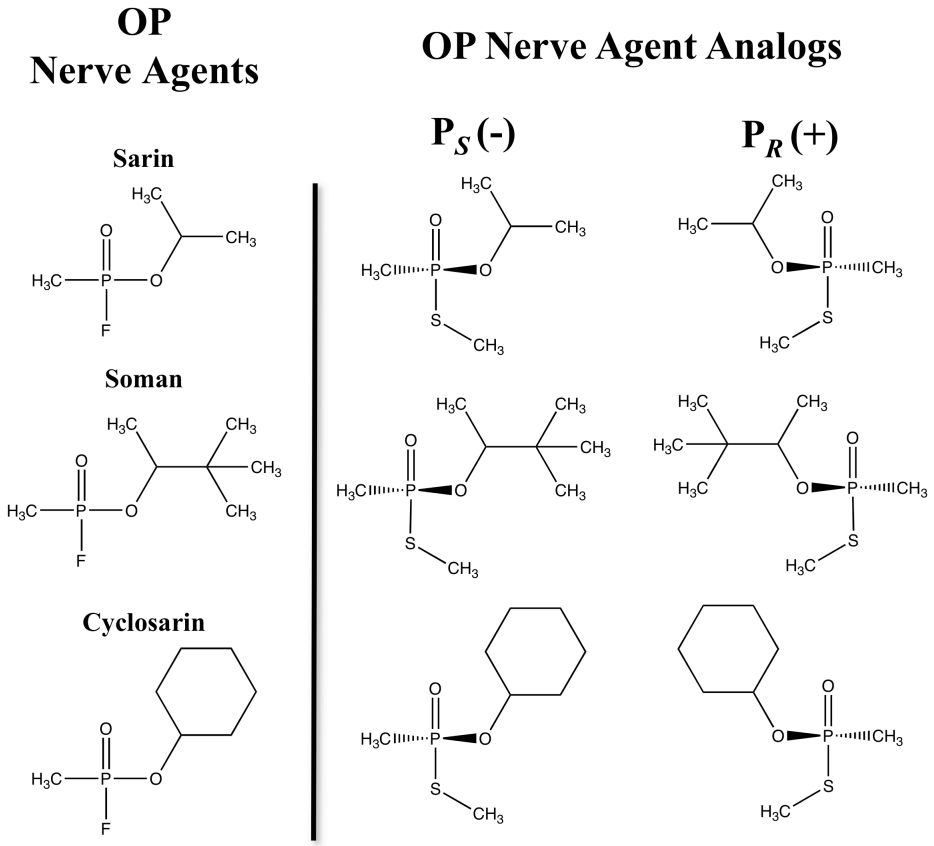

Figure 2.5 Organophosphate nerve agent analogs. Nerve agents contain a methyl, *O*-alkoxy, and good leaving group built on a central chiral phosphonate. The stereogenic OP nerve agent analogs contain a thiomethyl leaving group in place of the fluoride.

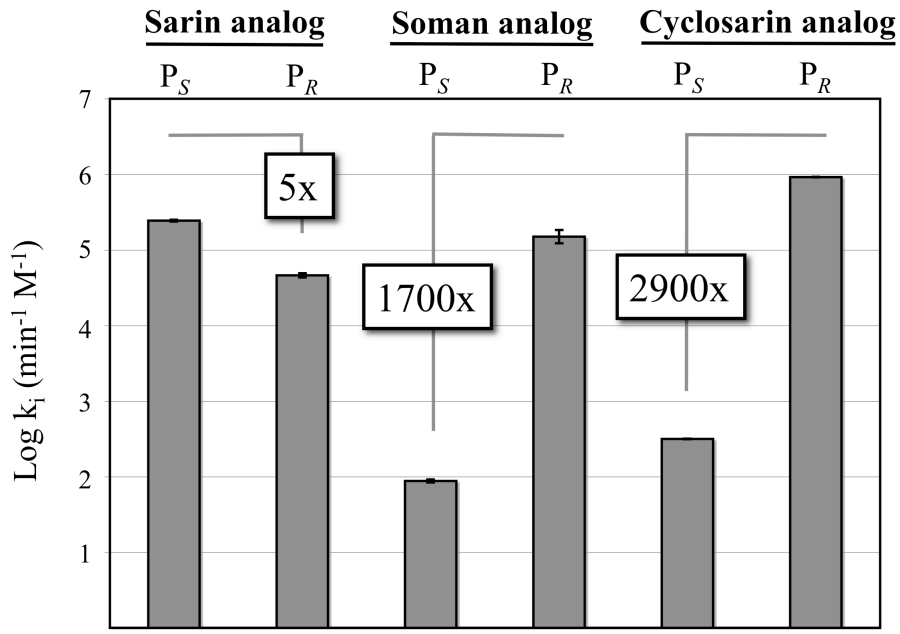

Analog Type		k_i (s^{-1} M^{-1})	K_d (M)	k_2 (s^{-1})	P_R/P_S
Sarin	P_S	4.10 ± 0.10 x 10^3	3.70 ± 0.20 x 10^{-7}	1.53 ± 0.02 x 10^{-3}	0.190
	P_R	0.77 ± 0.05 x 10^3	1.40 ± 0.20 x 10^{-6}	1.12 ± 0.01 x 10^{-3}	
Soman	P_S	1.46 ± 0.07	8.00 ± 2.00 x 10^{-4}	1.20 ± 0.01 x 10^{-3}	1705
	P_R	2.50 ± 0.50 x 10^3	2.20 ± 0.20 x 10^{-7}	0.55 ± 0.05 x 10^{-3}	
Cyclosarin	P_S	5.27 ± 0.07	1.70 ± 0.20 x 10^{-3}	9.00 ± 0.83 x 10^{-3}	2900
	P_R	1.53 ± 0.12 x 10^4	3.20 ± 0.10 x 10^{-7}	5.30 ± 0.50 x 10^{-3}	

Figure 2.6 Bimolecular rates of inhibition for hCE1 and nerve agent analogs. Plotted as log k_i, hCE1 exhibits strong enantiomeric P_R preference for soman and cyclosarin analogs, with only slight P_S sarin analog selectivity. Dissociation constants (K_d) are similar to authentic nerve agents, while phosphorylation rates (k_2) are 2-3 orders of magnitude slower. N=3, S.E.

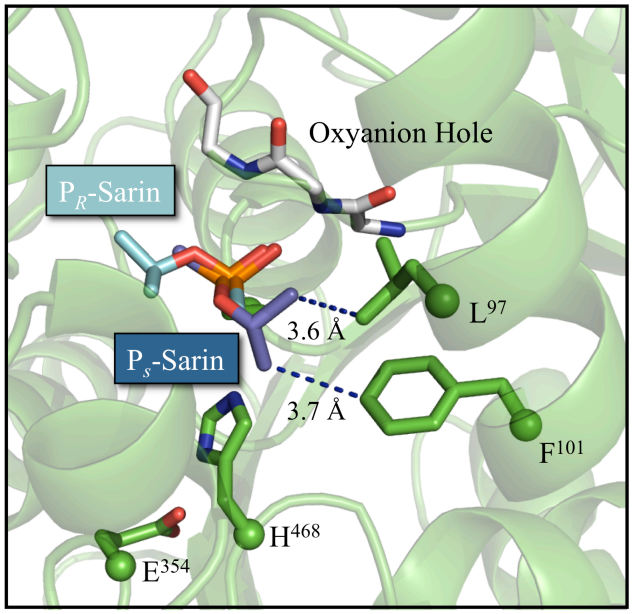

Figure 2.7 hCE1-sarin model. P_R and P_S enantiomers of sarin modeled in the hCE1 active site. The *O*-isopropyl group on P_S sarin makes hydrophobic contacts with Phe101 and Leu97, while P_R does not have any additional interactions.

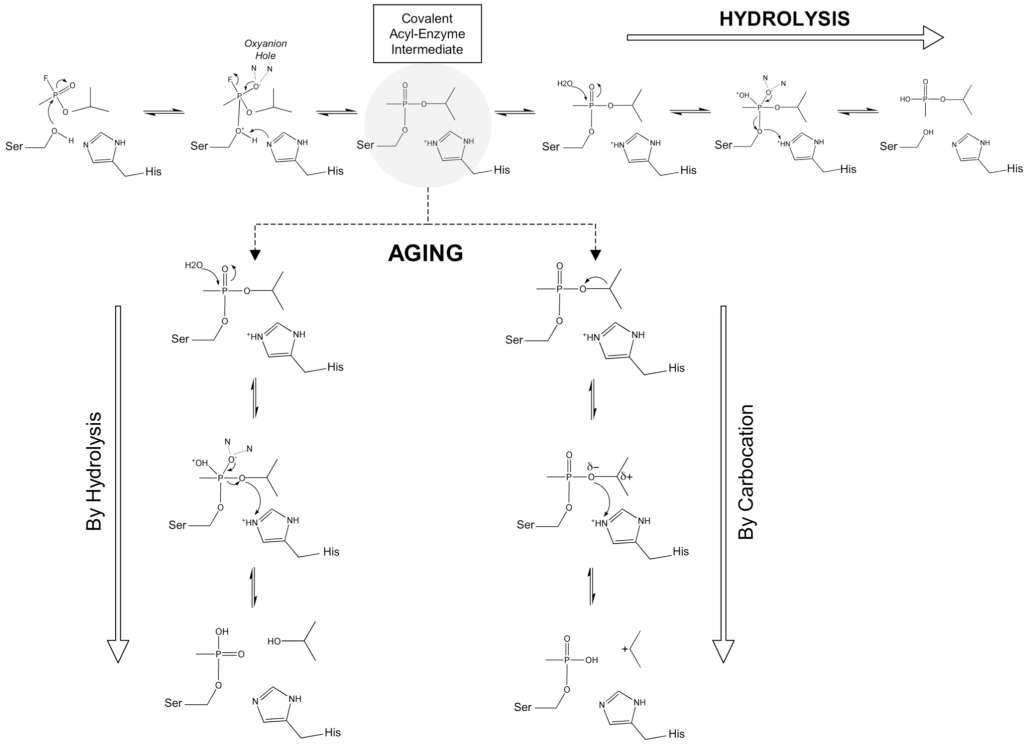

Scheme 2.2 Aging and hydrolytic pathways in serine hydrolases.

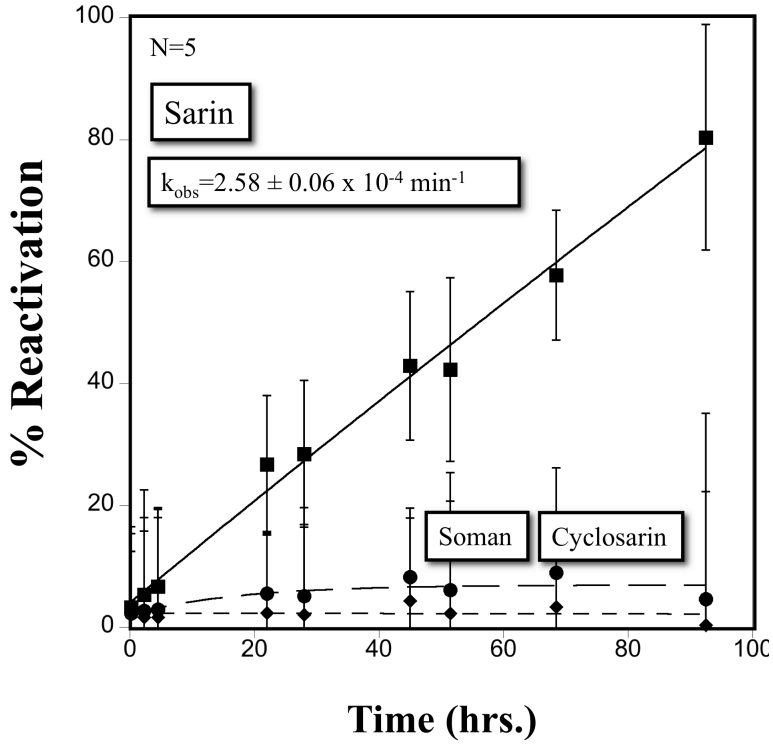

Figure 2.8 Spontaneous reactivation of racemic *bona fide* OP nerve agents by hCE1. Reactivation on occurs against sarin (■), with a half-time of reactivation of ~45 hours. Soman (•) and cyclosarin (◆) inhibited samples exhibit no reactivation.

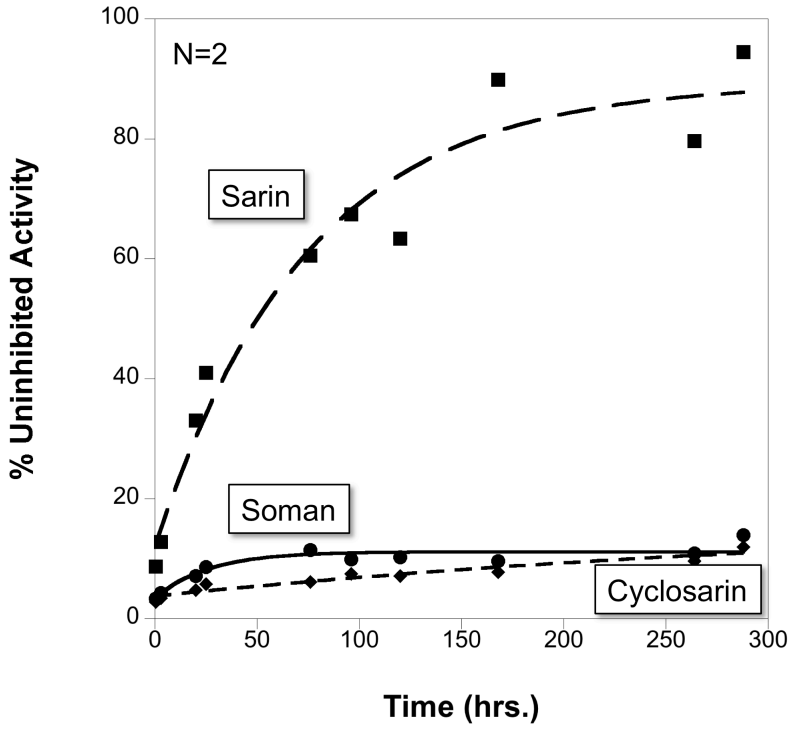

Figure 2.9 Maximal reactivation of racemic *bona fide* nerve agents by hCE1.

After 300 hours, sarin (■) inhibited samples are reactivated to 89 ± 5%, while soman (•) and cyclosarin (◆) inhibited samples remain permanently inhibited.

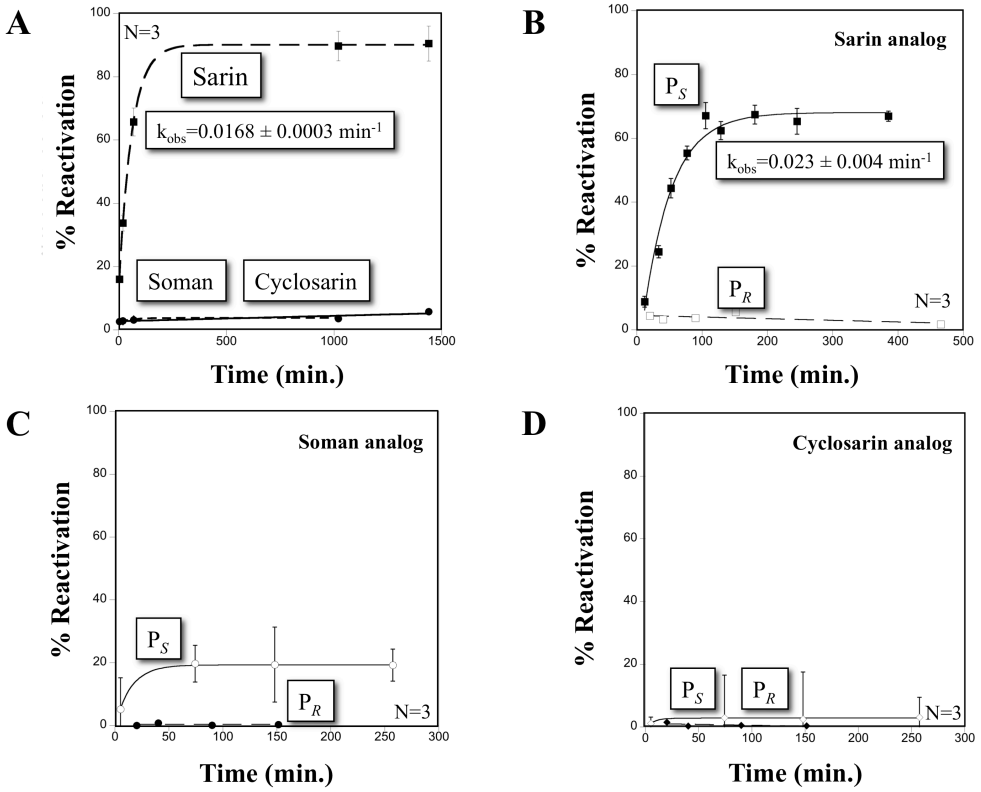

Figure 2.10 DAM assisted reactivation after inhibition by racemic *bona fide* OP nerve agents or stereospecific nerve agent analogs. A) Reactivation with racemic *bona fide* nerve agents. Recovery is only measured against sarin (■) with a half-time of reactivation of 41 minutes (N=3, S.E.). Soman (●) and cyclosarin (◆) did not reactivate. **B**) Reactivation of sarin analogs. The P_S isomer (■) reactivates with a half-time of 30 minutes (N=3, S.E.). P_R sarin (□) analog did not reactivate. **C**) Reactivation of soman analogs. Greatest recovery was measured in the P_S (○) enantiomer, while the P_R (●) analog remained inhibited. **D**) Reactivation of cyclosarin analogs. Negligible recovery was measured for either P_S (◇) or P_R (◆) cyclosarin analog.

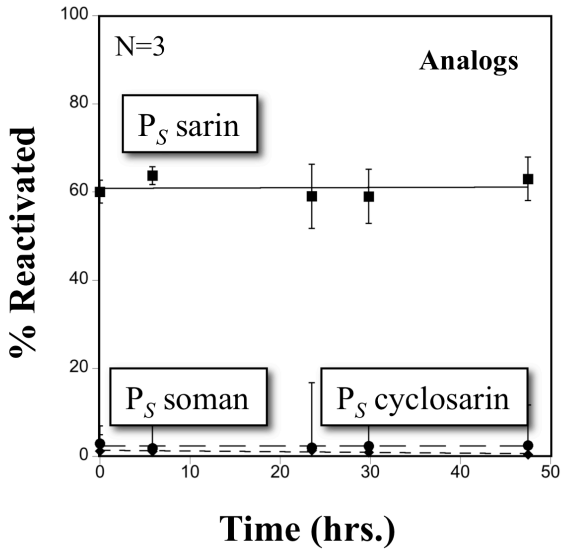

Figure 2.11 Determination of aging with P_S nerve agent analogs in hCE1. No aging was measured for the P_S species.

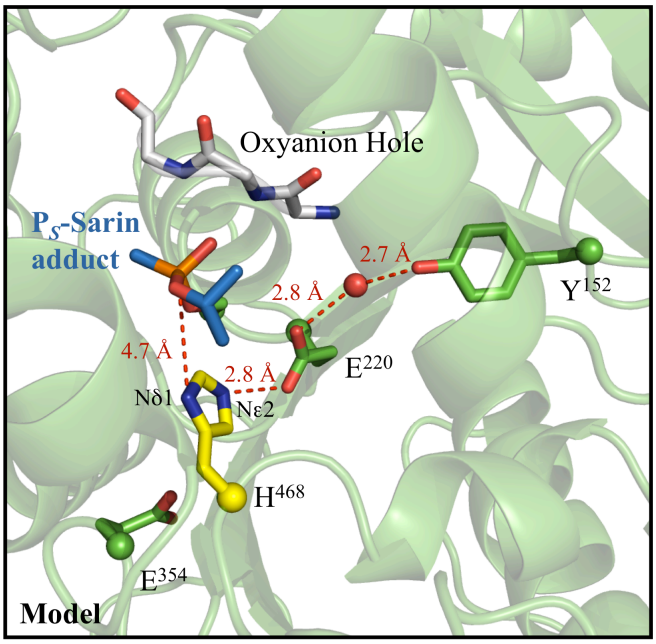

Figure 2.12 Model for spontaneous reactivation of P_S sarin by hCE1. In AChE, H468 has been observed to rotate away from E354 and interact with E221 after acylation. Modeling this shift in the hCE1 active site, there is an electronic network formed between Y152 (green) and H468 (yellow) that may either deprotonate Nε2 or allow Nδ1 of H468 to act as a general base for water activation. P_S sarin (blue) was modeled into the hCE1-soman structure (RSCB PSB access code 2HRQ (*18*)).

REFERENCES

1. Li, B., Nachon, F., Froment, M. T., Verdier, L., Debouzy, J. C., Brasme, B., Gillon, E., Schopfer, L. M., Lockridge, O., and Masson, P. (2008) Binding and hydrolysis of soman by human serum albumin, *Chem Res Toxicol 21*, 421-431.

2. Maxwell, D. M., and Brecht, K. M. (2001) Carboxylesterase: specificity and spontaneous reactivation of an endogenous scavenger for organophosphorus compounds, *J Appl Toxicol 21 Suppl 1*, S103-107.

3. Saxena, A., Sun, W., Luo, C., Myers, T. M., Koplovitz, I., Lenz, D. E., and Doctor, B. P. (2006) Bioscavenger for protection from toxicity of organophosphorus compounds, *J Mol Neurosci 30*, 145-148.

4. Yeung, D. T., Smith, J. R., Sweeney, R. E., Lenz, D. E., and Cerasoli, D. M. (2007) Direct detection of stereospecific soman hydrolysis by wild-type human serum paraoxonase, *Febs J 274*, 1183-1191.

5. Lenz, D. E., Yeung, D., Smith, J. R., Sweeney, R. E., Lumley, L. A., and Cerasoli, D. M. (2007) Stoichiometric and catalytic scavengers as protection against nerve agent toxicity: a mini review, *Toxicology 233*, 31-39.

6. Maxwell, D. M. (1992) The specificity of carboxylesterase protection against the toxicity of organophosphorus compounds, *Toxicol Appl Pharmacol 114*, 306-312.

7. Maxwell, D. M., Lieske, C. N., and Brecht, K. M. (1994) Oxime-induced reactivation of carboxylesterase inhibited by organophosphorus compounds, *Chem Res Toxicol 7*, 428-433.

8. Li, B., Sedlacek, M., Manoharan, I., Boopathy, R., Duysen, E. G., Masson, P., and Lockridge, O. (2005) Butyrylcholinesterase, paraoxonase, and albumin esterase, but not carboxylesterase, are present in human plasma, *Biochem Pharmacol 70*, 1673-1684.

9. Ross, M. K., and Crow, J. A. (2007) Human carboxylesterases and their role in xenobiotic and endobiotic metabolism, *J Biochem Mol Toxicol 21*, 187-196.

10. Maglott, D., Ostell, J., Pruitt, K. D., and Tatusova, T. (2007) Entrez Gene: gene-centered information at NCBI, *Nucleic Acids Res 35*, D26-31.

11. Redinbo, M. R., and Potter, P. M. (2005) Mammalian carboxylesterases: from drug targets to protein therapeutics, *Drug Discov Today 10*, 313-325.

12. Satoh, T., and Hosokawa, M. (2006) Structure, function and regulation of carboxylesterases, *Chem Biol Interact 162*, 195-211.

13. Ellgaard, L., Molinari, M., and Helenius, A. (1999) Setting the standards: quality control in the secretory pathway, *Science 286*, 1882-1888.

14. Bencharit, S., Morton, C. L., Xue, Y., Potter, P. M., and Redinbo, M. R. (2003) Structural basis of heroin and cocaine metabolism by a promiscuous human drug-processing enzyme, *Nat Struct Biol 10*, 349-356.

15. Bencharit, S., Morton, C. L., Hyatt, J. L., Kuhn, P., Danks, M. K., Potter, P. M., and Redinbo, M. R. (2003) Crystal structure of human carboxylesterase 1 complexed with the Alzheimer's drug tacrine: from binding promiscuity to selective inhibition, *Chem Biol 10*, 341-349.

16. Fleming, C. D., Bencharit, S., Edwards, C. C., Hyatt, J. L., Tsurkan, L., Bai, F., Fraga, C., Morton, C. L., Howard-Williams, E. L., Potter, P. M., and Redinbo, M. R. (2005) Structural insights into drug processing by human carboxylesterase 1: tamoxifen, mevastatin, and inhibition by benzil, *J Mol Biol 352*, 165-177.

17. Aldridge, W. N. (1953) 1. Two types of Esterase (A and B) Hydrolysing p-Nitrophenyl Acetate, Propionate and Butyrate, and a Method for their Determination, *Biochem J 53*, 110-117.

18. Fleming, C. D., Edwards, C. C., Kirby, S. D., Maxwell, D. M., Potter, P. M., Cerasoli, D. M., and Redinbo, M. R. (2007) Crystal structures of human carboxylesterase 1 in covalent complexes with the chemical warfare agents soman and tabun, *Biochemistry 46*, 5063-5071.

19. Hornberg, A., Tunemalm, A. K., and Ekstrom, F. (2007) Crystal structures of acetylcholinesterase in complex with organophosphorus compounds suggest that the acyl pocket modulates the aging reaction by precluding the formation of the trigonal bipyramidal transition state, *Biochemistry 46*, 4815-4825.

20. Millard, C. B., Kryger, G., Ordentlich, A., Greenblatt, H. M., Harel, M., Raves, M. L., Segall, Y., Barak, D., Shafferman, A., Silman, I., and Sussman, J. L. (1999) Crystal structures of aged phosphonylated acetylcholinesterase: nerve agent reaction products at the atomic level, *Biochemistry 38*, 7032-7039.

21. Epstein, T. M., Samanta, U., Kirby, S. D., Cerasoli, D. M., and Bahnson, B. J. (2009) Crystal structures of brain group-VIII phospholipase A2 in nonaged complexes with the organophosphorus nerve agents soman and sarin, *Biochemistry 48*, 3425-3435.

22. Hemmert, A., Otto, M. F., Wierdl, M., Edwards, C. C., Fleming, C. D., MacDonald, M., Cashman, J. R., Potter, P. M., Cerasoli, D. M., and Redinbo, M. R. (2010) Human Carboxylesterase 1 Stereoselectively Binds the Nerve Agent Cyclosarin and

Spontaneously Hydrolyzes the Nerve Agent Sarin, *Molecular Pharmacology IN PRESS*.

23. Morton, C. L., and Potter, P. M. (2000) Comparison of Escherichia coli, Saccharomyces cerevisiae, Pichia pastoris, Spodoptera frugiperda, and COS7 cells for recombinant gene expression. Application to a rabbit liver carboxylesterase, *Mol Biotechnol 16*, 193-202.

24. Wierdl, M., Tsurkan, L., Hyatt, J. L., Edwards, C. C., Hatfield, M. J., Morton, C. L., Houghton, P. J., Danks, M. K., Redinbo, M. R., and Potter, P. M. (2008) An improved human carboxylesterase for enzyme/prodrug therapy with CPT-11, *Cancer Gene Ther 15*, 183-192.

25. Lee, B. C., Le, D. T., and Gladyshev, V. N. (2008) Mammals reduce methionine-S-sulfoxide with MsrA and are unable to reduce methionine-R-sulfoxide, and this function can be restored with a yeast reductase, *J Biol Chem 283*, 28361-28369.

26. Potter, P. M., Pawlik, C. A., Morton, C. L., Naeve, C. W., and Danks, M. K. (1998) Isolation and partial characterization of a cDNA encoding a rabbit liver carboxylesterase that activates the prodrug irinotecan (CPT-11), *Cancer Res 58*, 2646-2651.

27. Kabsch, W. Xds, *Acta Crystallogr D Biol Crystallogr 66*, 125-132.

28. Collaborative Computation Project, N. (1994) The CCP4i suite: programs for protein crystallography, *Acta Crystallogr D Biol Crystallogr 50*.

29. Brunger, A. T., Adams, P. D., Clore, G. M., DeLano, W. L., Gros, P., Grosse-Kunstleve, R. W., Jiang, J. S., Kuszewski, J., Nilges, M., Pannu, N. S., Read, R. J., Rice, L. M., Simonson, T., and Warren, G. L. (1998) Crystallography & NMR system: A new software suite for macromolecular structure determination, *Acta Crystallogr D Biol Crystallogr 54*, 905-921.

30. Emsley, P., and Cowtan, K. (2004) Coot: model-building tools for molecular graphics, *Acta Crystallogr D Biol Crystallogr 60*, 2126-2132.

31. Laskowski, R., MacArthur, M., Moss, D., and Thornton, J. (1993) PROCHECK: a program to check the stereochemical quality of protein structures, *J. Appl. Cryst 26*, 283-291.

32. Bencharit, S., Morton, C. L., Howard-Williams, E. L., Danks, M. K., Potter, P. M., and Redinbo, M. R. (2002) Structural insights into CPT-11 activation by mammalian carboxylesterases, *Nat Struct Biol 9*, 337-342.

33. Sanson, B., Nachon, F., Colletier, J. P., Froment, M. T., Toker, L., Greenblatt, H. M., Sussman, J. L., Ashani, Y., Masson, P., Silman, I., and Weik, M. (2009)

Crystallographic Snapshots of Nonaged and Aged Conjugates of Soman with Acetylcholinesterase, and of a Ternary Complex of the Aged Conjugate with Pralidoxime (dagger), *J Med Chem*.

34. Gilley, C., MacDonald, M., Nachon, F., Schopfer, L. M., Zhang, J., Cashman, J. R., and Lockridge, O. (2009) Nerve agent analogues that produce authentic soman, sarin, tabun, and cyclohexyl methylphosphonate-modified human butyrylcholinesterase, *Chem Res Toxicol 22*, 1680-1688.

35. Forsberg, A., and Puu, G. (1984) Kinetics for the inhibition of acetylcholinesterase from the electric eel by some organophosphates and carbamates, *Eur J Biochem 140*, 153-156.

36. Aurbek, N., Thiermann, H., Szinicz, L., Eyer, P., and Worek, F. (2006) Analysis of inhibition, reactivation and aging kinetics of highly toxic organophosphorus compounds with human and pig acetylcholinesterase, *Toxicology 224*, 91-99.

37. Li, H., Schopfer, L. M., Nachon, F., Froment, M. T., Masson, P., and Lockridge, O. (2007) Aging pathways for organophosphate-inhibited human butyrylcholinesterase, including novel pathways for isomalathion, resolved by mass spectrometry, *Toxicol Sci 100*, 136-145.

38. Langenberg, J. P., De Jong, L. P., Otto, M. F., and Benschop, H. P. (1988) Spontaneous and oxime-induced reactivation of acetylcholinesterase inhibited by phosphoramidates, *Arch Toxicol 62*, 305-310.

39. Bartling, A., Worek, F., Szinicz, L., and Thiermann, H. (2007) Enzyme-kinetic investigation of different sarin analogues reacting with human acetylcholinesterase and butyrylcholinesterase, *Toxicology 233*, 166-172.

40. Volans, A. P. (1996) Sarin: guidelines on the management of victims of a nerve gas attack, *J Accid Emerg Med 13*, 202-206.

41. Shafferman, A., Ordentlich, A., Barak, D., Stein, D., Ariel, N., and Velan, B. (1996) Aging of phosphylated human acetylcholinesterase: catalytic processes mediated by aromatic and polar residues of the active centre, *Biochem J 318 (Pt 3)*, 833-840.

42. Reiner, E., and Aldridge, W. N. (1967) Effect of pH on inhibition and spontaneous reactivation of acetylcholinesterase treated with esters of phosphorus acids and of carbamic acids, *Biochem J 105*, 171-179.

Chapter 3. Structurally Guided Design of Human Carboxylesterase 1 into a Nerve Agent Hydrolyzing Enzyme

3.1 Catalytic Complication of OP Nerve Agents in hCE1

Human carboxylesterase 1 (hCE1) is a promiscuous liver hydrolase involved in the metabolism of compounds ranging from endobiotics like cholesteroyl esters to xenobiotics like pyrethroid pesticides or chemotherapy prodrugs. It has been postulated that broad-spectrum, generalized enzymes are evolutionary intermediates to specialized enzymes (*1*). Perhaps through structurally guided design, nerve agent hydrolysis activity can be engineered to compliment the predisposition of hCE1 to bind organophosphates. To understand how the protein can be modified for enhanced nerve agent hydrolysis, the limitations of the wild type enzyme need to be addressed.

hCE1 uses a serine catalytic triad to hydrolyze ester, thioester, and amide bonds (*2*). As illustrated in **Figure 3.1**, H468 forms a hydrogen bond at Nδ1 with E354, thereby polarizing and enabling the lone pair of electrons on Nε2 to deprotonate S221. S221 then acts as a nucleophile to attack the carbonyl center of an ester substrate. A tetrahedral transition state forms, which collapses to release an alcohol, resulting in an acyl-enzyme intermediate. The high pKa of the alcohol leaving group (pKa ~15) depronotates neighboring H468, enabling this catalytic base to activate a water molecule for hydrolysis.

The newly formed hydroxide ion can now attack the carbonyl center of the acyl-enzyme intermediate, forming a second tetrahedral transition state, which upon collapse cleaves the S221-substrate ester bond, regenerating the enzyme for another round of catalysis. Catalytic triads are one of the most efficient mechanisms for hydrolyzing substrates. Indeed, acetylcholine hydrolysis by AChE is one of the fastest known enzyme reactions (*3*).

The catalytic complication with nerve agents occurs after the first transition state **(Figure 3.2)** (*4*). As the pentahedral transition state collapses, the nerve agent leaving group, which has a much lower pKa than a conventional alcohol, dissociates but likely leaves H468 protonated. For example fluoride, the leaving group in sarin, soman, and cyclosarin, has a pKa of 4. The drastic difference in the chemical nature of the dissociating groups halts the mechanism since a catalytic base is not available for water activation (*5*). We hypothesized that if an additional base could be added into the hCE1 active site for water activation, enzyme function towards OPs could be enhanced.

Using the crystal structures of hCE1 in complex with soman and cyclosarin (RCSB PDB 2HRQ and 3K9B, respectively (*6, 7*)), we explored the active site for positions where a histidine or glutamic acid could be added. Histidine has a pKa of 6 and can act as both an acid or base at physiological pH, while Glu or Asp serves as the base in protein tyrosine phosphatases to efficiently hydrolyze phosphorylated substrates (*8*). As shown in **Figure 3.3**, residues V146 and L363 were selected based on their location above the acyl-enzyme intermediate for an S_N2 hydrolytic attack. In order to cleave the S221-OP phosphate bond, a water molecule would need to approach in-line with these atoms.

3.2 Site-directed mutagenesis of hCE1

Site-directed mutagenesis was utilized with custom-designed primers to introduce single mutations at positions 146 and 363. Primers are listed in **Table 3.1**. Briefly, mutations were introduced in the hCE1 gene (GenBank accession code NC_000016) contained within the ampicillin resistant pUC9 plasmid through 15 rounds of PCR with respective primers. After PCR, template plasmids were digested for 1 hr at 37^{o}C with *Dpn1* (Fermentas Life Sciences), transformed into DH5α cells, and colonies were grown overnight on ampicillin resistant plates. Single colonies were selected and further grown in LB suspension. Plasmids were then isolated and successful mutant incorporation was verified by DNA sequencing. To express mutant hCE1 in COS cells, the modified hCE1 gene was cloned into the mammalian expression vector, pCI-neo (Promega, Madison, WI). Briefly, using 30 rounds of PCR and custom designed 5' and 3' primers with flanking engineered *EcoR1* and *Sma1* (Fermentas Life Sciences) restriction sites, the 1.7 kb hCE1 gene was cloned out of pUC9 and ligated into the 5.4 kb pCI-neo using T4 DNA ligase. hCE1-containing plasmids were selected and isolated from colonies that incorporated successful ligations, then verified through *Pst1* (Frementas Life Sciences) digestion to confirm presence of gene in plasmid, followed by DNA sequencing. Endotoxin free (Quaigen) pCI-neo plasmids were then prepared and transfected into COS cells through electroporation as described in **Chapter 2.4**.

3.3 Spontaneous Reactivation of hCE1 mutations following nerve agent inhibition

In collaboration with the United Stated Army Medical Research Institute of Chemical Defense (USAMRICD) we tested over 50 designed mutants of hCE1 for spontaneous reactivation following sarin, soman, cyclosarin, or tabun inhibition. As reported

is **Chapter 2.8**, wild type hCE1 spontaneously reactivates following sarin inhibition, with a half-time of reactivation of ~45 hours (*7*), but remains permanently inhibited after soman, cyclosarin, and tabun exposure. Fifty μL of mutant hCE1 COS cell lysate was incubated with ~1000-fold molar excess of sarin, soman, cyclosarin, or tabun for approximately 10 minutes. Complete inactivation was verified by comparing the ability of the inhibited sample to hydrolyze 10 mM pNPB relative to an unexposed sample. All mutant enzymes were still capable of hydrolyzing pNBB (data not shown). Excess agent was removed by passing the sample over a PD MiniTrap G-25 desalting spin column (GE Healthcare) and eluate was diluted 1:10 into 100 mM phosphate buffer pH 7.4. Samples were then verified for complete agent removal by measuring the ability of flow-through fractions to further inhibit BChE. Rates of spontaneous reactivation (k_{obs}) and maximal percent reactivation (A_{max}) were determined by measuring the ability of nerve agent inhibited samples to hydrolyze pNPB compared to an uninhibited sample and fitting the data to equation 1:

$$A = A_0 + A_{max}(1 - e^{-k_{obs}t}) \quad (1)$$

where A was percent activity at time, t, and A_0 was the initial activity at t=0. The experiments were conducted in triplicate and data were analyzed with KaleidaGraph 4 (Synergy Software, Reading, PA). pNPB is a conventional ester substrate and hydrolysis is measured by following absorbance of *o*-nitrophenol at 410 nm on a microplate reader.

As shown in **Figure 3.4**, the designed dyad hCE1 mutant V146H/L363E was able to rapidly reactivate following inhibition by racemic sarin, soman, and cyclosarin. V146H/L363E remained inhibited after tabun exposure. This mutant completely hydrolyzed cyclosarin, with a half-time of reactivation of 68 ± 4 minutes at pH 7.4 and 25^{o}C, and returned to >90% uninhibited activity following sarin and soman inhibition with a half-times

of reactivation of 9 ± 1 hours and 11 ± 3 hours, respectively. This is the fastest reported rate of cyclosarin hydrolysis by a mutant esterase. A mutant form of BChE (G117H/E197Q) has been generated that reactivates following racemic soman inhibition, with a half-time of reactivation of 1.9 ± 0.2 hours (*9*). As mentioned in **Chapter 2.8**, wild type hCE1 cannot reactivate following cyclosarin or soman exposure.

3.4 Mutant controls of nerve agent hydrolysis

To understand the combination of V146H/L363E for cyclosarin hydrolysis we made control mutants and tested them for spontaneous reactivation following exposure to racemic sarin, soman, or cyclosarin. **Figure 3.5** reports the rates of spontaneous reactivation for each control mutant. V146H and L363Q enhance the rates of sarin hydrolysis, but their combination is less than additive, suggesting that these residues are not interacting in a functional manner. These mutants have no effect on cyclosarin hydrolysis. Soman hydrolysis is fastest with V146H but only recovers to approximately 10% uninhibited activity. The V146H/L363E mutant is almost as rapid as V146H against soman, but recovery is increased to 90 ± 3 %. L363E alone exhibits slight sarin and soman hydrolysis, but is most effective for cyclosarin (half-time of reactivation of 7 ± 1 hours). Adding V146Q to L363E further reduces the half time of cyclosarin hydrolysis to 3 hours, perhaps by positioning the carboxylate head group, but does little for sarin or soman reactivation. Only the synergistic mutant V146H/L363E is capable of rapidly reactivating after cyclosarin inhibition, and recovering near full activity following sarin and soman inhibition.

Tables 3.2-3.4 report the rates of spontaneous reactivation (k_{react}) and percent maximal recovered activity (A_{max}) for V146H, V146Q, L363E, L363Q, V146H/L363Q,

V146Q/L363E, and V146H/L363E hCE1 mutants towards sarin, soman, and cyclosarin. To emphasize the impact of each mutant we devised an adjusted rate of reactivation (Adjusted k_{react} = (k_{react}•A_{max}) / 100), which combines the rates of reactivation and percent maximal activity into one term. An ideal bioscavenger will exhibit both enhanced rates of reactivation and maximal recovery (*10*). Based on this selection criteria, the combination of V146H/L363E results in a 48,700-fold increased in the rate of cyclosarin hydrolysis compared to wild type.

3.5 pH profile of cyclosarin hydrolysis by V146H/L363E hCE1 mutant

The difference in free energy ($\Delta G = -RT \ln(k_{react}$ Mutant 1/k_{react} Mutant 2)) between the rates of cyclosarin hydrolysis of L363E and V146H/L363E is approximately 1 kcal/mol, suggesting a weak bond is being formed between the His and Glu. To explore how the V146H/L363E hCE1 mutants are interacting and determine whether a bond is being formed we measured the rates of spontaneous reactivation following cyclosarin inhibition from pH 4 to 9. The inflection points on the pH curve report the key ionizable states in cyclosarin hydrolysis. To cover this range, 10 mM buffers of sodium phosphate (pH 3.37, pH 7.06, and pH 10.01), potassium formate (pH 4.13, 5.13), potassium phosphate (pH 6.2), TRIZMA (pH 8.02), and sodium carbonate (pH 9.04) were used. Samples of purified V146H/L363E hCE1 mutant in 50 mM HEPES pH 7.4 were incubated with 10 nM cyclosarin for 5 minutes then confirmed for complete inhibition as previously described. Excess agent was removed and samples were diluted 1:10 into appropriate buffers. At various time points, aliquots were removed and assayed with 100 mM pNPB in 100 mM phosphate buffer pH 7.4 for CE activity. Rates of spontaneous reactivation were determined by fitting data to equation 1.

As shown in **Figure 3.6**, the pH profile exhibits only one pKa for the partnering E363 and H146. The inflection point near pH 6.2 is where H146 becomes deprotonated. On a small peptide His has a pKa of 6.04 and Glu exhibits a pKa of 4.07 (*11*). These values are environment dependent and may change, especially if H146 and E363 are interacting. Unfortunately, below pH 4, both inhibited and uninhibited enzyme samples became denatured and no consistent catalytic activity was measured; therefore the deprotonation event of E363 could not be accessed. However the highest rates of cyclosarin hydrolysis are observed below pH 6.2, in the pH range where E363 is deprotonated and H146 is positively charged. These observations support the conclusion that E363 is acting as the nucleophilic base for water activation and is stabilized by a charged H146 **(Figure 3.7)**. Once H146 becomes deprotonated, E363 is destabilized, perhaps changing rotamers to sample the outside aqueous environment.

3.6 Computational modeling of V146H/L363E hCE1

Based on these biochemical data E363 is most likely the nucleophilic base for water activation in cyclosarin reactivation and H146 stabilizes the position of this base. Using the crystal structures of wild type hCE1 in complex with soman and cyclosarin we used computational protein design algorithms to model in the V146H/L363E mutations and examined their structural relationship.

To prepare structures for computational design, a new residue type was created for S221 covalently inhibited by each of the OPs, GBX for sarin, GDX for soman, and GFX for cyclosarin. Following removal of all water molecules, saccharides, soman/cyclosarin, and extra monomers from the hCE1-soman and cyclosarin crystal structures (RCSB PDB 2HRQ,

3K9B (*6, 7*)), hydrogens were added into the protein structure using Molprobity (*12*). OP-inhibited S221 hydrogens were added using Accelrys Discovery Studio Visualizer 2.5 (Accelrys, San Diego, CA). Any strain or steric clashes in the structures were removed by performing 50 steps of conjugate gradient energy minimization.

Residues with side chains pointing towards and within 5 Å of the organophosphorus, V146, or L363 residues (residues 89, 90, 93, 96, 97, 100, 101, 145, 146, 220, 222, 252, 254, 255, 304, 318, 358, 359, 361, 363, 364, 388, 425, 426, and 468) were allowed to sample alternative conformations during the designs, but their identities were not modified. The crystallographic conformer at each designed position was also allowed. A standard backbone-dependent side chain rotamer library with expansions by one standard deviation about $\chi 1$ and $\chi 2$ was used (*13*). Prior to the modeling procedure, rotamer libraries for the various OPs (P_S sarin, P_R sarin, P_RC_R soman, P_RC_S soman, P_SC_R soman, P_SC_S soman, P_R cyclosarin, and P_S cyclosarin) were generated. These OP rotamer libraries introduced torsions in the phosphorus-alkoxy oxygen and alkoxy oxygen-carbon bonds of each *free* OP-bound serine residue, in 5° increments. The rotamers with conformational energies lower than a specified value (usually 0) were included in the OP rotamer library. Computational design was performed using the PHOENIX protein design software (X). The energy function used was based on the DREIDING force field and included a scaled van der Waals term, hydrogen bonding and electrostatic terms, and terms for implicit solvation and phi-psi propensities. Implicit solvation energies were evaluated using a model based on occluded volume. Amino acid phi-psi propensities were derived and applied following the method of Shortle (*14*). Sequence optimization was carried out with FASTER.

Figure 3.8A illustrates the energy minimized model of V146H/L363E hCE1 in complex with P_R cyclosarin. From this structure it is apparent that E363 and H146 form an ion pair, but not a salt bridge. Salt bridges require that the side-chain charged group centroids are within a 4.0 Å distance and at least one pair of Asp/Glu side-chain carbonyl oxygen and Arg/Lys/His side-chain nitrogen atoms are also within this distance (*15*). According to the computational model V146H/L363E fulfills the second criteria, but not the first. The distance between Oε1 on the E363 anionic carboxylate head group and the cationic Nε2 is 4 ± 1 Å at a 140^o angle, but the distance between charged centroids is at least 5 ± 1 Å. Rather, H146 and E363 form a nitrogen-oxygen (N-O) bridge (*16*). This stabilizing electrostatic interaction has been observed via NMR in multiple protein structures (*16, 17*).

A conventional salt bridge would tie up E363, thereby eliminating the potential to activate a water molecule. Through this N-O bridge, however, E363 stabilized for nucleophilic attack. A water molecule can be positioned between E363 Oε1 and the cyclosarin phosphonyl center, at a distance of 3.2 Å between each group and the water molecule **(Figure 3.8B)**. The ability of this dyad to promote hydrolysis for cyclosarin more rapidly than soman and sarin is likely caused by the difference in *O*-alkoxy groups between the agents. The branched isopropyl and pinacolyl alkoxy groups in sarin and soman most likely exhibit greater degrees of rotational freedom than the spatially constrained cyclosarin cyclohexyl group, thereby limiting hydrolytic attack.

3.7 Effect of nerve agent binding by V146H/L363E hCE1 mutant

Researchers have been trying to develop mutant esterases for the last 20 years that exhibit enhanced rates of reactivation towards OP nerve agents (*5, 9*). The previously

described G117H/E197Q BChE mutant was the most successful cholinesterase variant thus far (*9*). The deficiency with this mutant however, is that by enhancing the rate of reactivation, the ability of this enzyme to bind nerve agents is greatly diminished. For example, the ability of G117H/E197Q BChE to bind soman is reduced over 1000-fold compared to WT, making this mutant an ineffective *in vivo* nerve agent scavenger. The loss in binding affinity was attributed to G117H blocking OP entry into the active site (*9*).

Using the stereogenic thiomethylated nerve analogs previously described in **Chapter 2.7** we determined the bimolecular rates of inhibition (k_i) and dissociation constants (K_d) of V146H/L363E hCE1 for these compounds (*7*). Samples of purified V146/L363E hCE1 at 100 nM were inhibited at room temperature with increasing concentrations of stereogenic OP nerve agent analogs. Aliquots of enzyme incubated with stereoisomer analogs of sarin (P_R, P_S), soman (P_R, P_S), and cyclosarin (P_R, P_S) were removed at various time points (up to 1 hr) and the level of active enzyme that remained was determined by comparing pNPB hydrolysis relative to an uninhibited sample. These data, collected at 410 nm and 25 ^oC on a Pherastar microplate reader (BMG Labtech), were corrected for spontaneous pNPB hydrolysis and fit to equation 3 (*18*):

$$\frac{\Delta t}{\Delta \ln v} = \frac{K_d}{k_2} * \frac{1}{[IX](1-\alpha)} + \frac{1}{k_2} \qquad \textbf{(3)}$$

where K_d was the dissociation constant, k_2 the unimolecular phosphorylation rate constant, v the remaining percent enzyme activity, [IX] was the OP analog concentration, α was $[S]/(K_M + [S])$, in which [S] was the substrate concentration and K_M was the Michaelis-Menton constant. All experiments were performed in triplicate. Data were analyzed in KaleidaGraph 4 (Synergy Software, Reading, PA) to determine k_i ($k_i = k_2 / K_d$) values.

As shown in **Figure 3.9**, the V146H/L363E hCE1 mutant did not drastically reduce the overall bimolecular rates of inhibition of this mutant for the nerve agent analogs. Indeed, the dyad addition enhanced the enzymes affinity towards P_S soman and cyclosarin isomers compared to wild type. **Table 3.5** details the effects of V146H/L363E on nerve agent analog binding. The slight differences in k_i between wild type and the dyad mutant are from the slower rates of phosphonylation (k_2) in the novel enzyme (*7*), which could be associated with active site changes induced by the mutants. These slower rates however are balanced by the enhanced binding affinity (K_d) of V146H/L363E for each analog. The mutant enzyme drastically reduced the previous absolute P_R stereoprefence, especially for the cyclosarin analog. The P_R/P_S binding ratio was reduced from 2900 in the wild type enzyme to only 45 for the mutant (*7*). Overall these data confirm that unlike the G117H/E197Q BChE, the tight binding affinity of carboxylesterases for OP nerve agents was not diminished in the V146H/L363 hCE1 mutant.

3.8 An Efficient Enzyme

Through the V146H/L363E dyad addition we increased the Adjusted rate of reactivation for cyclosarin 48,000-fold over wild type while still maintaining nM binding affinity. Combining these two terms (k_{cat}/K_m) describes an enzyme's efficiency (*19*). Because it is believed reactivation is the slowest step in the enzymatic pathway, we approximate that $k_{react} \approx k_{cat}$. Additionally, the K_d towards the thiomethylated cyclosarin analog is representative of the K_d for *bona fide* agents (*7, 20*). By combining these terms we arrive at a k_{cat}/K_m of V146H/L363E hCE1 for cyclosarin of 1.8×10^3 M^{-1} s^{-1}, four orders of magnitude more efficient than the soman hydrolyzing G117H/E197Q BChE (*9*). When

compared to other rational protein designs towards hemisubstrates, or enzymes that bind a given substrate but have no catalytic activity on that substrate, we have created the current most efficient enzyme described to date **(Table 3.6)**. Other designed enzymes include peptidase activity into cyclophilin through a Ser-His-Asp catalytic triad addition, phosphatase activity in phospho- (serine/threonine/tyrosine) binding proteins by adding a catalytic cysteine, thioester hydrolysis in glutathione transferase A1-1 with a nucleophilic His addition, and oxaloacetate decarboxylesterase into 4-oxalocrotonate tautomerase by generating a N-terminal tertiary amine to induce Schiff base formation (*21-24*). In terms of all designed enzymes, rationally, computationally, or evolutionarily, the most efficient enzyme, so far, resulted from the combination of *de novo* protein design and directed evolution (*25*). The Kemp elimination pathway designed into a TIM barrel exhibits a k_{cat}/K_m of 2.6 x 10^3 M^{-1} s^{-1}, approximately 1.5x more efficient than V146H/L363 hCE1.

3.9 Conclusion

Despite the dramatic increase in the rate of spontaneous reactivation of V146H/L363E hCE1 towards cyclosarin, this mutant enzyme is still too slow to be used as a catalytic bioscavenger. The ideal catalytic bioscavenger candidate must bind nerve agents on the nM scale and exhibit reactivation rate constants on the order of 1 min^{-1}, we are still two-orders of magnitude away from that benchmark (personal communication with Dr. Douglas Cerasoli, USAMRICD). The rate-limiting step in the reaction pathway may now be product release, so we are in the process of making mutations that open up the active site pocket, potentially further enhancing the rate of nerve agent hydrolysis. Indeed, as shown in

Chapter 5, a loop truncation to open up the active site pocket greatly enhanced that rate of oxime induced sarin hydrolysis compared to wild type hCE1.

3.10 Figures and Tables

Figures and tables are listed in the same order they appear in the text of chapter 3.

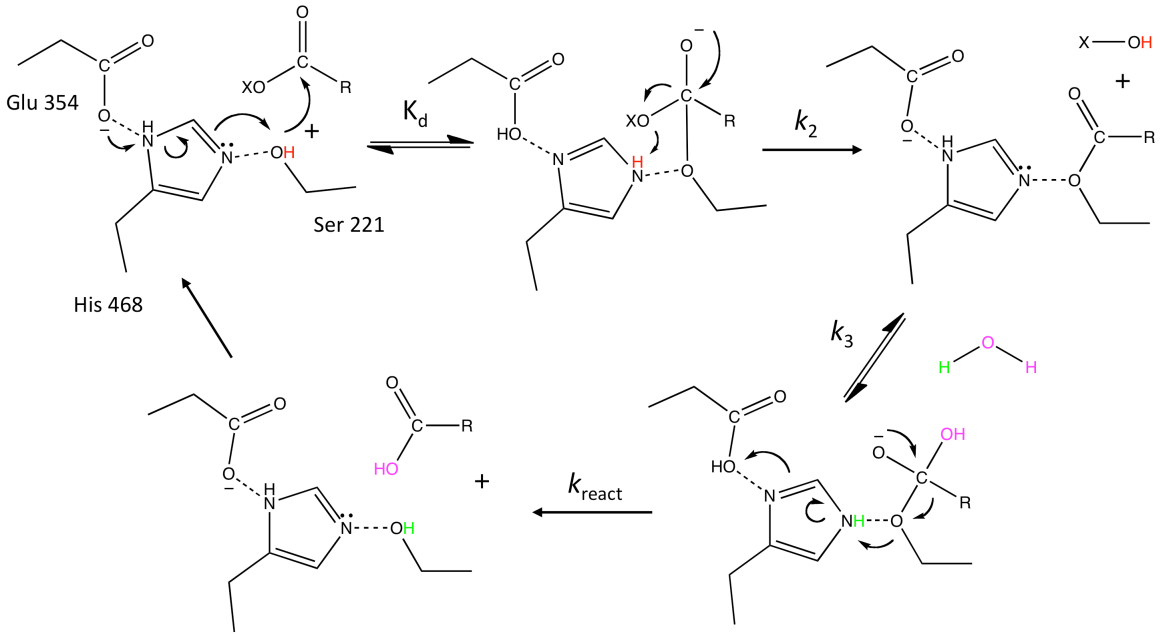

Figure 3.1 Ester hydrolysis by hCE1. H468 deprotonates S221, leading to a nucleophilic attack of an ester substrate. Upon collapse of the tetrahedral intermediate, an alcohol dissociates, deprotonating H468, resulting in an acyl enzyme intermediate. H468 then activates a water molecule for nucleophilic attack on the acyl carbonyl center, forming a second transition state. Finally, the newly formed carboxylic acid dissociates from S221, regenerating the enzyme for another round of catalysis.

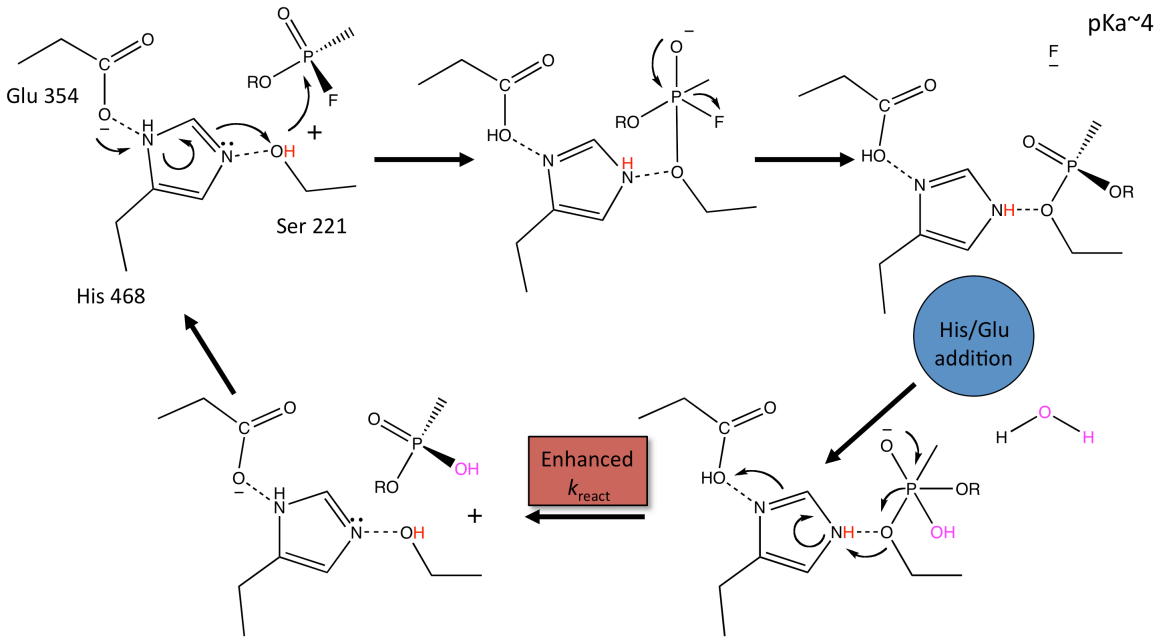

Figure 3.2 Catalytic complication of nerve agent inhibition in esterases. After resolve of the initial pentahedral transition state, the departing fluoride has a much lower pKa than the traditional ester alcohol, likely leaving H468 protonated. Adding a base (His or Glu) into the active site may enable water activation and reactivation of S221.

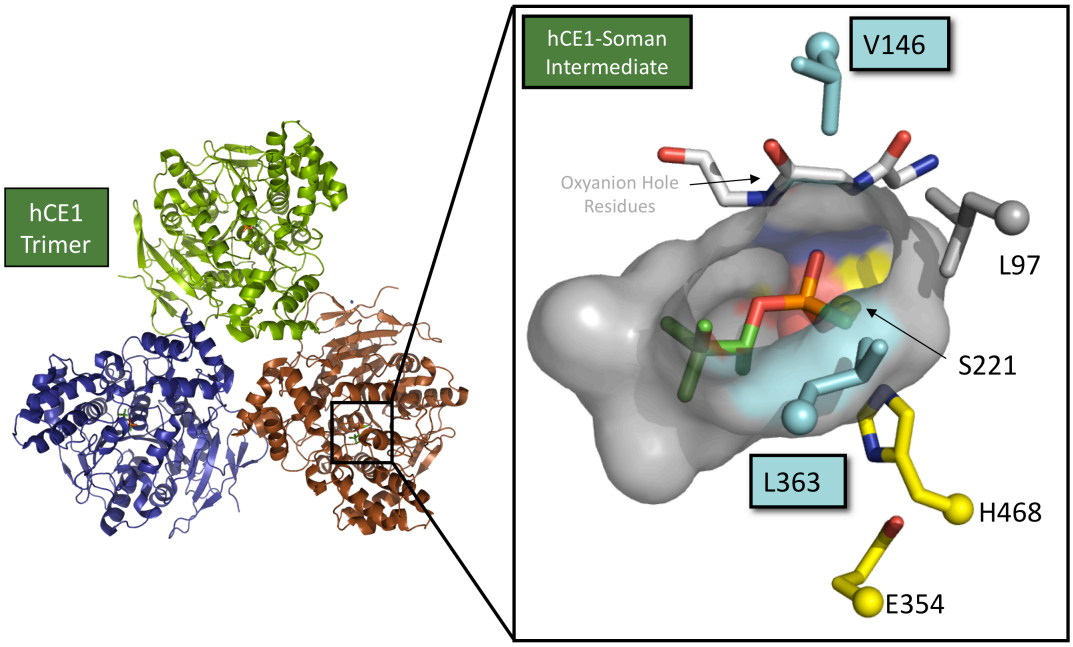

Figure 3.3 Active site of human carboxylesterase 1 covalently inhibited with soman. The active site residues S221, H468, and E354 (yellow), are surrounded by hydrophobic residues (grey surface), including L97 (grey), V146, and L363 (light blue).

Table 3.1 Primers used for mutant incorporation in hCE1.

Mutant hCE1 Plasmid	Custom DNA Primer Sequence
V146H	Forward: 5'-ggaggggggctgatgCACggtgcggcatcaacc-3' Reverse: 5'-ggttgatgccgcaccGTGcatcagccccctcc-3'
V146Q	Forward: 5'-ggaggggggctgatgCAggtgcggcatcaacc-3' Reverse: 5'-ggttgatgccgcacccTGcatcagccccctcc-3'
L363E	Forward: 5'-ggctggttgattccaatgGAgatgagctatccactctccg-3' Reverse: 5'-cggagagtggatagctcatcTCcattggaatcaaccagcc-3'
L363Q	Forward: 5'-ggctggttgattccaatgCAgatgagctatccactctccg-3' Reverse: 5'-cggagagtggatagctcatcTGcattggaatcaaccagcc-3'

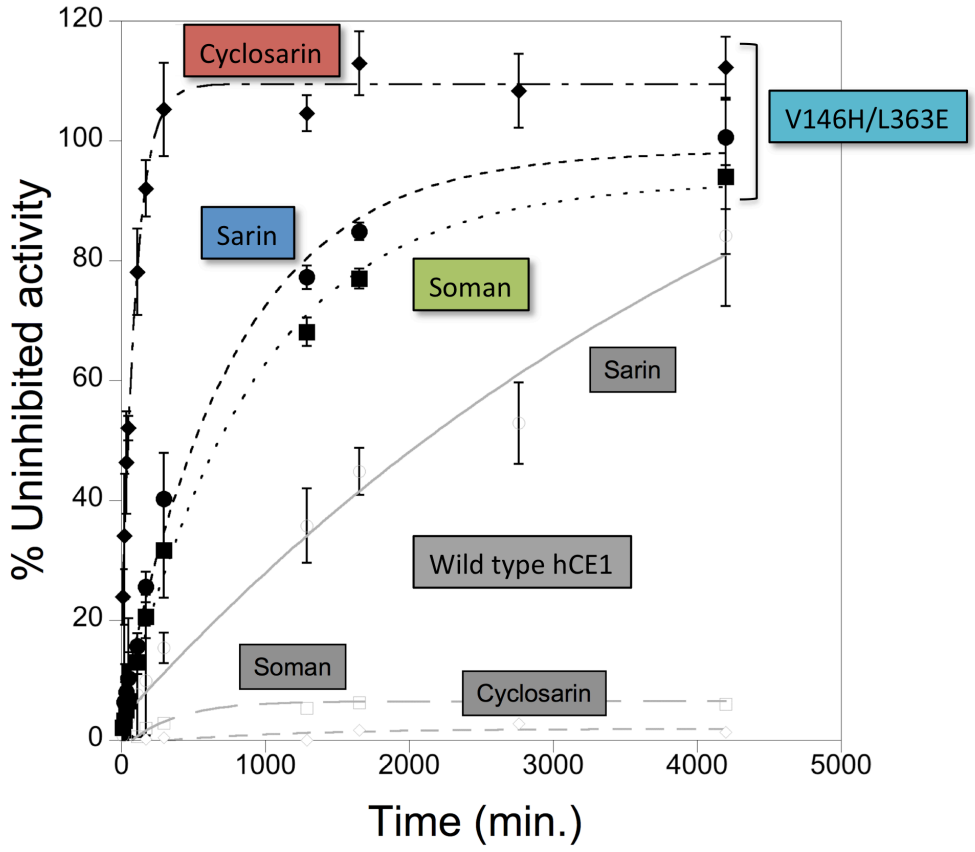

Figure 3.4 Rates of spontaneous reactivation for V146H/L363E hCE1 mutant. Reactivation in the presence of sarin (●), soman (■) and cyclosarin (◆). Sarin is hydrolyzed 4.5x faster than wild type, soman ~100x faster, and cyclosarin >1000x faster. For comparison, reactivation of wild type enzyme is shown in grey (*7*). N=3, S.E.

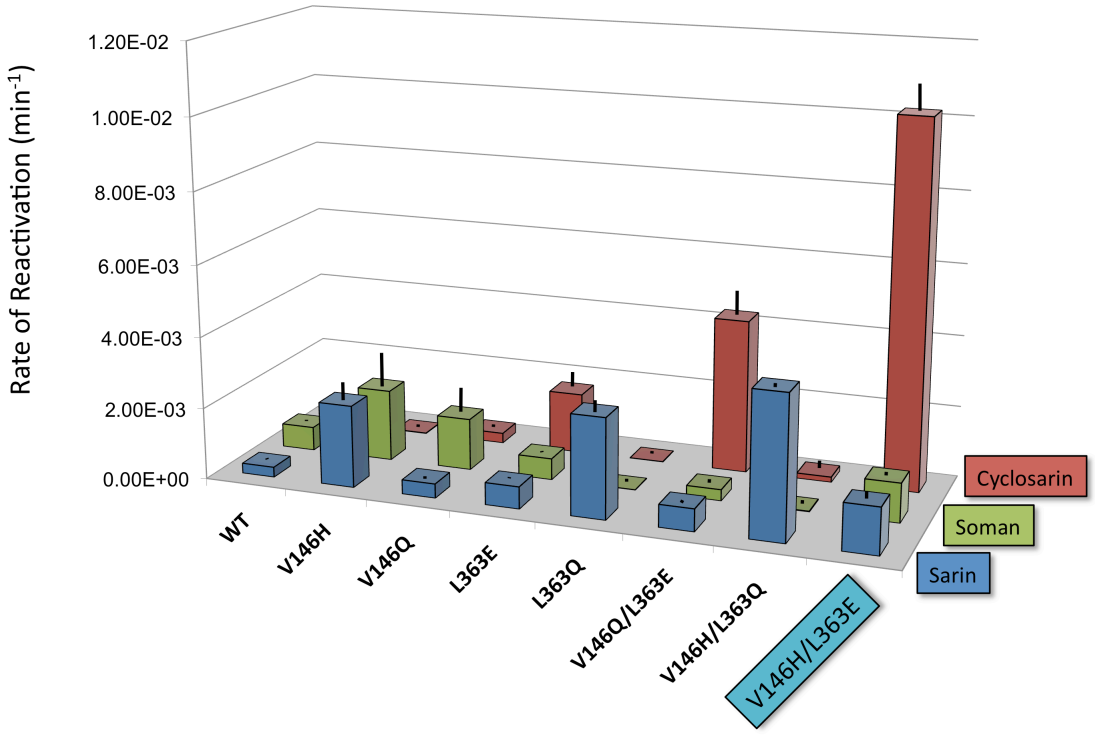

Figure 3.5 Rates of spontaneous reactivation for control mutants. V146H and L363Q recover following sarin and soman inhibition, but cannot hydrolyze cyclosarin. L363E can spontaneously reactivate following cyclosarin inhibition, but slowly recovers after sarin and soman exposure. V146Q/L363E may assist in stabilizing the carboxylate base, but the synergistic combination of V146H/L363E exhibits broad-spectrum nerve agent hydrolysis. N=3, S.E.

	k_{react} (min^{-1})	A_{max} (%)	Adjusted k_{react} (min^{-1})	Fold enhancement (WT/MUT)
WT	$2.8 \pm 0.5 \times 10^{-4}$	84 ± 6	$2.4 \pm 0.6 \times 10^{-4}$	-
V146H	$2.3 \pm 0.5 \times 10^{-3}$	86 ± 3	$2.0 \pm 0.5 \times 10^{-3}$	8
V146Q	$4 \pm 1 \times 10^{-4}$	80 ± 8	$3 \pm 1 \times 10^{-4}$	1
L363E	$6.2 \pm 0.2 \times 10^{-4}$	75 ± 8	$4.6 \pm 0.6 \times 10^{-4}$	2
L363Q	$2.8 \pm 0.2 \times 10^{-3}$	51 ± 2	$1.4 \pm 0.2 \times 10^{-4}$	6
V146H/L363Q	$4.0 \pm 0.1 \times 10^{-3}$	65 ± 7	$2.6 \pm 0.4 \times 10^{-3}$	14
V146Q/L363E	$6.3 \pm 0.7 \times 10^{-4}$	90 ± 3	$5.7 \pm 0.8 \times 10^{-4}$	2
V146H/L363E	$1.3 \pm 0.2 \times 10^{-3}$	93 ± 3	$1.2 \pm 0.2 \times 10^{-3}$	5

Table 3.2 Reactivation kinetics by hCE1 mutants following sarin inhibition. pH 7.4, 25°C, N=3, S.E. Adjusted k_{react} = (k_{react} x A_{max}) / 100, Fold enhancement = Adjusted k_{react} Mut / Adjusted k_{react} WT

N.R. is no-reactivation (<1 x 10^{-5} min^{-1}), [a](*7*)

	k_{react} (min^{-1})	A_{max} (%)	Adjusted k_{react} (min^{-1})	Fold enhancement (WT/MUT)
WT	$7 \pm 3 \times 10^{-4}$	8 ± 1	$5 \pm 3 \times 10^{-5}$	-
V146H	$2 \pm 1 \times 10^{-3}$	10 ± 1	$2 \pm 1 \times 10^{-4}$	4
V146Q	$1.5 \pm 0.7 \times 10^{-3}$	16 ± 2	$2 \pm 1 \times 10^{-4}$	4
L363E	$6 \pm 1 \times 10^{-4}$	66 ± 8	$4 \pm 1 \times 10^{-4}$	7
L363Q	N.R.	N.R.	N.R.	N.R.
V146H/L363Q	N.R.	N.R.	N.R.	N.R.
V146Q/L363E	$3.1 \pm 0.5 \times 10^{-4}$	82 ± 5	$2.6 \pm 0.5 \times 10^{-4}$	5
V146H/L363E	$1.1 \pm 0.1 \times 10^{-3}$	91 ± 3	$1.0 \pm 0.1 \times 10^{-3}$	19

Table 3.3 Reactivation kinetics by hCE1 mutants following soman inhibition. pH 7.4, 25°C, N=3, S.E. Adjusted k_{react} = (k_{react} x A_{max}) / 100, Fold enhancement = Adjusted k_{react} Mut / Adjusted k_{react} WT

N.R. is no-reactivation (< 1×10^{-5} min^{-1}), [a](*7*)

	k_{react} (min^{-1})	A_{max} (%)	Adjusted k_{react} (min^{-1})	Fold enhancement (WT/MUT)
WT	N.R.	N.R.	N.R.	-
V146H	$1.5 \pm 0.1 \times 10^{-5}$	21 ± 3	$3.2 \pm 0.6 \times 10^{-6}$	16
V146Q	$2.8 \pm 0.7 \times 10^{-4}$	12 ± 1	$3 \pm 1 \times 10^{-5}$	171
L363E	$1.7 \pm 0.4 \times 10^{-3}$	100 ± 8	$1.9 \pm 0.5 \times 10^{-3}$	9,300
L363Q	N.R.	N.R.	N.R.	-
V146H/L363Q	N.R.	N.R.	N.R.	-
V146Q/L363E	$4.3 \pm 0.4 \times 10^{-3}$	100 ± 2	$4.3 \pm 0.4 \times 10^{-3}$	21,500
V146H/L363E	$1.02 \pm 0.07 \times 10^{-2}$	95 ± 3	$9.7 \pm 0.9 \times 10^{-3}$	48,700

Table 3.4 Reactivation kinetics by hCE1 mutants following cyclosarin inhibition. pH 7.4, 25°C, N=3, S.E. Adjusted k_{react} = (k_{react} x A_{max}) / 100, Fold enhancement = Adjusted k_{react} Mut / Adjusted k_{react} WT

N.R. is no-reactivation (< 1×10^{-5} min^{-1}), [a](*7*)

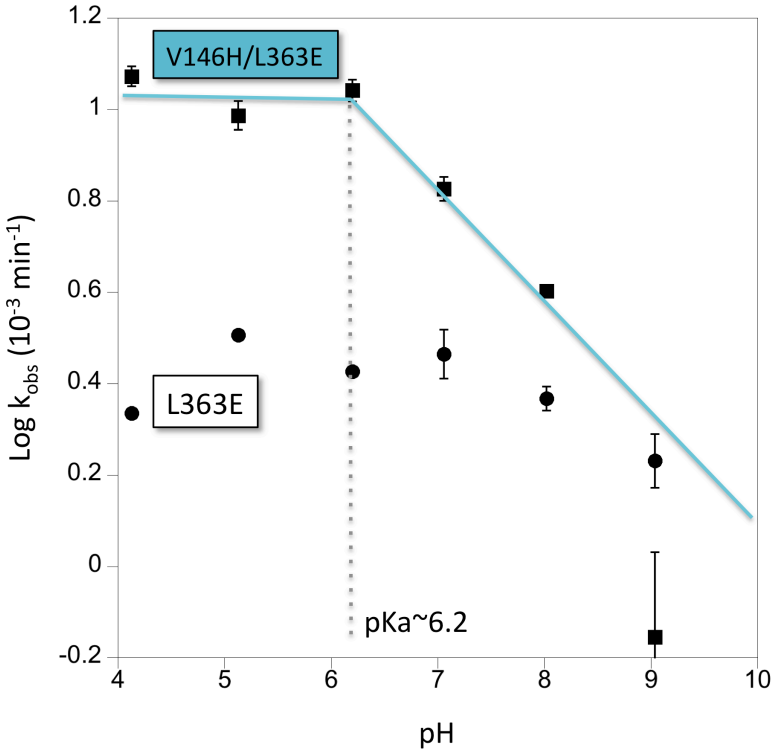

Figure 3.6 pH profile for spontaneous cyclosarin hydrolysis by V146H/L363E hCE1. The reactivation profile of V146H/L363E hCE1 against cyclosarin from pH 4 to 10 has a sharp inflection point at pH 6.2. This corresponds with the pKa of H146. The pKa of E363 is below pH 4 and therefore not accessible by this experiment. These data show that the most active form of the mutant enzyme for cyclosarin hydrolysis is when E363 is deprotonated and H146 is charged. H146 hCE1 exhibited no reactivation following cyclosarin inhibition. N=3, S.E.

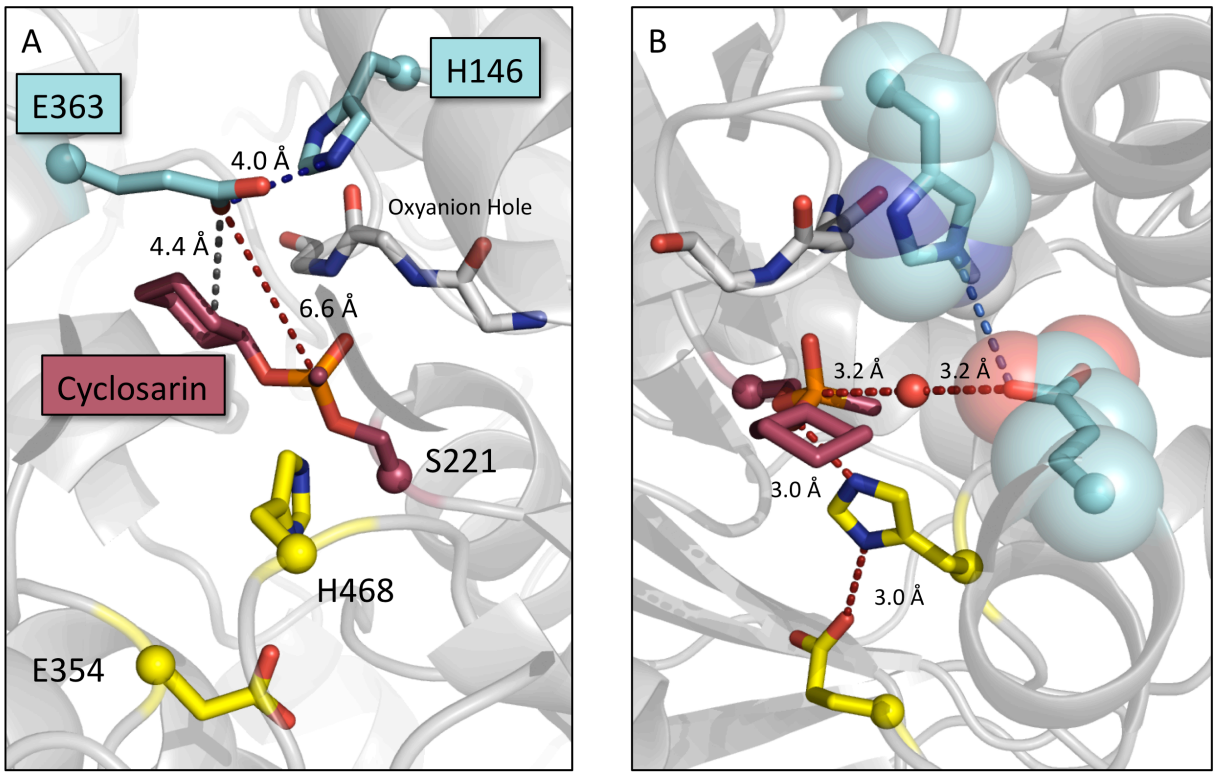

Figure 3.7 Energy minimized structures of V146H/L363E hCE1 mutant with cyclosarin.

A) The mutated E363 and H146 sit above the active site pocket. E363 Oε1 forms an N-O bridge (4 Å) with Nε2 of H146 and is 4.4 Å away from the cyclosarin cyclohexyl ring. B) View rotated by ~90°, E363 is 6.6 Å away from the phosphate center, a modeled water can fit 3.2 Å away from the key atoms. Atomic surface shown.

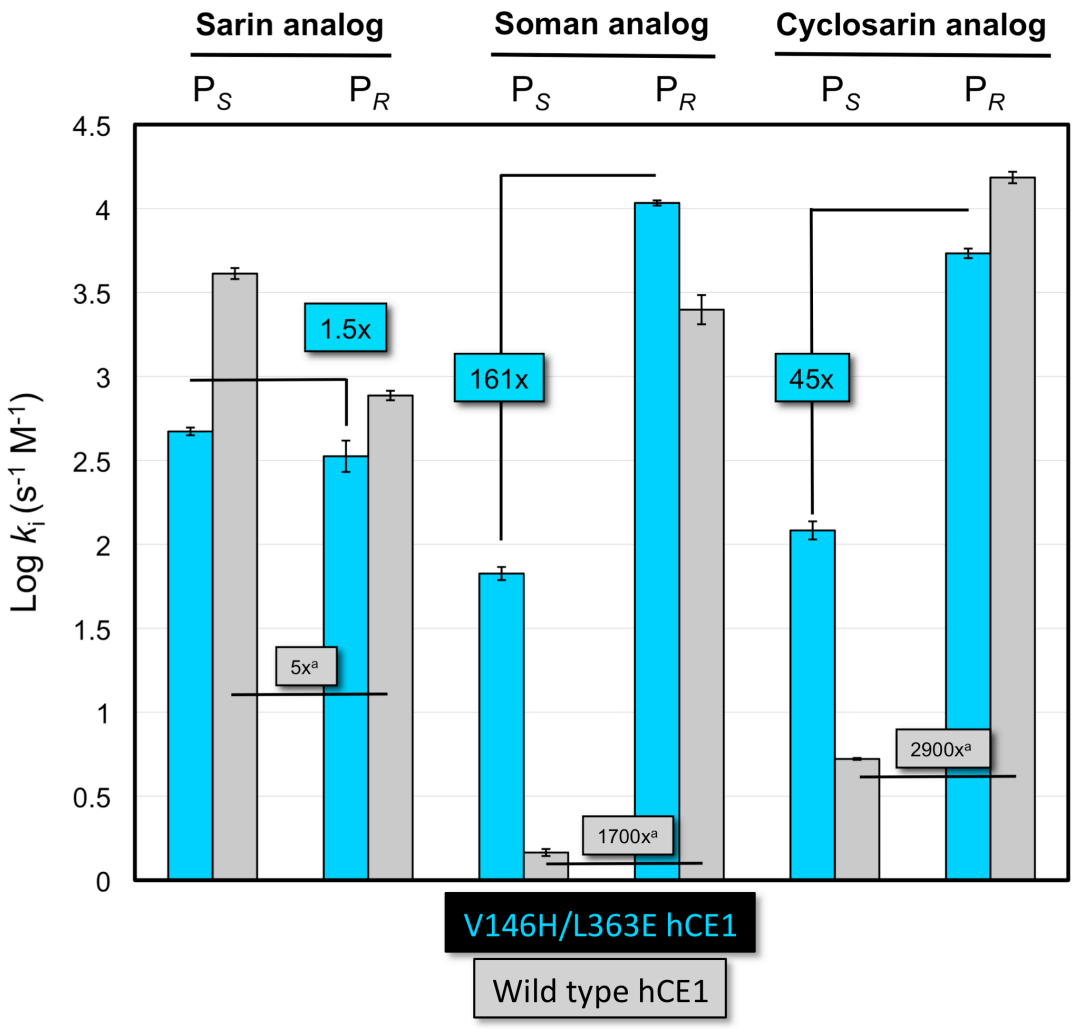

Figure 3.8. Bimolecular rate constants of inhibition for V146H/L363E with thiomethylated OP nerve agent analogs. The P_R/P_S ratios for V146H/L363E with soman and cyclosarin analogs are greatly reduced compared to WT enzyme, suggesting that these mutations have enhanced P_S binding affinity [a](*7*).

Analog Type		k_i (s^{-1} M^{-1})	k_i MUT / k_i WT[a]	K_d (M)	k_2 (s^{-1})	P_R/P_S
Sarin	P_S	470 ± 20.0	0.11	$9 \pm 1 \times 10^{-7}$	$4 \pm 1 \times 10^{-4}$	1.5
	P_R	340 ± 70.0	0.43	$3.5 \pm 0.8 \times 10^{-6}$	$1.2 \pm 0.3 \times 10^{-3}$	
Soman	P_S	67 ± 6.0	46	$8 \pm 2 \times 10^{-6}$	$5.1 \pm 0.1 \times 10^{-4}$	161
	P_R	$1.08 \pm 0.04 \times 10^{4}$	4	$1.01 \pm 0.05 \times 10^{-7}$	$1.40 \pm 0.01 \times 10^{-5}$	
Cyclosarin	P_S	121 ± 15.0	23	$5.2 \pm 0.7 \times 10^{-6}$	$6.3 \pm 0.3 \times 10^{-4}$	45
	P_R	$5.4 \pm 0.4 \times 10^{3}$	0.35	$9.5 \pm 0.6 \times 10^{-8}$	$5.1 \pm 0.4 \times 10^{-4}$	

Table 3.5 Inhibition constants of V146H/L363E hCE1 with nerve agent analogs. The bimolecular rates of inhibition (k_i) are similar in magnitude to WT [a](*7*). V146H/L363E hCE1 exhibits smaller dissociation constants (K_d) than WT, but slightly slower rates of phosphonylation (k_2).

Natural Enzyme	Designed Activity	Mutation(s)	Enzymatic Efficiency ($M^{-1}s^{-1}$)
Butyrylcholinesterase	Soman hydrolysis[a]	G117H/E197Q	0.11
Glutathione Transferase A1-1	Thioester hydrolysis[b]	A216H	2.60
4-Oxalocrotonate Tautomerase	Oxaloacetate decarboxylase[c]	P1A	114
Phospho(serine/threonin/tyrosine) Binding Protein	Phosphatase activity[c]	G120C	490
Cyclophilin	Protease activity[c]	A91S/F104H/ N106D	1675
Human Carboxylesterase 1	Cyclosarin hydrolysis	V146H/L363E	1789

Table 3.6 Enzymatic efficiency of rational designed enzymes. The designed V146H/L363E hCE1 mutant is the most efficient rationally designed enzyme towards a hemisubstrate. The above listed rationally designed enzymes are other examples where the natural protein bound the desired substrate, but was not capable of performing the designed activity. [a](*9*), [b](*24*), [c](*26*)

REFERENCES

1. Aharoni, A., Gaidukov, L., Khersonsky, O., Mc, Q. G. S., Roodveldt, C., and Tawfik, D. S. (2005) The 'evolvability' of promiscuous protein functions, *Nat Genet 37*, 73-76.

2. Redinbo, M. R., and Potter, P. M. (2005) Mammalian carboxylesterases: from drug targets to protein therapeutics, *Drug Discov Today 10*, 313-325.

3. Shen, T., Tai, K., Henchman, R. H., and McCammon, J. A. (2002) Molecular dynamics of acetylcholinesterase, *Acc Chem Res 35*, 332-340.

4. Lenz, D. E., Broomfield, C. A., Yeung, D., Masson, P., Maxwell, D. M., and Cerasoli, D. M. (2008) Nerve Agent Bioscavengers: Progress in Development of a New Mode of Protection against Organophosphorus Exposure, in *Chemical Warfare Agents: Chemistry, Pharmacology, Toxicology, and Therapeutics* (Romano Jr., J. A., Lukey, B. J., and Salem, H., Eds.) 2nd ed., CRC Press, Boca Raton, FL.

5. Millard, C. B., Lockridge, O., and Broomfield, C. A. (1995) Design and expression of organophosphorus acid anhydride hydrolase activity in human butyrylcholinesterase, *Biochemistry 34*, 15925-15933.

6. Fleming, C. D., Edwards, C. C., Kirby, S. D., Maxwell, D. M., Potter, P. M., Cerasoli, D. M., and Redinbo, M. R. (2007) Crystal structures of human carboxylesterase 1 in covalent complexes with the chemical warfare agents soman and tabun, *Biochemistry 46*, 5063-5071.

7. Hemmert, A., Otto, M. F., Wierdl, M., Edwards, C. C., Fleming, C. D., MacDonald, M., Cashman, J. R., Potter, P. M., Cerasoli, D. M., and Redinbo, M. R. (2010) Human Carboxylesterase 1 Stereoselectively Binds the Nerve Agent Cyclosarin and Spontaneously Hydrolyzes the Nerve Agent Sarin, *Molecular Pharmacology IN PRESS*.

8. Denu, J. M., and Dixon, J. E. (1998) Protein tyrosine phosphatases: mechanisms of catalysis and regulation, *Curr Opin Chem Biol 2*, 633-641.

9. Millard, C. B., Lockridge, O., and Broomfield, C. A. (1998) Organophosphorus acid anhydride hydrolase activity in human butyrylcholinesterase: synergy results in a somanase, *Biochemistry 37*, 237-247.

10. Lenz, D. E., Yeung, D., Smith, J. R., Sweeney, R. E., Lumley, L. A., and Cerasoli, D. M. (2007) Stoichiometric and catalytic scavengers as protection against nerve agent toxicity: a mini review, *Toxicology 233*, 31-39.

11. Voet, D., Voet, J. G., and Pratt, C. W. (2002) *Fundamentals of Biochemistry upgrade*, Upgrade Edition ed., John Wiley & Sons, Inc., New York.

12. Chen, V. B., Arendall, W. B., 3rd, Headd, J. J., Keedy, D. A., Immormino, R. M., Kapral, G. J., Murray, L. W., Richardson, J. S., and Richardson, D. C. (2009) MolProbity: all-atom structure validation for macromolecular crystallography, *Acta Crystallogr D Biol Crystallogr 66*, 12-21.

13. Dunbrack, R. L., Jr., and Cohen, F. E. (1997) Bayesian statistical analysis of protein side-chain rotamer preferences, *Protein Sci 6*, 1661-1681.

14. Shortle, D. (2003) Propensities, probabilities, and the Boltzmann hypothesis, *Protein Sci 12*, 1298-1302.

15. Kumar, S., and Nussinov, R. (1999) Salt bridge stability in monomeric proteins, *J Mol Biol 293*, 1241-1255.

16. Kumar, S., and Nussinov, R. (2002) Relationship between ion pair geometries and electrostatic strengths in proteins, *Biophys J 83*, 1595-1612.

17. Kumar, S., and Nussinov, R. (2002) Close-range electrostatic interactions in proteins, *Chembiochem 3*, 604-617.

18. Aurbek, N., Thiermann, H., Szinicz, L., Eyer, P., and Worek, F. (2006) Analysis of inhibition, reactivation and aging kinetics of highly toxic organophosphorus compounds with human and pig acetylcholinesterase, *Toxicology 224*, 91-99.

19. Wolfenden, R. (2006) Degrees of difficulty of water-consuming reactions in the absence of enzymes, *Chem Rev 106*, 3379-3396.

20. Forsberg, A., and Puu, G. (1984) Kinetics for the inhibition of acetylcholinesterase from the electric eel by some organophosphates and carbamates, *Eur J Biochem 140*, 153-156.

21. Brik, A., D'Souza, L. J., Keinan, E., Grynszpan, F., and Dawson, P. E. (2002) Mutants of 4-oxalocrotonate tautomerase catalyze the decarboxylation of oxaloacetate through an imine mechanism, *Chembiochem 3*, 845-851.

22. Quemeneur, E., Moutiez, M., Charbonnier, J. B., and Menez, A. (1998) Engineering cyclophilin into a proline-specific endopeptidase, *Nature 391*, 301-304.

23. Wishart, M. J., Denu, J. M., Williams, J. A., and Dixon, J. E. (1995) A single mutation converts a novel phosphotyrosine binding domain into a dual-specificity phosphatase, *J Biol Chem 270*, 26782-26785.

24. Hederos, S., Broo, K. S., Jakobsson, E., Kleywegt, G. J., Mannervik, B., and Baltzer, L. (2004) Incorporation of a single His residue by rational design enables thiol-ester hydrolysis by human glutathione transferase A1-1, *Proc Natl Acad Sci U S A 101*, 13163-13167.

25. Khersonsky, O., Rothlisberger, D., Dym, O., Albeck, S., Jackson, C. J., Baker, D., and Tawfik, D. S. (2009) Evolutionary Optimization of Computationally Designed Enzymes: Kemp Eliminases of the KE07 Series, *J Mol Biol 28*, 28.

26. Toscano, M. D., Woycechowsky, K. J., and Hilvert, D. (2007) Minimalist active-site redesign: teaching old enzymes new tricks, *Angew Chem Int Ed Engl 46*, 3212-3236.

Chapter 4. Novel Enzyme-Based Nerve Agent Identification Device

4.1 Nerve Agent Detection

Military warfighters and HAZMAT emergency first responders are trained to recognize the signs and symptoms of nerve agent exposure. These acetylcholine based muscarinic and nicotinic effects are best described by the nemonic SLUDGE (salivation, lacrimation, urination, defecation, gastrointestinal pains, and emesis). The onset and intensity of these conditions, determined by route and length of exposure, can be partially mitigated by post-exposure therapies. As described in Chapter 1.4, current treatments for OP poisoning include injections of atropine and a critical strong-nucleophile oxime (*1*). One deficiency of this therapy however is that there is no broad-spectrum oxime. For example 2-PAM can reactivate AChE inhibited by sarin or the V-agents, while another oxime, Obidoxime, is only effective against sarin, tabun, and the V-agents (*2*). Between the four oximes currently suitable for therapeutic use, exposure to G- or V-agents can all be effectively treated **(Figure 4.1)** (*2*). Thus, to utilize the already available oximes, it is essential to accurately and quickly identify the specific nerve agent(s) present in an attack.

The current point nerve agent identification technologies employed by the U.S. military and HAZMAT first-responders include electronic and colorimetric detectors (*3-5*). Electronic devices, such as the JCAD produced by Smiths Detection, utilizes Differential Ion

Mobility Spectroscopy (DMS) to detect and identify chemical agent vapors. These devices are effective at identifying low levels of toxins, but are costly, bulky, require external power, and constant calibration (*4*). Colorimetric detectors such as the M256A1 kit, M8/M9 paper, or Agentase CAD-kit are no-power methods to detect chemical agents, but cannot distinguish between different nerve agents and are known to suffer from a high rates of false positives (*3*). The read-out on these colorimetric devices only discriminates between G- and V-agents, thereby significantly limiting administration of the best oxime antidote. An ideal device would provide robust, rapid, no power and cost-effective identification of specific nerve agents.

4.2 hCE1 Mutants for Nerve Agent Detection

Despite the impressive increases in spontaneous rates of reactivation with the designed hCE1 mutants, these enzymes are still too slow to be utilized as effective bioscavengers. Indeed, even with the 48,700-fold increase in cyclosarin hydrolysis, the V146H/L363E hCE1 mutant would still only behave as a stoichiometric bioscavenger, regenerating every hour. Additionally, because of the intrinsic active site architecture, these hCE1 mutants still exhibit a strong preference for the less toxic stereoisomers of most G-agents. These two factors may limit the prophylactic potential of designed hCE1 enzymes, but these mutant proteins are ideally positioned to aid in nerve agent detection and identification.

During the mutant design process it was observed that certain mutants exhibited unique hydrolytic specificity towards each agent **(Figure 4.2)**. For example V146H/L363Q hCE1 only reactivates following sarin inhibition, with a half-time of reactivation of ~2

hours, while V146H/L363E hCE1 reactivates following cyclosarin inhibition with a half-time of approximately 1 hr. Unlike the necessity of a catalytic bioscavenger to return to maximal activity after nerve agent inhibition, enzymes used for detection and identification may only partially reactivate since the rate of reactivation is the most important characteristic. Additionally, in some mutants this rate can be further enhanced through oxime assistance.

4.3 Ability of hCE1 Mutants to Identify Nerve Agent Analogs

Through a secondary colorimetric substrate assay following nerve agent inhibition, we tested the ability of the novel hCE1 mutant L97K to detect and identify nerve agent analogs. This single mutation exhibits spontaneous reactivation against *bona fide* soman, with a half time of reactivation of 73 minutes, and can also recover following sarin inhibition, ($t_{1/2} \sim 6$ hours). L97K does not reactivate following racemic cyclosarin or tabun inhibition. Using the thiomethylated nerve agent analogs, 50 µL of COS cells containing wild type or the hCE1 L97K mutant were exposed to 1 mM sarin, soman, or cyclosarin analogs. Following inhibition for 10 minutes, aliquots were diluted 1:10 into 10 mM para-nitrophenol butyrate (pNPB) at pH 7.4. hCE1 cleaves this ester substrate to release *o*-nitrophenol, a small molecule that absorbs light in the visible spectrum. Analytically, this hydrolysis event is measured through absorbance at 410 nm, while qualitatively the sample will turn yellow. Differences in color change could be observed 30 seconds after colorimetric substrate addition for soman and sarin analogs **(Figure 4.3)**. This rapid color change may either be attributed to the L97K mutant hydrolyzing sarin and soman analogs, or the mutant was poorly inhibited compared to wild type enzyme.

4.4 Detection Limits of hCE1 Mutants

One challenge with current protein-based nerve agent detection devices is that the enzyme catalyzed colorimetric readout can be swamped out by excess OP sample. With the above-mentioned thiomethylated nerve agent analogs we determined the detection range of the V146H/L363Q hCE1 mutant with sarin, soman, and cyclosarin analogs. Fifty μL of COS enzyme containing sample was inhibited with nerve agent analog concentrations ranging from 10 μM to 4 mM for 10 minutes, prior to 10 mM pNPB substrate addition. These analogs have previously been shown to form identical adducts to OP nerve agents (*6*) but as previously mentioned, have 1,000-fold reduced potency stemming from the slower rates of phosphonylation (k_2) (*7*). As shown in **Figure 4.4** the V146H/L363Q mutant optimally differentiates between nerve agent analogs from 10 μM to 1 mM, suggesting that *bona fide* agents should be detected between 10 nM to 1 μM, below or near the nerve agent LD_{50} (800 nM) (*8*).

4.5 Mutant Incorporation in Nerve Agent Identifying Device

We are currently working on entrapping these mutant enzymes for a small, hand-held device that requires no power to detect and identify various agents. A spatially separated array should enable the identification of all known nerve agents. As illustrated in **Figure 4.5**, each OP will have a unique visual readout. V146H/L363Q will reactivate sarin, L97K will identify soman, and V146H/L363E hydrolyzes cyclosarin. AChE will also be incorporated into the device to enable VX and tabun detection. As described in **Chapter 2.5**, hCE1 does not react with VX; therefore each of the hCE1 mutants will remain available for substrate hydrolysis, while AChE will be inhibited. Lastly, all the enzymes are inhibited by tabun, but

inclusion of the oxime obidoxime into the buffer solution will rapidly reactivate AChE. As previously mentioned hCE1 does not interact with this charged oxime.

4.6 Summary

With this technology in mind, we recently incorporated Identizyme Defense Technologies, and applied for a Department of Defense Phase I SBIR grant to further fund the development of this device. The storage and operational conditions, effects of field interferents on detection, and detection/identification range against *bona fide* agents still need to be tested. We anticipate that this type of device can replace the antiquated M256A1 chemical agent detection kit currently used by the U.S. military. The University of North Carolina at Chapel Hill has filed a provisional U.S. patent for these enzymes and their use for nerve agent and pesticide detection (USSN: 61/267,591)

4.7 Figures and Tables

Figures are listed in the same order they appear in the text of chapter 4.

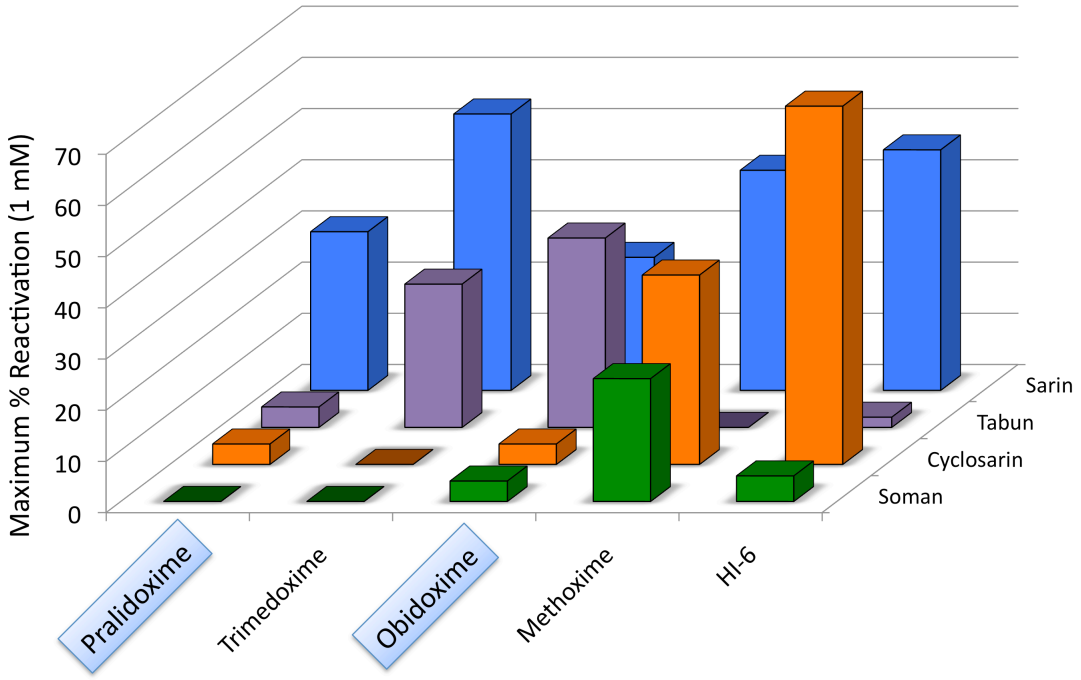

Figure 4.1 Comparison of oxime efficacy for acetylcholinesterase reactivation. Current administered oximes for nerve agent exposure include pralidoxime and obidoxime. As illustrated however, these oximes are ineffective against soman or cyclosarin. Additionally, there is no broad-spectrum oxime (*2*). Identification of a given agent could facilitate administration of the most effective antidote.

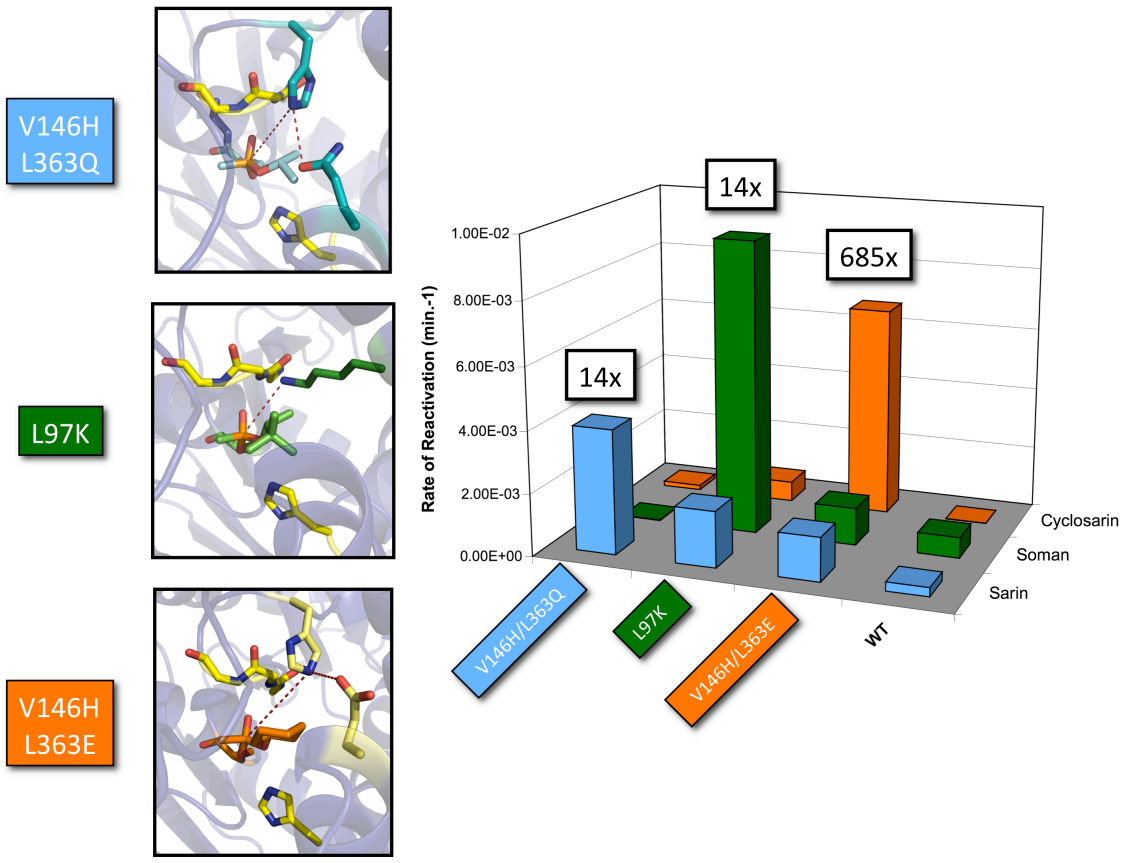

Figure 4.2 Spontaneous rates of reactivation of hCE1 mutants towards G-agents. The mutants V146H/L363Q, L97K, and V146H/L363E all exhibit unique rates of reactivation against each G-agent. V146H/L363Q reactivates after sarin inhibition, L97K rapidly recovers after soman exposure, and V146H/L363E can hydrolyze cyclosarin. These mutations are shown modeled into the hCE1 active site.

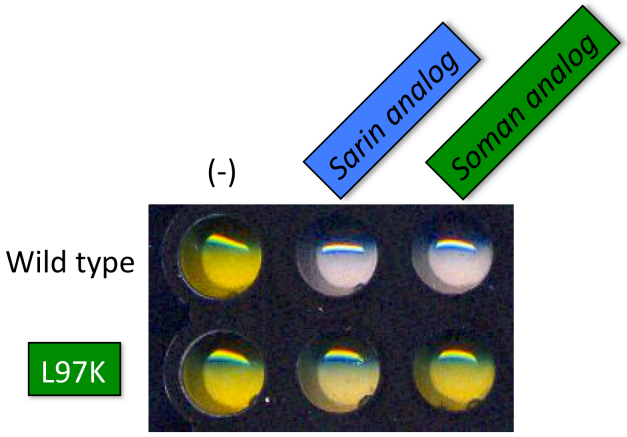

Figure 4.3 Nerve agent analog identification by hCE1 mutant. Following a 10 minute incubation with either sarin or soman nerve agent analogs, there is a clear visual difference wild type and L97K hCE1 to hydrolyze pNPB. This scan was taken 30 seconds after pNPB addition. No inhibitor was present in (-). Soman identification by L97K may either be from OP analog hydrolysis or lack of mutant inhibition in the 10 minute exposure.

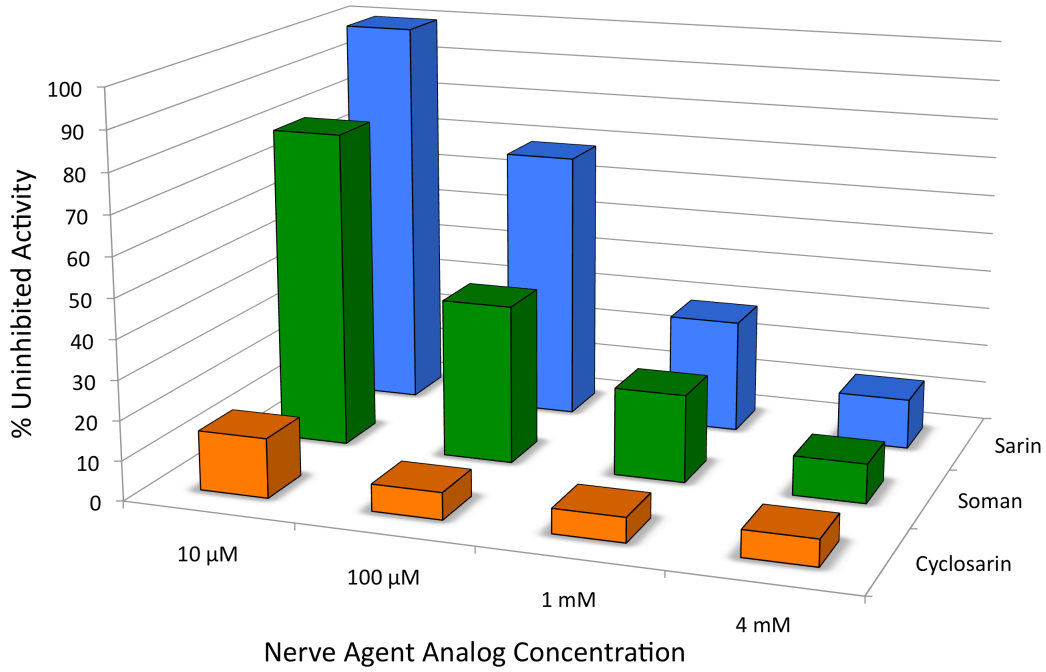

Figure 4.4 Detection and identification range of hCE1 with nerve agent analogs. The hCE1 mutant V146H/L363Q can detect and differentiate between nerve analogs most effectively at 100 µM. Due to the thiomethyl leaving group, these analogs are ~1000x less potent inhibitors of esterases (*7*), suggesting that the hCE1 mutant will be able to identify nerve agents below one LD_{50} (800 nM (*8*)).

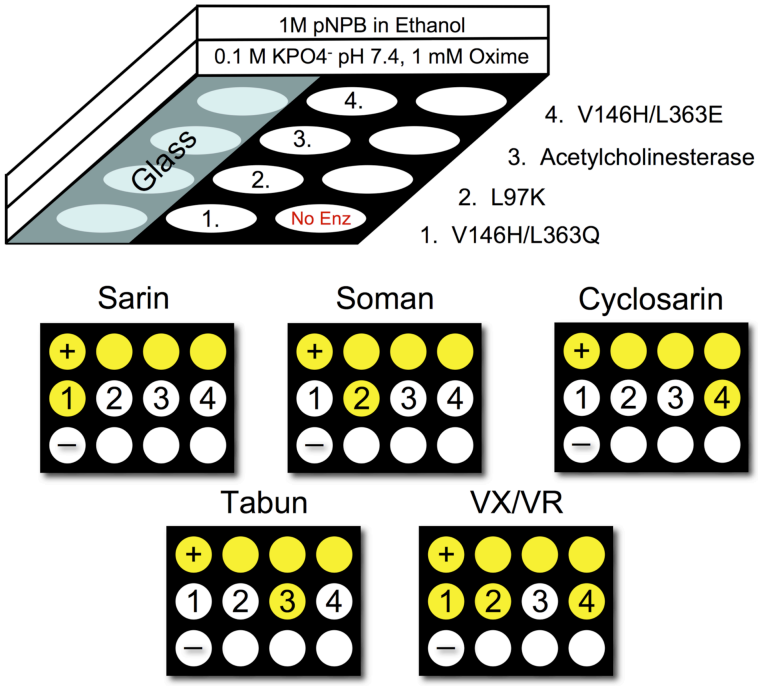

Figure 4.5 Enzyme-based nerve agent identifying device. By spatially separating the various hCE1 mutants along with acetylcholinesterase, we could generate a no-power device that may rapidly detect and identify all known OP nerve agents. Such a device could enable efficient identification and antidote administration.

REFERENCES

1. Gray, A. P. (1984) Design and structure-activity relationships of antidotes to organophosphorus anticholinesterase agents, *Drug Metab Rev 15*, 557-589.

2. Kuca, K., Jun, D., and Bajgar, J. (2007) Currently used cholinesterase reactivators against nerve agent intoxication: comparison of their effectivity in vitro, *Drug Chem Toxicol 30*, 31-40.

3. Seto Y, K.-K. M., Kouichiro T, Ohsawa I, Matsushita K, Sekiguchi H, Itoi T, Iura K, Sano Y, Yamashiro S. (2005) Sensing technology for chemical-warfare agents and its evaluation using authentic agents, *Sensors and Actuators B 108*, 193-197.

4. Hill, H. H., Martin S.J. (2002) Conventional analytical methods for chemical warefare agents, *Pure Appl. Chem. 74*, 2281-2291.

5. Program, D. o. D. C. a. B. D. (2009) Annual Report to Congress.

6. Gilley, C., MacDonald, M., Nachon, F., Schopfer, L. M., Zhang, J., Cashman, J. R., and Lockridge, O. (2009) Nerve agent analogues that produce authentic soman, sarin, tabun, and cyclohexyl methylphosphonate-modified human butyrylcholinesterase, *Chem Res Toxicol 22*, 1680-1688.

7. Hemmert, A., Otto, M. F., Wierdl, M., Edwards, C. C., Fleming, C. D., MacDonald, M., Cashman, J. R., Potter, P. M., Cerasoli, D. M., and Redinbo, M. R. (2010) Human Carboxylesterase 1 Stereoselectively Binds the Nerve Agent Cyclosarin and Spontaneously Hydrolyzes the Nerve Agent Sarin, *Molecular Pharmacology IN PRESS*.

8. Lenz, D. E., Broomfield, C. A., Yeung, D., Masson, P., Maxwell, D. M., and Cerasoli, D. M. (2008) Nerve Agent Bioscavengers: Progress in Development of a New Mode of Protection against Organophosphorus Exposure, in *Chemical Warfare Agents: Chemistry, Pharmacology, Toxicology, and Therapeutics* (Romano Jr., J. A., Lukey, B. J., and Salem, H., Eds.) 2nd ed., CRC Press, Boca Raton, FL.

Chapter 5. Structural and Biochemical Differences of Mammalian Carboxylesterases

5.1 Mammalian Carboxylesterases

Human carboxylesterase 1 (hCE1) is a primary hydrolytic drug-metabolizing enzyme found in the liver (*1*). This serine hydrolase, however, is only one of many mammalian carboxylesterases. Even though these promiscuous enzymes bind a wide range of xenobiotics and catalyze hydrolytic and transesterification reactions, they also exhibit unique catalytic rates for these various compounds (*2*). For example, human intestinal carboxylesterase (hiCE) hydrolyzes the ester prodrug, Irinotecan (CPT-11), 90 times more efficiently than hCE1 (*3*). This chemotherapeutic is cleaved to form 7-ethyl-10-hydroxycamptothecin (SN-38), a potent topoisomerase inhibitor (*4*). Additionally, the rat serum carboxylesterase (rsCE) exhibits 15-fold faster rates of spontaneous reactivation against organophosphate (OP) nerve agents than hCE1 (*5*).

As we and others have shown, these enzymes are robust to mutations, many of which can enhance catalytic activity (*3, 6*). Indeed, as presented in Chapter 3, two mutations in hCE1 increased the rate of reactivation after OP inhibition above that measured with rsCE. Also, by altering 7 amino acids in hCE1, researchers were able to enhance CPT-11 hydrolysis in this enzyme to hiCE levels (*3*). To understand the structural constraints that lead to differing CE activities we performed multiple sequence

alignments across a range of human and rodent carboxylesterases to identify functionally essential differences.

5.2 Liver carboxylesterase acyl-loop identification

All mammalian carboxylesterases belong to the α/β serine hydrolase superfamily, and share the conserved beta-sheet backbone surrounded by helices and loops (*7*). As shown in **Figure 5.1**, sequence alignments of multiple mammal carboxylesterase, both from liver and serum, reveal three diverging sequence clusters (GenBank accession numbers hCE1 AAA35649, rabbit liver CE AAC3925, rat liver CE CAA46391, mouse liver CE CAA73388, mouse serum CE AAA63297, rsCE CAA55241, and hiCE CAA70831). These are the 18-residues N-terminal signal peptide, a 15-residue section in the middle of the protein alignment, and the 4-residue ER retention sequence. The initial and latter sequences determine cellular localization and retention and will be different for each protein (*7, 8*), but the 15-residue difference between the liver and serum/intestinal CEs is unique. It is worth noting that human do not express a serum carboxylesterase, which can be attributed to the conserved KDEL like C-retention sequence (HIEL in hCE1, HTEL in hiCE) (*8*). Both the rat and mouse serum CEs have non-retaining sequences (TEHK) (*9*).

As shown in the hCE1-soman crystal structure (RSCB PDB 2HRQ), these 15 residues correspond to a long, flexible loop that covers the top of the active site **(Figure 5.2)** (*10*). This loop has been termed the acyl-loop, based on interactions with acyl-enzyme intermediates in AChE and BChE (*10*). In these cholinesterases the acyl-loop dips into the active site pocket, while in hCE1 it covers the top, like a lid on a can. The

only existing mammalian carboxylesterase crystal structures are for hCE1 and rCE, both of which contain these 15 residues, although it was disordered in rCE. This region typically exhibits high crystallographic temperature factors, and was also completely disordered in the hCE1-cyclosarin model (*6, 11*). To understand the structural significance of this loop we utilized InsightII (Acclerys, San Diego) and hCE1 as a template, and constructed a homology model of rsCE and hiCE, both of which do not contain the acyl-loop. These enzymes share 68% and 42% sequence homology with hCE1, respectively. As shown in **Figure 5.3,** without the acyl loop, the active site opening of rsCE is significantly larger than hCE1. Based on this observation, we hypothesized that this enhanced entrance might facilitate the unique catalytic activities observed in non-loop containing enzymes compared to hCE1.

5.3 hCE1 acyl-loop deletion

To test this hypothesis, we truncated the acyl loop in wild type hCE1 and determined the effect this deletion had on enzymatic activity. Initially, by overlaying the hCE1 and rsCE models we identified appropriate deletion sites that would not affect additional secondary structure. As listed in **Table 5.1**, custom primers were designed that omitted residues 301-313 and mutated residues 314-320 to match the shorter rsCE linker. Two batches of PCR were performed, the first consisted of separate reactions of pUC9 hCE1 template plasmid replicating with either the sense or antisense primers only. The second batch combined equal volumes of each reaction to complete deletion and mutant incorporation. After PCR, template strands were digested with *Dpn1* for 1 hr. at 37^{o}C and then transformed into DH5α cells. As described in **Chapter 2.4** successful mutants

were sequence verified, cloned into the pCI-neo mammalian expression vector, and expressed in COS cells (*3*). This loop deletion and linker mutation was coined the loop deletion (LD) mutant. Based on the rsCE homology model, additional mutations were engineered into hCE1 LD, to make the hCE1 active site more "rat serum-like". As shown in **Table 5.1**, these are identified as LD_1 through LD_4.

5.4 Enzymatic Changes in hCE1 LD Mutant.

Table 5.2 reports the effect of each LD mutant on CE activity, SN-38 production, spontaneous rate of sarin hydrolysis, and rate of oxime-assisted sarin hydrolysis compares to wild type protein. Carboxylesterase activity was determined by measuring the rate of *o*-nitrophenol production per mg enzyme at 410 nm following addition of 3 mM *o*-nitrophenol acetate (oNPA), a conventional substrate. To correct for differences in CE expression within transfected COS cells, the enzyme activity values were corrected for the level of immunoreactive CE protein as determined from western blot analyses (*3*). Wild type hCE1 produces approximately 2520 ± 60 nM/min/mg. The LD hCE1 mutant reduced this rate in half and further mutations within the active site pocket reduced oNPA hydrolysis to about 3% the wild type activity. The most dramatic decrease came after the addition of L388N. This mutation is in the active site "side-door", a secondary opening to the active site that has been implicated in cocaine transesterification with ethanol or product release following CPT-11 hydrolysis (*11, 12*). It is unknown what role this side-door plays in rsCE. Since protein expression levels were normalized a reduction in carboxylesterase activity may suggest a decrease in promiscuous activity towards this substrate.

Conversion of CPT-11 into SN-38 was monitored by incubating cell extracts with 5 mM CPT-11 for 1 h in 50 mM HEPES (pH 7.4) at 37^{o}C. An equal volume of acidified methanol was added to terminate the reactions and particulate matter was removed by centrifugation at 100,000 g for 5 min at 4^{o}C. Concentrations of both drugs in the supernatant were then determined by high-performance liquid chromatography (*3*). As previously mentioned, wild type hCE1 poorly hydrolyzes CPT-11, with an average activity of 0.36 ± 0.017 nM/min/mg protein. hiCE, which is missing the acyl-loop, hydrolyzes CPT-11 approximately 90 times more efficiently (*3*). The rates of hydrolysis between these two enzymes aren't drastically different (1.49 nmol/min/mg vs. 0.36), but hiCE binds CPT-11 approximately 25 times tighter than hCE1 (3.35 μM vs. 82.8 μM) (*3*). As shown in **Table 5.2**, the loop deletion mutants enhanced the rate of SN-38 production up to 62-fold over wild type enzyme. This large increase matches a rate enhancement achieved by other researchers in mutating the hCE1 active site to be more "rabbit-liver" like (hCE1m6) (*3*).

As shown in **Figure 5.4,** two structural features are consistent among the three CPT-11 hydrolyzing enzymes (hiCE, hCE1m6, and hCE1 LD_4). These enzymes all contain an open active-site entrance, either through absence of the acyl-loop or engineered disorder, and they all exhibit a patch of polar residues near the active sites side door. Irinotecan is a large, multi-ringed, substrate covalently modifies with a dipiperdine group to enhance solubility (*4*). In order for a carboxylesterase to cleave this substrate, the solubilizing group would sit deep into the active site pocket, while the larger SN-38 moiety resides where the acyl-loop would be positioned. By removing the acyl-loop from hCE1, this space is now available to accommodate the large substrate. In

the hCE1m6 mutant, a helix adjacent to the acyl-loop was mutated to mirror a disordered loop in rCE. The second structural feature is a patch of polar resides near the active-site side door. In hiCE there is an arginine, hCE1m6 contains a glutamine, and hCE1 LD_4 has two asparagines. In hCE1m6 and hCE1 LD_4 is was only after the addition of these polar residues that maximum CPT-11 activity was achieved (*3*). These residues may be important to support the SN-38 lactone on the critical E ring, which would be positioned in that region. To support these ideas, additional measurements such as binding constant determination are required and underway.

Rates of reactivation following nerve agent inhibition were carried out as described in **Chapters 2.8 and 2.9**. Briefly, COS cell lysates expressing wild type or mutant hCE1 were incubated with ~1000-fold molar excess of racemic sarin. After confirmation of complete inhibition, excess agent was removed and samples were diluted into solutions with and without 1 mM DAM prior to activity determination relative to an uninhibited sample (*6, 10*). Removal of the acyl-loop and mutation of the hCE1 active site to resemble the rsCE did not dramatically increase the rates of spontaneous reactivation towards sarin. rsCE spontaneously reactivates after sarin inhibition 13x faster than hCE1 (*5*). These modifications did however increase the rate of oxime-assisted reactivation 15x after sarin inhibition in hCE1 LD_4 compared to wild type (*6*). The half time for reactivation of this mutant is now ~2 minutes, within the benchmark range for a catalytic bioscavenger (*13*). Removing the acyl-loop may have enhanced DAM binding by removing the a barrier into the active site. This will be confirmed by determining the Michaelis-Menton kinetics of this mutant with DAM. Additionally, we

are combining the V146H/L363E mutant with LD_4 to potentially generate a mutant that eliminates any kinetic slowdown caused by product release.

5.5 Summary

Overall these initial data suggest that the 15-residue acyl-loop lid that caps the hCE1 active plays an important role in substrate access and binding. Additional measurements need to be made to determine the kinetics effects of the loop deletion. We are the first to observe this 15-amino acid difference in esterases and are excited to finish the experiments required to build a complete story.

5.6 Figures and Tables

Figures are listed in the same order they appear in the text of chapter 5.

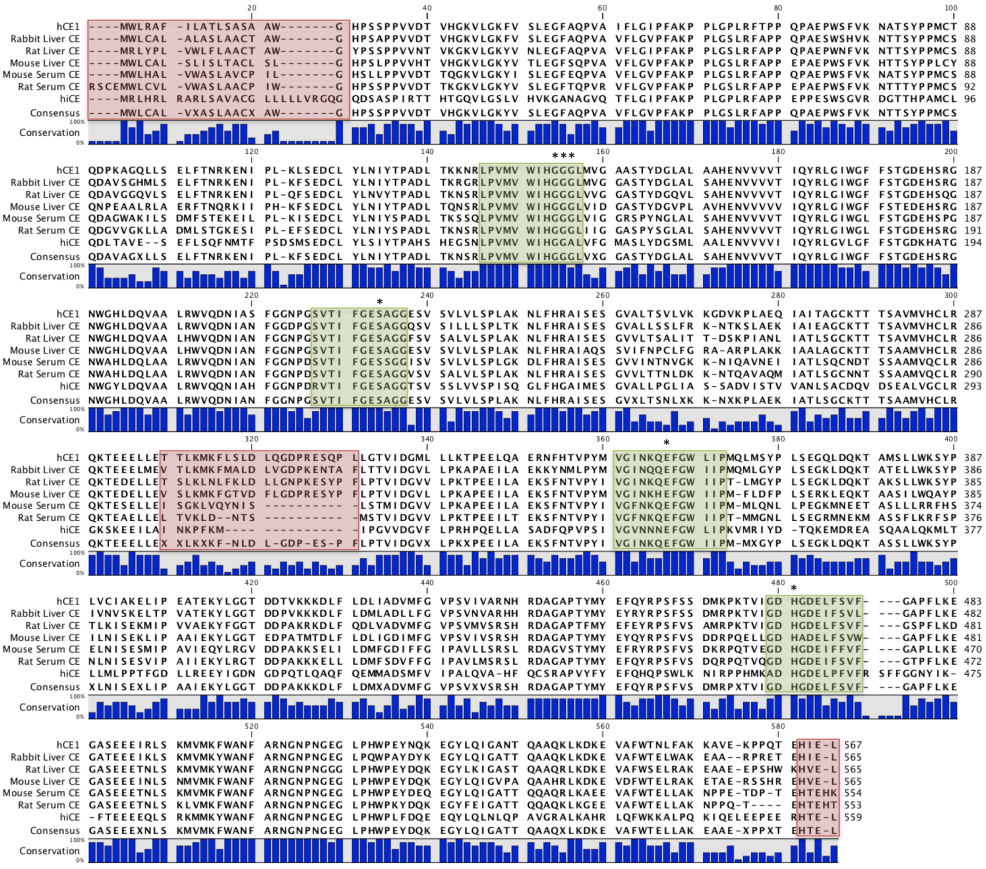

Figure 5.1 Multiple sequence alignment of mammalian carboxylesterases. From this sequence alignment of human, rabbit, rat, mouse carboxylesterases, three divergent regions can be identified (red boxes). The 18-residue N-terminal leader sequence directs newly synthesized protein to the endoplasmic reticulum (ER). Additionally the C-terminal 4-residue retention sequence either aids in retention of CE within the ER, or allows the enzyme to enter the serum. The 15-amino acid patch around residue 320 is the acyl-loop. These CEs all share high homology in the catalytic machinery (green boxes).

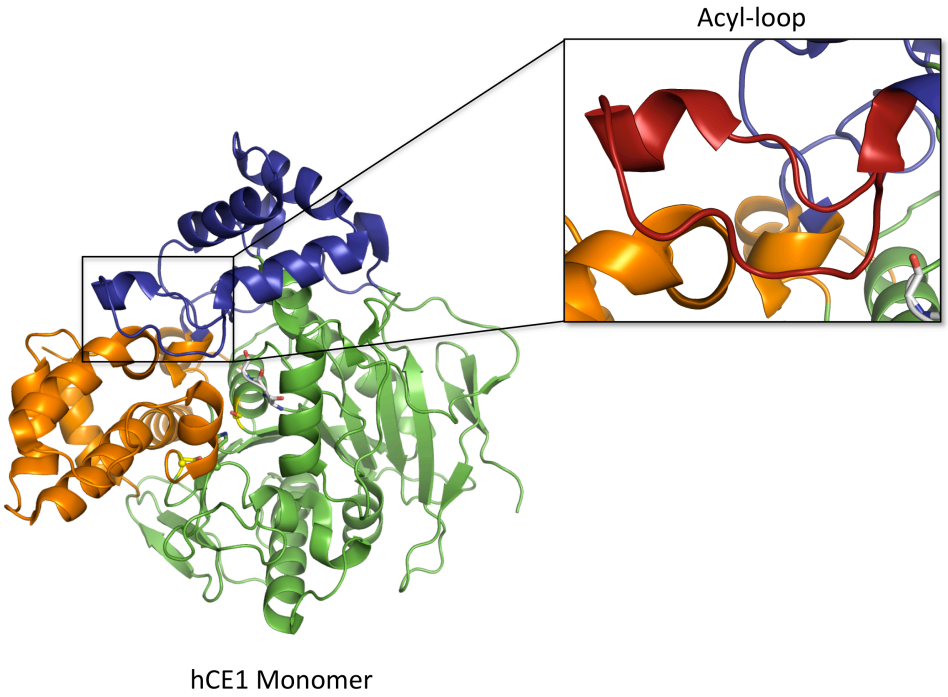

Figure 5.2 Acyl-loop in wild type hCE1. The 15-residue acyl-binding loop is positioned above the active site (red inset) and may regulate access into this cavity. This loop is found in all liver CEs, but not in serum or human intestinal enzymes.

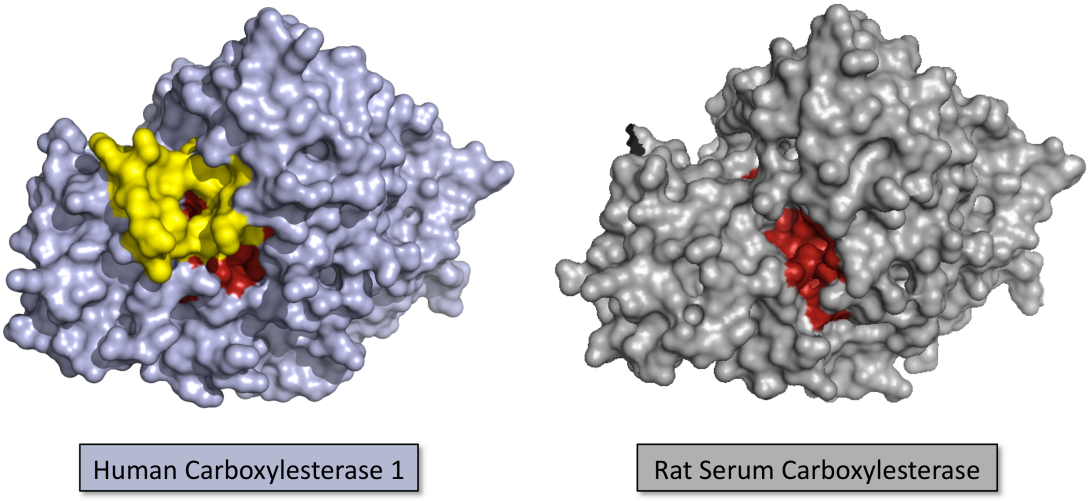

Figure 5.3 Homology model of rsCE. Rat serum carboxylesterase (rsCE) does not contain the 15-residue acyl loop (yellow) found in hCE1. Without this loop, the rsCE active site (red) is more open.

hCE1 Mutant		Designed Primer
LD	Sense	5’-ggagctcttggagacgacattgaaaCTgCAGAaCAccAGtAtgAgcactg-3’
(Δ301-313 + LDNTSMS)	Antisense	5’-cagtgcTcaTaCTggTGtTCTGcAGtttcaatgtcgtctccaagagctcc-3’
LD_1	Sense	5’-gtggcgtggccctcacttctAAtctggtgaagaaaggtgatgt-3’
(LD + V254N)	Antisense	5’-acatcacctttcttcaccagaTTagaagtgagggccacgccac-3’
LD_2	Sense	5’-tcctgtggaagtcctatcccAAtgtttgcattgctaaggaact-3’
(LD_1 + L388N)	Antisense	5’-agttccttagcaatgcaaacaTTgggataggacttccacagga-3’
LD_3	Sense	5’-aagacctgttcctggacttgTtCgcagatgtgatgtttgg-3’
(LD_2 + I421F)	Antisense	5’- ccaaacatcacatctgcGaAcaagtccaggaacaggtctt-3’
LD_4	Sense	5’-cttgatagcagatgtgTtCtttggtgtcccatctgtgatt-3’
(LD_3 + M425F)	Antisense	5’- aatcacagatgggacaccaaaGaAcacatctgctatcaag -3’

Table 5.1 Custom designed primers for hCE1 LD mutants. Based on sequence alignments between hCE1 and rsCE custom primers were designed to excise the acyl-loop and include the rsCE linker. Further mutations were engineered that altered the hCE1 active site to mirror respective amino acids in rsCE.

	CE activity	SN-38 produced	Rate of Sarin Reactivation	DAM assisted hCE1 reactivation
	Fold activity compared to wild type (Mut/WT)			
hCE1	1.00	1.00	1.00	1.00
hCE1 LD	0.54	8.53	2.16	N.D.
hCE1 LD1	0.30	33.78	0.94	N.D.
hCE1 LD2	0.07	1.85	N.D.	N.D
hCE1 LD3	0.02	53.14	N.D.	N.D.
hCE1 LD4	0.03	61.59	1.78	15.06

Table 5.2 Effects of LD mutations on various CE substrates. By removing the 15-residue acyl-loop and mutating the hCE1 active site, activity towards conventional carboxylesterase substrates was decreased while hydrolysis of SN-38 enhanced 60-fold. N.D. is no detected.

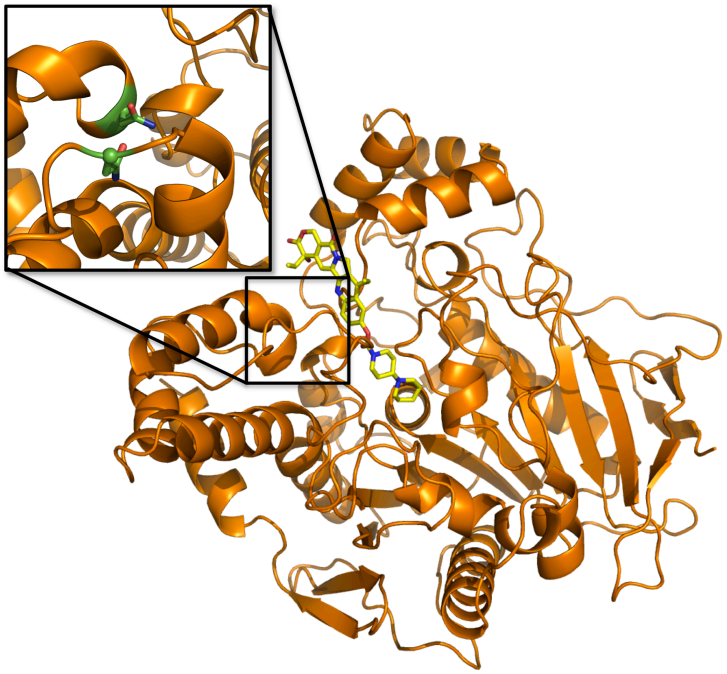

Figure 5.4 Homology model of hCE1 LD_4 with CPT-11. By removing the acyl-binding loop and adding a patch of polar residues (N254 and N388, green inset) near the enzyme's "side-door", we enhanced the hydrolysis of CPT-11 up to 60-fold over wild type hCE1. These structural features are also found in hiCE and rsCE.

REFERENCES

1. Ross, M. K., and Crow, J. A. (2007) Human carboxylesterases and their role in xenobiotic and endobiotic metabolism, *J Biochem Mol Toxicol 21*, 187-196.

2. Holmes, R. S., Cox, L. A., and Vandeberg, J. L. (2009) A new class of mammalian carboxylesterase CES6, *Comp Biochem Physiol Part D Genomics Proteomics 4*, 209-217.

3. Wierdl, M., Tsurkan, L., Hyatt, J. L., Edwards, C. C., Hatfield, M. J., Morton, C. L., Houghton, P. J., Danks, M. K., Redinbo, M. R., and Potter, P. M. (2008) An improved human carboxylesterase for enzyme/prodrug therapy with CPT-11, *Cancer Gene Ther 15*, 183-192.

4. Redinbo, M. R., Stewart, L., Kuhn, P., Champoux, J. J., and Hol, W. G. (1998) Crystal structures of human topoisomerase I in covalent and noncovalent complexes with DNA, *Science 279*, 1504-1513.

5. Maxwell, D. M., and Brecht, K. M. (2001) Carboxylesterase: specificity and spontaneous reactivation of an endogenous scavenger for organophosphorus compounds, *J Appl Toxicol 21 Suppl 1*, S103-107.

6. Hemmert, A., Otto, M. F., Wierdl, M., Edwards, C. C., Fleming, C. D., MacDonald, M., Cashman, J. R., Potter, P. M., Cerasoli, D. M., and Redinbo, M. R. (2010) Human Carboxylesterase 1 Stereoselectively Binds the Nerve Agent Cyclosarin and Spontaneously Hydrolyzes the Nerve Agent Sarin, *Molecular Pharmacology IN PRESS*.

7. Hosokawa, M. (2008) Structure and catalytic properties of carboxylesterase isozymes involved in metabolic activation of prodrugs, *Molecules 13*, 412-431.

8. Potter, P. M., Wolverton, J. S., Morton, C. L., Wierdl, M., and Danks, M. K. (1998) Cellular localization domains of a rabbit and a human carboxylesterase: influence on irinotecan (CPT-11) metabolism by the rabbit enzyme, *Cancer Res 58*, 3627-3632.

9. Alexson, S. E., Finlay, T. H., Hellman, U., Svensson, L. T., Diczfalusy, U., and Eggertsen, G. (1994) Molecular cloning and identification of a rat serum carboxylesterase expressed in the liver, *J Biol Chem 269*, 17118-17124.

10. Fleming, C. D., Edwards, C. C., Kirby, S. D., Maxwell, D. M., Potter, P. M., Cerasoli, D. M., and Redinbo, M. R. (2007) Crystal structures of human carboxylesterase 1 in covalent complexes with the chemical warfare agents soman and tabun, *Biochemistry 46*, 5063-5071.

11. Bencharit, S., Morton, C. L., Howard-Williams, E. L., Danks, M. K., Potter, P. M., and Redinbo, M. R. (2002) Structural insights into CPT-11 activation by mammalian carboxylesterases, *Nat Struct Biol 9*, 337-342.

12. Bencharit, S., Morton, C. L., Xue, Y., Potter, P. M., and Redinbo, M. R. (2003) Structural basis of heroin and cocaine metabolism by a promiscuous human drug-processing enzyme, *Nat Struct Biol 10*, 349-356.

13. Lenz, D. E., Broomfield, C. A., Yeung, D., Masson, P., Maxwell, D. M., and Cerasoli, D. M. (2008) Nerve Agent Bioscavengers: Progress in Development of a New Mode of Protection against Organophosphorus Exposure, in *Chemical Warfare Agents: Chemistry, Pharmacology, Toxicology, and Therapeutics* (Romano Jr., J. A., Lukey, B. J., and Salem, H., Eds.) 2nd ed., CRC Press, Boca Raton, FL.